

UC Santa Barbara

UC Santa Barbara Electronic Theses and Dissertations

Title

Multidimensional Synthesis of Organic Materials

Permalink

<https://escholarship.org/uc/item/7hb9c2fh>

Author

Sample, Caitlin Sarah

Publication Date

2020

Peer reviewed|Thesis/dissertation

UNIVERSITY OF CALIFORNIA

Santa Barbara

Multidimensional Synthesis of Organic Materials

A dissertation submitted in partial satisfaction of the
requirements for the degree Doctor of Philosophy
in Materials

by

Caitlin S. Sample

Committee in charge:

Professor Craig J. Hawker, Co-Chair

Professor Christopher M. Bates, Co-Chair

Professor Ram Seshadri

Professor Matthew E. Helgeson

March 2020

The dissertation of Caitlin S. Sample is approved.

Professor Matthew E. Helgeson

Professor Ram Seshadri

Professor Christopher M. Bates, Committee Co-Chair

Professor Craig J. Hawker, Committee Co-Chair

March 2020

Multidimensional Synthesis of Organic Materials

Copyright © 2020

by

Caitlin S. Sample

ACKNOWLEDGEMENTS

I owe so much of my development, both professional and personal, to my advisors, Craig Hawker and Chris Bates. Craig took me on as a mathematically inclined materials scientist with very little chemistry knowledge, and under his guidance I have not only learned so much about chemical synthesis and characterization, but also about the importance of personal responsibility, scientific curiosity, and collegial respect. From my third year onwards, I had the pleasure of being co-advised by Chris Bates, who brought a new and valuable perspective to my work; he was generous with his time and effort whenever needed, helping to guide my projects and papers to a higher level. I'll also never mistake a hyphen for an en dash again.

In addition to my official advisors, I've been fortunate to be surrounded by many other faculty members that have offered advice and support throughout my grad school career. Ram Seshadri was immensely supportive of both my work here at UCSB and my aspirations for the future. Matt Helgeson was always quick with an insightful if challenging question about my research, both as a committee member and a part of IRG-3. Rachel Segalman and Javier Read de Alaniz offered thoughtful discussions to help push me in new directions. Frank Leibfarth, while not at UCSB by the time I arrived, encouraged me in deciding to come here and has welcomed me into the greater polymer community ever since.

One of the most difficult and most important lessons I've learned in grad school is that it is not only acceptable but rather imperative to ask for help, and I have received so much from my fellow group members over the years. I would not be the scientist I am today without the influence of Nisha Handa, Eisuke Goto, Yingdong Luo, Will Gutekunst, Zak Page, Neil Dolinski, Emre Discekeci, David Lunn, Athina Anastaski, Sang-Ho Lee, Shaoguang Li,

Morgan Bates, Jing Ren, Jeffrey Self, Lindsay Robinson, Eileen Seo, Zhishuai Geng, Allison Abdilla, Manny Zayas, Yvonne Diaz, Benjaporn Narupai, Reggie Bou Zerdan, Zac Hudson, Revital Kaminker, Abby Knight, Daniel Klinger, Jimmy Lawrence, Kaila Mattson, Brenden McDearman, Alaina McGrath, Saemi Poelma, Christian Pester, Nic Treat, Cynthia Wang, and so many more. I've appreciated all your contributions to my journey from day one to now.

I would be absolutely remiss if I neglected to thank the talented undergraduates and other interns that I've been so lucky to work with. Valerie Lensch is one of the brightest young scientists I've ever met, and her intellectual and experimental contributions to the poly(silyl ether work) and silicone vulcanization were key to their success. My thanks also go out to my summer interns, Brooke Versaw, Fern Boonchaiphruak, and Alex Fusi, who were able to accomplish so much in so little time—I expect great things of you all.

I owe an enormous debt of gratitude to the technical and administrative staff that have helped me throughout grad school. Without Rachel Behrens, Amanda Strohm, Jerry Hu, Hongjun Zhou, Dmitriy Uchenik, and James Pavlovich, the majority of my research would have not been possible. Samantha Crossno, Marisol Cedillo Dougherty, Mary McGuan, Sylvia Vogel, Julie Standish, Jocelyn Guzman, and Tawny Hernandez have tolerated my dozens of questions and requests for help these past five years, and I thank them for that as well as all of the work they do to keep the MRL and Materials Department running smoothly.

Outside of lab, I've been blessed by the most supportive group of friends anyone could ask for. Anastasia and Julija, I am so happy that coincidence brought us together from the very beginning; you are the kindest, funniest, all-around-best people I could have imagined going through grad school with. And for the rest of the Bouncy Castle crew—Neil, Ben, Emily, Madi, Richard, Christian, Emma, Sean, and Sophia—I thank you for keeping me grounded and happy

throughout the highs and lows of these past few years. Grad school isn't easy, but you all made it so much easier.

I don't know where to begin in thanking my partner-in-crime and partner-in-life, Jeffrey. You have filled the last and most stressful years of my doctoral career with laughter, and I've enjoyed every minute of it. I cannot imagine what my life would be without you inspiring me to be my best self, and I am eternally grateful for your compassion, intelligence, and creativity. I cannot wait to see what further adventures our future holds, and nothing seems daunting with you by my side. And of course, I owe you thanks for my faithful writing companion, Gaia Nala.

Finally, I dedicate this dissertation to my parents. You have been my greatest cheerleaders from day one, and although you never pushed me to follow in your footsteps, it was impossible not to be inspired by your passion for science and your dedication to the pursuit of knowledge. I know that you would have supported me in whatever I chose to do, but you've made a challenging path easier with your love and encouragement. I am so grateful to have you both in my corner, and I could not have asked for a better team. From the very bottom of heart, I love you, and I thank you.

VITA OF CAITLIN S. SAMPLE

March 2020

EDUCATION

Bachelor of Science in Materials Science and Engineering and Applied Mathematics, Massachusetts Institute of Technology, June 2014

Doctor of Philosophy in Materials, University of California, Santa Barbara, March 2020 (expected)

PUBLICATIONS

Sample, CS; Lee, S-H; Li, S; Bates, MW; Lensch, V; Versaw, BA; Bates, CM; Hawker, CJ. “Metal-free room-temperature vulcanization of silicones via borane hydrosilylation.” *Macromolecules*, **2019**, *52*, 7244–7250. DOI: 10.1021/acs.macromol.9b01585

Sample, CS; Lee, S-H; Bates, MW; Ren, JM; Lawrence, J; Lensch, V; Gerbec, JA; Bates, CM; Li, S; Hawker, CJ. “Metal-free synthesis of poly(silyl ether)s under ambient conditions.” *Macromolecules*, **2019**, *52*, 1993–1999. DOI: 10.1021/acs.macromol.8b02741

Sample, CS; Goto, E; Handa, NV; Page, ZA; Luo, Y; Hawker, CJ. “Modular synthesis of asymmetric rylene derivatives.” *J. Mater. Chem. C.*, **2017**, *5*, 1052–1056. DOI: 10.1039/C6TC05139A

Sample, CS; Xu, AK; Swartz, SM; Gibson, LJ. “Nanomechanical properties of wing membrane layers in the house cricket (*Acheta domestica* Linnaeus).” *J. Insect Physiol.*, **2015**, *74*, 10–15. DOI: 10.1016/j.jinsphys.2015.01.013

Lee, H; **Sample, C**; Cohen, RE; Rubner, MF. “pH-programmable sequential dissolution of multilayer stacks of hydrogen-bonded polymers.” *ACS Macro Lett.*, **2013**, *2*, 924–927. DOI: 10.1021/mz400398s

Salem, IB; Guillermic, RM; **Sample, C**; Leroy, V; Saint-Jalmes, A; Dollet, B. “Propagation of ultrasound in aqueous foams: bubble-size dependence and resonance effects.” *Soft Matter*, **2013**, *9*, 1194–1202. DOI: 10.1039/C2SM25545F

Dollet, B; Erpelding, M; Guillermic, RM; **Sample, C**; Pierre, J; Saint-Jalmes, A; Crassous, J. “Probing acoustics of liquid foams by optical diffusive wave spectroscopy.” *J. Acoust. Soc. Am.*, **2013**, *133*, 3373. DOI: 10.1121/1.4805787

CONFERENCE PRESENTATIONS

Sample, CS; Lee, S-H; Bates, MW; Lensch, V; Bates, CM; Li, S; Hawker, CJ. “Metal-free synthesis of poly(silyl ethers) with tunable degradation.” *Gordon Research Conference on Polymers*, South Hadley, MA, **2019**. Poster.

Sample, CS; Bates, MW; Lensch, V; Boonchaiphruk, L.; Bates, CM; Hawker, CJ. “Metal-binding polysiloxane networks through borane-catalyzed vulcanization.” *257th ACS National Meeting*, Orlando, FL, **2019**. Oral & Poster.

Sample, CS. “Metal-free synthesis of functional silicones.” *Materials Research Outreach Program*. Santa Barbara, CA, **2019**. Invited Talk.

Sample, CS; Lee, S-H; Li, S; Schulze, M; Lensch, V; Versaw, B; Bates, CM; Hawker, CJ. “A metal-free route to vulcanization of silicone networks.” *National Graduate Research Polymer Conference*. Minneapolis, MN, **2018**. Oral.

Sample, CS; Lee, S-H; Li, S; Schulze, M; Lensch, V; Versaw, B; Bates, CM; Hawker, CJ. “Functional silicone networks via metal-free vulcanization.” *255th ACS National Meeting*. New Orleans, LA, **2018**. Oral.

Sample, CS; Dolinski, ND; Anastasaki, A; Lunn, DJ; Discekici, E; Hawker, CJ. “Photomediated approach for patterned bottlebrush networks.” *253rd ACS National Meeting*, San Francisco, CA, **2017**. Poster.

Sample, CS; Handa, NV; Hawker, CJ. “A novel and versatile synthetic strategy for asymmetric perylene diimide derivatives.” *250th ACS National Meeting*, Boston, MA, **2015**. Oral.

AWARDS

Graduate Research Fellowship, *National Science Foundation*, **2014–2019**.

Chancellor’s Fellowship, *University of California*, **2014–2019**.

Honorable Mention Oral Presentation, *National Graduate Research Polymer Conference*, **2018**.

MENTORSHIP AND TEACHING EXPERIENCE

Valerie Lensch, *Research Internships in Science and Engineering*, **2017–2019**.

Alexander Fusi, *Cooperative International Science and Engineering Internships*, **2019**.

Laksamon Boonchaiphruk, *Intern from Chulalongkorn University*, **2018**.

Brooke Versaw, *Future Leaders in Advanced Materials*, **2017**.

Teaching Assistant, *Materials 10*, **2015**.

ABSTRACT

Multidimensional Synthesis of Organic Materials

by

Caitlin S. Sample

At the core of materials science is a simple but essential rule: structure informs function. It follows, then, that the ability to control the structure of organic molecules is key to the development of highly functional organic materials. At the small-molecule level, this means taking advantage of the diversity of synthetic transformations available to control the spatial arrangements of atoms within the molecular structure. For example, the synthesis of asymmetric perylene diimides for organic semiconductors is realized by choosing a naphthalic starting material over the traditional perylene core, and the substitutions made possible by this approach have a dramatic effect on the electronic and optical properties as well as the potential for subsequent functionalization. Small-molecule functionality becomes of great important as we move to higher dimension systems, such as polymers. Macromolecular synthesis requires a careful selection of functional monomer and appropriate catalyst. The synthetic route demonstrated herein shows that the polyaddition of bis(silanes) and diketones can be achieved via borane-catalyzed hydrosilylation to generate poly(silyl ethers) with varied thermal properties and degradation behavior. By exchanging one of the small-molecule starting components —bis(silanes)—for hydrosilane-containing polymers, we shift from the synthesis

of discrete polymer chains to unimolecular silicone networks, in which chemical crosslinks give the resultant thermosets the mechanical integrity needed to perform as engineering materials. As a further handle for structural manipulation, triggers for external stimuli can be used to give spatiotemporal control over material properties. In the final case study discussed in this dissertation, the combination of two forms of stimuli is demonstrated. Light is used to spatially program the macroscopic structure of thiol–ene networks, while the inclusion of dynamic boronic ester bonds allows for thermal relaxation at the nanoscopic scale. The interplay between these stimuli allows for 3D printing of objects that can relax stress, self-heal, and be reprocessed into entirely new parts. In each of the examples presented, we harness fundamental concepts from organic chemistry to gain control over chemical and physical structure, enabling the generation of functional organic materials across multiple length scales.

TABLE OF CONTENTS

Chapter 1 Introduction	1
1.1 Organic n-Type Semiconductors	2
1.2 Asymmetric Rylene Diimides.....	3
1.3 Structure–Function in Polymers	4
1.4 Poly(Silyl Ethers).....	6
1.5 Organoborane Catalysis	7
1.6 Metal-Free Synthesis of PSEs and Silicones	8
1.7 Vat Polymerization 3D Printing.....	10
1.8 Covalent Adaptable Networks	11
1.9 Conclusion	13
Chapter 2 Modular Synthesis of Asymmetric Perylene Diimides	14
2.1 Abstract.....	14
2.2 Introduction.....	15
2.3 Results and Discussion	16
2.3.1 Synthetic Approach.....	16
2.3.2 Imide Substitution.....	19
2.3.3 Bay Substitution.....	20
2.3.4 Higher-Order Rylenes.....	22
2.4 Conclusions.....	24
2.5 Experimental.....	25
2.5.1 Materials	25

2.5.2 Methods.....	25
2.5.3 Synthesis	26
2.6 Supplemental Results.....	29
Chapter 3 Poly(Silyl Ethers) via Borane-Catalyzed Hydrosilylation	34
3.1 Abstract.....	34
3.2 Introduction.....	35
3.3 Results and Discussion	38
3.3.1 Small-Molecule Model Reaction	38
3.3.2 Polymerization Conditions.....	39
3.3.3 Expansion of Monomer Scope.....	42
3.3.4 Physical and Thermal Properties	45
3.3.5 Hydrolysis	47
3.4 Conclusions.....	48
3.5 Experimental.....	49
3.5.1 Materials	49
3.5.2 Methods.....	49
3.5.3 Synthesis	50
3.5 Supplemental Results.....	52
Chapter 4 Metal-Free Vulcanization of Silicone Networks.....	54
4.1 Abstract.....	54
4.2 Introduction.....	55
4.3 Results and Discussion	58
4.3.1 Development of Vulcanization	58

4.3.2 Varied Crosslinker Scope	58
4.3.3 Varied Prepolymer Scope	60
4.3.4 Hydrolysis	62
5.3.5 Introduction of Functionality	64
4.4 Conclusions.....	67
4.5 Experimental	68
4.5.1 Materials	68
4.5.2 Methods.....	68
4.5.3 Synthesis	69
4.6. Supplemental Results.....	72
4.6.1 Hydrolysis Analysis	72
4.6.2 Functionalization of PMHS	73
Chapter 5 3D Printing of Boronic-Ester Vitrimers	74
5.1 Abstract.....	74
5.2 Introduction.....	75
5.3 Results and Discussion	77
5.3.1 Resin Formulation.....	77
5.3.2 Varied Concentration of Boronate	80
5.3.3 3D Printing of Boronate Resins	83
5.4 Conclusions and Future Directions	85
5.5 Experimental	87
5.5.1 Materials	87
5.5.2 Methods.....	87

5.5.3 Synthesis	90
5.6 Supplemental Results.....	91
Chapter 6 References	94

Chapter 1

Introduction

From a materials perspective, one of the greatest strengths of organic synthesis is the ability to control structure across multiple length scales. In the design of organic materials, there are a wealth of transformations allowing for the precise arrangement of nearest-neighbor atoms at the nanoscale, the architecture of higher-order polymers and network topology at the microscale, and the overall macroscale form of the final material. It is the role of the materials scientist to bridge the gap between organic chemistry and materials engineering by identifying the potential of synthetic developments to produce novel functional materials. In this dissertation, four such examples will be presented. The first is a case study in purely small-molecule synthesis, with a modular approach allowing for precise control over asymmetric substitutions of rylenes for organic semiconductor applications.¹ The second and third extend synthetic control to macromolecular systems by taking advantage of borane catalysis to generate organosilicon polymers² and networks.³ The fourth and final example spans length-scales from nano to macro, as the inclusion of dynamic boronate bonds in a photo-curable resin

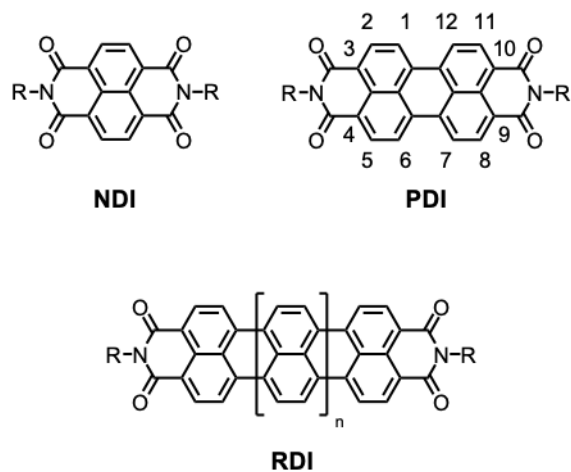
enables 3D printing of self-healing, reconfigurable materials. Despite the range of synthetic approaches used and the diversity of materials that result, each of these studies demonstrate the fundamental interplay between synthetic and structural control.

1.1 Organic n-Type Semiconductors

The finest precision that organic synthesis affords is at the nanoscale, by allowing for the selective arrangement of bonded atoms within a single molecule. This atomistic-level control, and the wide diversity of structures that it affords, is one of the reasons that organic molecules are of great interest as an alternative to traditional inorganic semiconductors. In addition to their relatively low cost, ease of processing, and mechanical robustness, organic semiconductors can have substituents that are both structurally variable and precisely located, enabling the targeted synthesis of candidate molecules. These synthetic approaches have succeeded in identifying several high performing *p*-type systems, in which the charge carriers are predominantly holes.⁴ However, the development of corresponding n-type materials, in which conduction is driven directly by the movement of electrons, has been more limited.⁵

Some of the most promising n-type semiconductors are rylene diimides, which contain a conjugated, naphthalene-based core bookended by electron-withdrawing dicarboxylic imides (Scheme 1.1). The electronic properties of various naphthalene dimides (NDIs), perylene diimides (PDIs), and higher-order rylene dimides (RDIs) have been the subject of substantial investigation in the past two decades,⁶⁻¹² and much of the breadth of the field is owed to the structural versatility of the rylene scaffold. While all rylene scaffolds share a similar polycyclic structure, they vary not only by the number of repeating naphthalene units within the core but also by the substitutions at the imide position and along the ortho and bay positions of the core.¹³ These modifications allow for the generation of a suite of materials suitable for a range

of applications, as well as the continual optimization of processability and electronic performance.

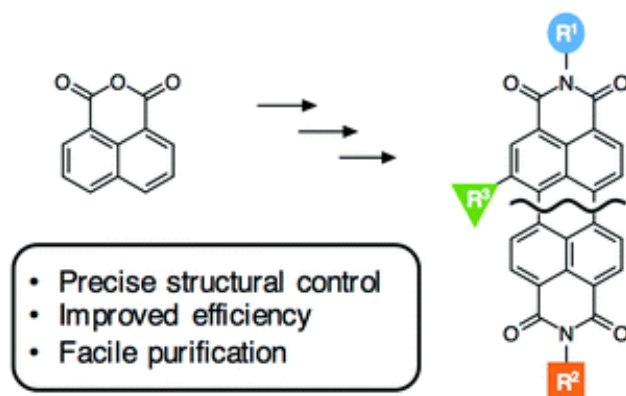


Scheme 1.1 Structures of naphthalene diimide (NDI), perylene diimide (PDI), and higher-order rylene diimides (RDI). The PDI core positions are notated, including the ortho (2, 5, 8, and 11) and bay (1, 6, 7, and 12) positions.

1.2 Asymmetric Rylene Diimides

While this tunability is powerful, the symmetric nature of rylenes means that chemistries to add substituents are non-selective with regards to equivalent positions, e.g., the 1 and 7 bay positions. This inherent symmetry is a limitation on the versatility of the rylene library; consider, for instance, the case of imide substitution. It is not difficult to conceive of an application in which a PDI containing two separate imide substituents is desired, for instance a solubilizing group on one side and a functional handle for incorporation along a polymer backbone on the other. The traditional approach of condensing a symmetric perylene core with the appropriate amine is inefficient, as even at sub-stoichiometric equivalents of amine, the

result is a statistical mixture of the di-, mono-, and unsubstituted perylenes.^{14,15} To overcome this challenge, we envisioned a modular synthetic approach that, instead of beginning with the intact perylene, takes advantage of the separate functionalization of two distinct naphthalene halves that are subsequently fused to form the core of the final PDI (Scheme 1.2). Chapter 2 of this dissertation presents the development of this synthetic pathway for a library of asymmetric perylenes and rylene derivatives, as well as the electronic and optical characterization of the resulting molecules.



Scheme 1.2 Modular synthesis of rylene derivatives showing naphthalic starting material and advantages of approach.

1.3 Structure–Function in Polymers

While the generation of a small molecule is a fitting case study for the precision of organic synthesis, much of the field of organic materials design is concerned with larger macromolecular systems, e.g., polymers. Polymeric materials such as plastics are ubiquitous in modern life, and as such, the improved synthesis of commodity materials and increased access to novel structures are of great societal importance. For any given polymerization, there are two fundamental considerations. Firstly, monomer choice plays a key role in structural

determination, as the monomeric units are the building blocks for the resultant macromolecule. Secondly, while some monomers are able to react spontaneously, the majority of reactions require some form of catalysis in order to proceed; the catalyst used depends on a variety of factors, including monomer functionality, catalyst expense, and compatibility with desired application.

The core of any polymer design is first and foremost monomer selection, for that choice informs the polymeric structure and, in turn, its properties. A key example of structure–function relationship comes from consideration of the backbone. Most polymer backbones are purely organic in composition, containing primarily C–C or C–O constituent bonds. For the simplest example of a linear, aliphatic polymer, the conformational freedom of these bonds lends flexibility to the chains they comprise, but their relatively poor bond strength results in a low maximum working temperature. What would be the outcome, however, if the carbon were to be replaced by silicon, an atom with the same vacancy and similar bonding behavior? While the Si–Si bond is weaker than its C–C counterpart, the Si–O bond that makes up the backbone of the most common silicon-containing polymer class, polysiloxanes, is substantially stronger.¹⁶ As a result, polysiloxanes exhibit much increased thermal stability in comparison to hydrocarbon polymers, making them better suited for high temperature applications. In addition, polysiloxanes improve upon the flexibility of carbon-based backbones, with polydimethylsiloxane having one of the lowest glass transition temperatures of any commodity polymer at around $-125\text{ }^{\circ}\text{C}$. Although both silicon and carbon share a tetrahedral bonding arrangement, the Si–O bond has the dual advantages of increased bond length and larger bond angle (Figure 1.1), giving more freedom of movement due to reduced steric interaction between neighboring groups.^{17,18}

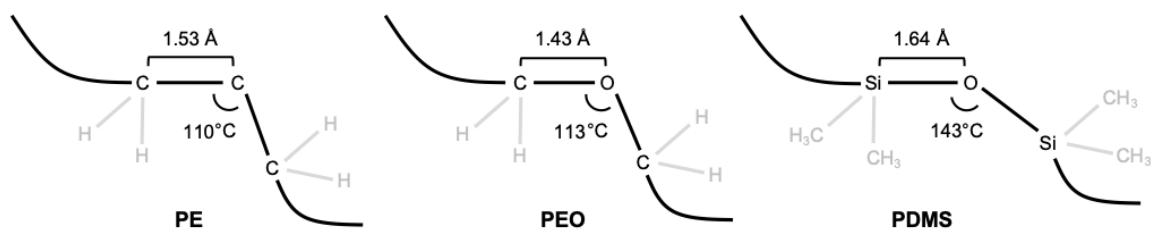


Figure 1.1 Selected sections of the structures of polyethylene (PE), poly(ethylene oxide) (PEO), and polydimethylsiloxane (PDMS) showing relevant bond lengths and angles.

1.4 Poly(Silyl Ethers)

In addition to polysiloxanes, a growing family of silicon-based polymers is that of poly(silyl ethers) (PSEs), which contain a silyl ether (Si–O–C) group within the repeat unit. PSEs share many of the advantages of polysiloxanes, including thermal stability and flexibility, with the added benefit of improved degradability due to the inclusion of labile silyl ether linkages. A variety of monomer species and catalytic systems have been investigated for the synthesis of PSEs, but the polymerization strategies can be broadly divided into two classes: polycondensation and polyaddition. Both are forms of step-growth polymerization (a term deprecated by IUPAC in 1994 but still in widespread use in the field today),¹⁹ in which the polymerization of a self-reactive bifunctional monomer or a mixture of two inter-reactive difunctional monomers gives rise to polymeric chains. Polycondensation is the subset of step-growth polymerizations in which the bond formation reaction produces a molecular side product, often but not always water, hence the term “condensation.” Many of the earliest developments in PSE synthesis were polycondensation reactions, but these tend to require higher temperatures, while lower atom economy leads to the evolution of hydrogen chloride or other byproducts.^{20–24} In addition to inherent issues associated with management and

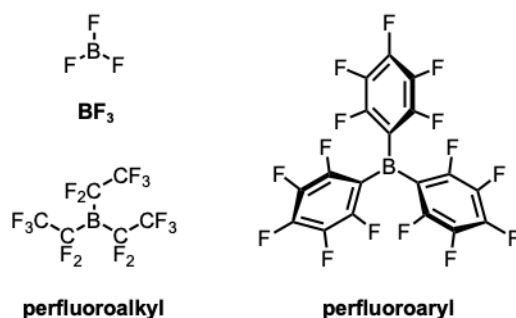
removal of unwanted side products, the *in situ* generation of acid is particularly detrimental in PSE synthesis. Due to the lability of the Si–O–C group under acidic conditions, production of acid leads to competition between the growth and degradation of the polymer chains.

In contrast, the polyaddition class of step-growth polymerizations exhibits ideal atom economy, with the intermolecular reactions involved yielding no extraneous products. Therefore, the bulk of PSE synthetic development has shifted to these systems, with a particular focus on hydrosilylation reactions, in which a hydrogen is added across an unsaturated bond. The wide scope of possible substrates and diversity of candidate catalysts make hydrosilylation a rich avenue to PSE synthesis, with a number of strategies developed in recent decades.^{25–31} While these systems have been employed to successfully generate PSEs, the procedures typically require elevated temperatures, extended reaction times, or a combination of the two. In addition, the catalysts used are all metal-based, which tend to be derived from expensive, limited resources and can have deleterious effects in applications such as biomedicine, electronics, and optics. We were interested, therefore, in developing a system that would be both highly efficient and metal-free.

1.5 Organoborane Catalysis

To that end, we turned to the family of organoborane Lewis acid catalysts. The trihalide BF_3 (Scheme 1.3) is the archetypical Lewis acid; three highly electronegative fluorine atoms give the central boron a strongly electron deficient character. Additionally, due to the electronic nature of boron, the compound adopts a trigonal planar geometry that permits easy access to the Lewis acidic core. Despite the potency of BF_3 , its practical application suffers due to its high moisture sensitivity and volatility. It was hypothesized that perfluoroalkyl analogs would have improved hydrolytic stability, but their synthesis revealed a tendency for rapid

decomposition.³² Instead, the frontrunner for stable boron-based Lewis acids became perfluoroaryl derivatives, in which the aryl boron bonds are more stable than the previous systems and the strongly electron withdrawing perfluoroaryl groups imbue the resultant catalyst with an even higher degree of Lewis acidity than BF_3 itself.³³



Scheme 1.3 Structures of BF_3 and representative perfluoroalkyl and perfluoroaryl boranes.

1.6 Metal-Free Synthesis of PSEs and Silicones

As a result of these advantages, the tri-substituted tris(pentafluorophenyl)borane, or $\text{B}(\text{C}_6\text{F}_5)_3$, has emerged as a particularly powerful and versatile catalyst. Originally synthesized by Massey and Park in the 1960s, the moisture tolerant and easily handled $\text{B}(\text{C}_6\text{F}_5)_3$ has seen a renaissance of investigation in recent decades. Of particular interest to the synthesis of PSEs was work by Piers and Park showing the ability of $\text{B}(\text{C}_6\text{F}_5)_3$ to catalyze hydrosilylation reactions of aldehydes, ketones and esters,³⁴ which was subsequently demonstrated to occur via the electron deficient boron center abstracting the Si–H hydride and thereby allowing for nucleophilic attack of the carbonyl on the activated silicon.³⁵ Inspired by the efficiency of these reactions, as well as the wide scope of diketone monomers available, we developed a $\text{B}(\text{C}_6\text{F}_5)_3$ -catalyzed strategy for the polymerization of PSEs (Figure 1.2). This approach, as well as the

thermal properties and degradation behavior of the resulting polymers, is discussed in further detail in Chapter 3.

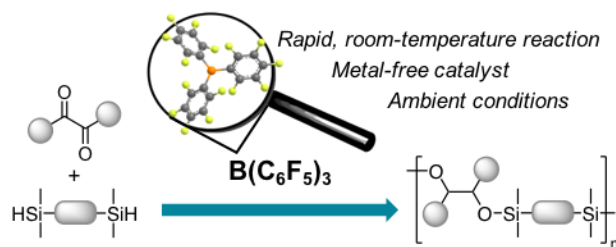


Figure 1.2 $B(C_6F_5)_3$ -catalyzed synthesis of poly(silyl ethers) from diketone and bis(silane) monomers.

Additionally, we extended this strategy from linear polymers to higher-order silicone networks by using those same diketone monomers to crosslink commercially available hydride-functional polysiloxanes. These siloxane derivatives are the same precursors used in conventional platinum-based addition curing, in which hydrosilylation of vinyl groups gives vulcanization. By using shared starting materials in a solvent-free approach, the $B(C_6F_5)_3$ -catalyzed system requires little deviation from traditional manufacturing techniques, while offering a room-temperature, metal-free route to materials with similar thermomechanical properties and improved optical properties to the Pt-cured materials (Figure 1.3). Furthermore, the ability for the resultant silicones to be decorated with functional handles inaccessible to the platinum system is demonstrated, with these vulcanization and functionalization results presented in Chapter 4.

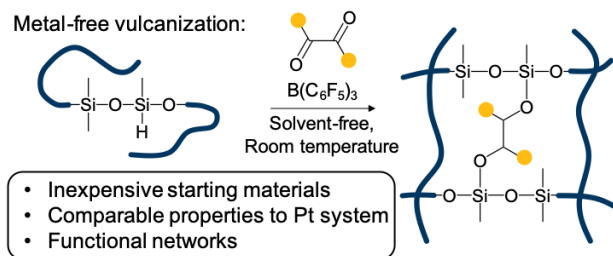


Figure 1.3 Room-temperature vulcanization of silicones via borane-catalyzed hydrosilylation.

1.7 Vat Polymerization 3D Printing

While the silicone networks generated via borane-catalyzed hydrosilylation can have some degree of three-dimensional control through casting in molds, we can achieve even greater influence over macroscopic structure by harnessing a curing chemistry with a spatiotemporally resolved stimulus. In particular, our group has taken advantage of light as a potent tool for surface patterning.^{36–40} In three dimensions, photocuring produces objects with well-defined geometries, and no technique has demonstrated the power of that approach more clearly than vat polymerization 3D printing. In vat polymerization processes such as stereolithography (SLA) or digital light processing (DLP), the desired part is 3D-printed by selectively exposing a photosensitive resin to patterned light, typically in a layer-by-layer fashion.^{41,42} The photoactive chemistry within the resin, typically radical or cationic polymerization, quickly generates a solid part solely in the regions that undergo light exposure. The rapidity of this approach, as well as the fine resolution afforded by typical focal lengths, have made vat polymerization 3D printers an increasingly attractive alternative to more traditional extrusion-based systems.⁴³

However, one area in which vat polymerization lags behind extrusion-based 3D printers is in sustainability, particularly with regards to the end-of-life fate of the printed parts. While

extrusion techniques such as fused filament fabrication (FFF) produce parts that are often recyclable, wherein old parts can be reprocessed into filament for further printing, vat-polymerized parts are generally doomed to accumulate in landfills. The key difference in these two destinies lies with the microscale structure produced by the two chemistries—more specifically, the connectivity of the constituent polymers (Figure 1.4). FFF filaments are thermoplastic in nature, which means entangled polymers provide a solid structure at lower temperatures but soften and eventually flow upon heating; this thermal dependence allows for both the extrusion process as well as a high degree of recyclability. Conversely, the photocuring chemistries of vat polymerization give rise to chemically crosslinked networks, in which permanent covalent bonds prevent reconfiguration. To reduce the amount of waste generated by this subset of 3D printing strategies, there is substantial interest in developing hybrid materials that combine capability of thermosets to be photocured with the reprocessability of thermoplastics.



Figure 1.4 Schematic of polymer network showing contrast between physical crosslinks of thermoplastics (left) and chemical crosslinks of thermosets (right).

1.8 Covalent Adaptable Networks

The challenge of developing recyclable thermosets is a decades-old problem and a highly active area of polymer research. One particular focus has been on the development of

reprocessable thermosets in the form of covalent adaptable networks (CANs). These networks are chemically crosslinked, but their structure contains dynamic covalent bonds that are able to undergo reversible exchange reactions, allowing for relaxation of stress, self-healing, and remolding. CANs are divided into a dissociative subset, in which bonds are broken during exchange, and an associative subset, in which the network structure is preserved throughout the process. Leibler et al. coined the term vitrimer to describe associative CANs with their study on carboxylate transesterification,⁴⁴ but several additional associative chemistries have been developed, including allyl sulfides,⁴⁵ olefins,⁴⁶ urethanes,⁴⁷ vinylogous urethanes,⁴⁸ triazoles,⁴⁹ and alkylated thioethers.⁵⁰ The wide range of dynamic covalent bonds available presents a wealth of opportunity for resin formulation aimed towards producing reprocessable 3D-printed parts.

The primary design criteria for selecting the appropriate dynamic chemistry for vat polymerization are as follows: radical-stable to survive the chosen photocuring process, compatible with other functionalities present in the resin, and catalyst-free to avoid issues with leaching during post-processing and the lifetime of the part. With these in mind, boronic ester transesterification emerged as an appealing candidate. The bond exchange of boronic esters has been demonstrated to occur efficiently without the need for extraneous catalyst or elevated temperatures that might degrade the material.⁵¹ In addition to this associative pathway, boronic esters can also rapidly rearrange via dissociative exchange in the presence of water, allowing for hydrolysis-induced, room-temperature self-healing.⁵² Furthermore, the stability of boronate moieties towards radical chemistries has also been shown.^{53,54} As such, we synthesized a boronic-ester-containing diene monomer for use in thiol–ene-based 3D printing, the results of which are found in Chapter 5.

1.9 Conclusion

The four studies presented in this dissertation allow us to explore the various length-scales associated with the development of organic materials. First, the production of asymmetric perylene diimides and rylene derivatives demonstrates the importance of synthetic development to tailor the nanoscale molecular structure. As we move from nanoscopic to micro- and mesoscopic materials, we see how the combination of catalyst and substrate selection plays a key role in the generation of both linear organosilicon polymers as well as crosslinked silicone networks. Finally, we harness light's ability for spatial patterning to control the macroscopic structure of 3D-printed vitrimers, in which the nanoscale rearrangement of dynamic boronic ester bonds has a dramatic effect on the material properties. Throughout this work, the fundamental relationship between structure and function is readily apparent.

Chapter 2

Modular Synthesis of Asymmetric Perylene Diimides

Reproduced from Sample, C. S.; Goto, E.; Handa, N. V.; Page, Z. A.; Luo, Y.; Hawker, C. J. Modular Synthesis of Asymmetric Rylene Derivatives. *J. Mater. Chem. C* **2017**, *5*, 1052–1056. with permission from the Royal Society of Chemistry.

2.1 Abstract

The modular synthesis of asymmetric rylenes from naphthalic anhydride derivatives is presented. Imidization, Suzuki-Miyaura coupling, and cyclodehydrogenation reactions are utilized for the generation of novel functional rylenes with these three core transformations providing significant flexibility over the final structure. The combination of simple purification and high yields enables access to asymmetric rylenes with functional handles at the imide position and site-specific incorporation of bay position substituents. The resulting library of

perylene and bisnaphthalimide-anthracene derivatives showcase the presented methodology and the ability to tune optoelectronic and electrochemical properties.

2.2 Introduction

Rylenes encompass a large family of molecules that are comprised of naphthalene units joined at the peri-position,⁵⁵ including well-known and sought-after perylene diimides (PDIs). PDIs were originally used as dyes due to their high molar absorptivity and excellent chemical, thermal, light, and air stability.⁵⁶ More recently, other attractive properties of PDIs have emerged, such as high fluorescence quantum yield⁵⁷ and strong electron accepting (n-type) character,⁵ leading to applications of PDIs and other rylenes in fluorescent light collectors,^{58,59} dye lasers,^{60–62} electrophotography,⁶³ organic field-effect transistors,^{64–66} and organic photovoltaics.^{65,67} In particular, asymmetric substitution at the imide position has resulted in improved solubility and functionality, granting access to multichromophoric systems,^{68,69} supramolecular architectures,⁷⁰ and incorporation into polymers for organic electronic applications.^{71–73}

While asymmetric PDIs are attractive, their synthesis has proven challenging. In contrast to their symmetric counterparts, which are produced readily through the condensation of perylene-3,4,9,10-tetracarboxylic dianhydride (PTCDA) with aliphatic primary amines or anilines,⁷⁴ asymmetric PDIs are not typically accessible through direct imidization given the increased reactivity of the singly substituted monoimide species.⁷⁵ Instead, the typical approach involves an inefficient (< 30% overall yield) stepwise synthesis; imidization of PTCDA with one amine, partial hydrolysis to the monoanhydride monoimide, and imidization with a second amine.^{15,76,77} A one-step synthesis of asymmetric PDIs in \approx 40% yield was recently developed in our group by taking advantage of the difference in reactivity between

alkyl- and aryl-amines, however the scope of products are limited to alkyl/alkyl and aryl/aryl combinations.⁷⁸

In seeking to further expand the availability and structural diversity of asymmetric perylenes, we report a modular approach to a wider range of functional asymmetric rylene derivatives. This strategy is enabled by the disconnection of the perylene/rylene core to give the readily available naphthalic anhydride starting material (Figure 4.1). By having a common initial building block (substituted naphthalimide—one half of PDI), the functionalization and purification is greatly simplified. As a result, high yielding imidization, followed by Suzuki–Miyaura coupling and cyclodehydrogenation reactions could be utilized to achieve the asymmetric PDI targets in greater than 40% yield.

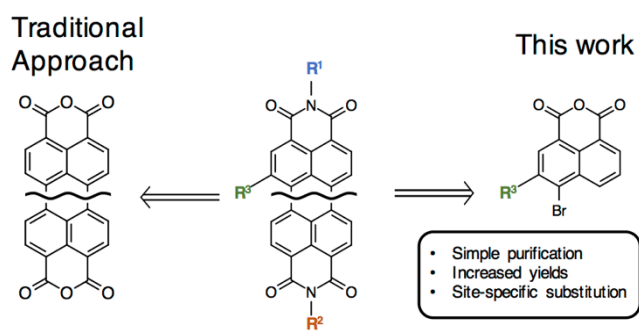


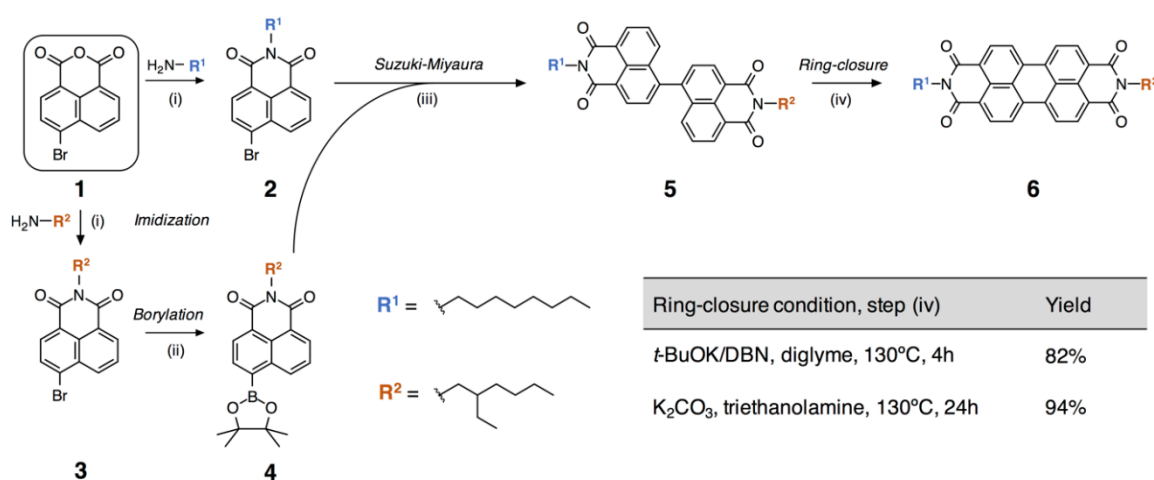
Figure 4.1 Retro-synthetic comparison of asymmetric rylene synthesis through the traditional approach starting from PTCDA versus the presented methodology from naphthalic anhydride derivatives.

2.3 Results and Discussion

2.3.1 Synthetic Approach

The general synthetic protocol to asymmetric PDIs is represented in Scheme 4.1. Bromination of the inexpensive (\approx \$50 kg⁻¹) commercial reagent “naphthalic,” to produce 4-

bromo-1,8-naphthalic anhydride (**1**), followed by imidization, is easily achieved by reacting with the desired primary amine in ethanol (EtOH) at reflux. The reaction mixture changes from an opaque to translucent solution after 2 hours due to improved solubility as **1** is converted to the imide, for example 4-bromo-1,8-naphthalimide **2** (*n*-octyl) and **3** (2-ethylhexyl) in near quantitative yields. The robust nature of this process allows for facile reaction monitoring and product purification. Following imide diversification, Miyaura borylation of **3** then leads to the boronic ester naphthalimide **4**, which could be cross coupled by Suzuki–Miyaura cross-coupling with a different bromo-naphthalimide **2** derived from the same bromo-substituted starting material, **1**. This results in clean conversion to the desired asymmetric product (**5**), which is easily purified through standard techniques.



Scheme 4.1 Representative synthesis of asymmetric PDI **1**. (i) EtOH, reflux, 4 h, 87% (**2**) and 85% (**3**); (ii) Pd(dppf)Cl₂, bis(pinacolato)diboron, KOAc, p-dioxane, 100 °C, 24 h, ≈ quantitative; (iii) K₂CO₃ (aq.), Pd(PPh₃)₄, toluene, 100 °C, 12 h, 67%; (iv) K₂CO₃, triethanolamine, 130 °C, 24 h, 94%. Comparison between reaction yields for two ring-closure conditions is provided as an inset.

A base-catalyzed cyclodehydrogenation ring closure of **5** was then investigated for formation of the asymmetric PDI **6**. Initial cyclodehydrogenation attempts employed potassium *tert*-butoxide (*t*-BuOK) and 1,5-diazabicyclo[4.3.0]non-5-ene (DBN) in diglyme,⁷⁹

however the reaction provided inconsistent yields. As an alternative, potassium carbonate (K_2CO_3) in ethanolamine at elevated temperature (130 °C) was investigated for cyclization, but this procedure leads to transimination of less sterically hindered side-chains (e.g., *n*-alkyl) by ethanolamine (Figure 4.5, Supplemental Results).⁸⁰ Triethanolamine was selected as an alternative to ethanolamine,⁸¹ and the change from primary amine to tertiary amine was found to mitigate transimination, while providing excellent yields ($\approx 94\%$). The conversion from **5** to **6** can be monitored using proton NMR (Figure 4.2a), particularly in the aromatic region as the five peaks of the Suzuki-coupled diad (**5**) collapse to two doublets (**6**) with formation of the perylene core. Additionally, the success of the ring closing can also be observed by eye due to the substantial bathochromic shift in absorbance (≈ 150 nm) from **5** (yellow solution) to **6** (bright red solution), shown as an inset in Figure 4.2b.

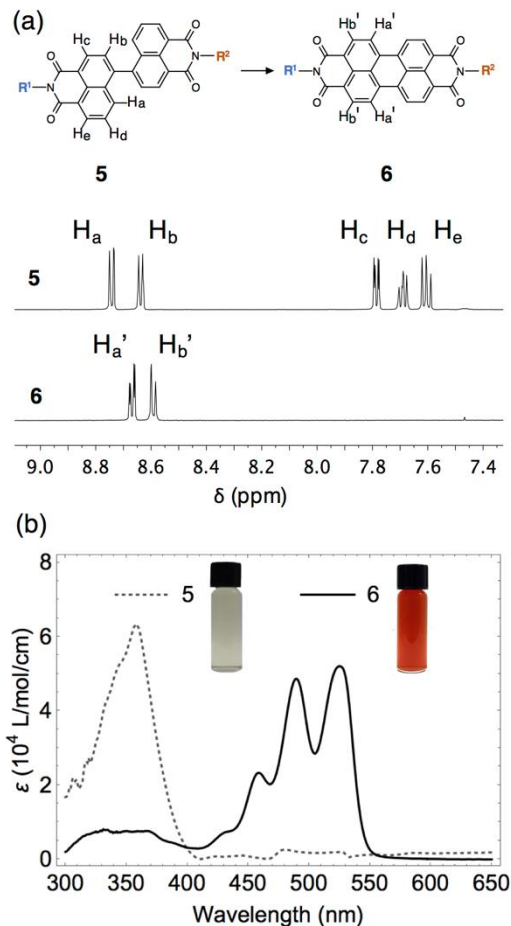


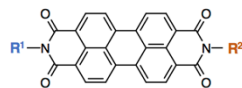
Figure 4.2 Monitoring of ring-closure reaction to convert **5** to **6**. (a) Structures with corresponding ^1H NMR, showing diagnostic aromatic protons. (b) Absorption spectra (100 μM in dichloromethane) and corresponding images of **5** and **6** (5 mM in dichloromethane).

2.3.2 Imide Substitution

To highlight the versatility of the aforementioned methodology, a library of functional asymmetric PDIs was synthesized, as shown in Table 4.1. Given the modular nature of this strategy, side chains can be easily mixed and matched. For example, partnering naphthalimide **4** containing a solubilizing 2-ethylhexyl chain with functional naphthalimides bearing a carboxylic acid or alkene chain to give asymmetric PDIs **7** and **8** respectively. Moreover, two orthogonal functionalities, such as a carboxylic acid and alkene can be easily paired with this

approach to give **9**. Overall, the yields range from 41% to 51%, as compared to < 30% for traditional methods.

Table 4.1 Asymmetric PDIs (**6–9**) synthesized with varying imide substituents. Overall yields account for all synthetic steps.



Entry	R ¹	R ²	Overall Yield
6			51%
7			44%
8			42%
9			41%

2.3.3 Bay Substitution

While varying imide substituents on PDIs is a facile route to increase solubility and incorporate functional handles, modifications at the **1**, **6**, **7**, and **12** (bay) positions on the perylene core directly influence the optoelectronic properties of the molecule. As with direct imide substitutions towards asymmetric PDIs, reactions at the perylene core typically produce mixtures of mono-, di-, tri-, and tetra-substitution that are challenging to separate, reducing reaction yields and leading to impure samples.⁸² The power of this modular strategy is that by constructing the central perylene core in a step-wise fashion starting from discrete naphthalic units, precise control over the location of the bay substitution in the final PDI is possible. Functional naphthalic anhydrides are commercially available, which provide easy access to

alkoxy-functional naphthalimides, such as methoxy-substituted naphthalimide (**10**), through Williamson-ether synthesis (Figure 4.3a). Suzuki–Miyaura coupling of **10** with a boronic ester naphthalimide (**11**), bearing no bay-substituents and a functional (alkene) imide chain, produces a PDI that is asymmetric at both the imide and bay positions (**12**). It was immediately apparent that methoxy substitution altered the electronic properties of the perylene core, given the visual difference in color for solutions of **12** (pink) relative to non-bay substituted PDIs (**6–9**, red) (Figure 4.3b). UV-Vis absorption spectroscopy quantified this observation, revealing a 30 nm bathochromic shift for methoxy-substituted PDI (**12**) relative to unsubstituted PDI (**6**) (Figure 4.3b). Additionally, cyclic voltammetry (CV) measurements show that bay substitution with an electron-donating methoxy group leads to an increase in reduction potentials for **12** (–1.19 and –1.50 V) relative to **6** (–1.11 and –1.41 V) (Figure 4.6, Supplemental Results), providing further evidence that bay substitution can be used to directly tune the electronic properties of PDIs.

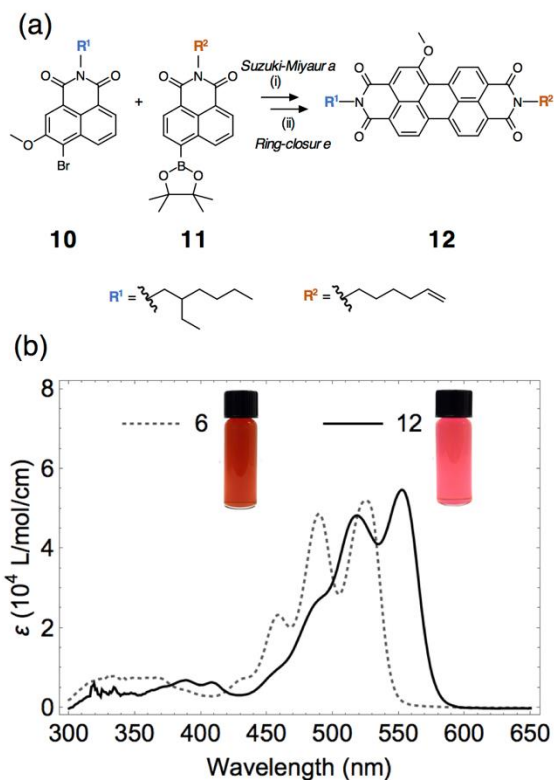


Figure 4.3 (a) Representative synthesis of bay-substituted PDI **12**. (i) K_2CO_3 (aq), $Pd(PPh_3)_4$, toluene, $100\text{ }^\circ C$, 12 h, 63%; (ii) K_2CO_3 , triethanolamine, $130\text{ }^\circ C$, 20 h, 91%. (b) Absorption spectra ($100\ \mu M$ in dichloromethane) and corresponding images of **6** and **12** (5 mM in dichloromethane).

2.3.4 Higher-Order Rylenes

As a final demonstration of modularity of this approach a novel core-extended rylene derivative was synthesized based on a structure inspired by pentarylene⁸² and an aminoanthraquinone-based rylene.⁸³ As shown in Figure 4.4a, the reaction of two equivalents of borylated naphthalimide (**13**) with 1,5-dibromoanthracene (**14**) produces a dinaphthalimide-anthracene triad (**15**). In contrast to the synthesis of electron-deficient cores, such as perylene, a two-step ring closure is required for the anthracene-based derivative due to the greater electron density and corresponding lower acidity of the aromatic protons.⁸⁴ The first ring closure was accomplished using traditional Lewis-acid chemistry with iron(III) chloride to give

the partially closed derivative, **16**, which was used directly for the second ring-closing step. Employing different conditions (K_2CO_3 in ethanolamine or triethanolamine) then gives the final rylene product (**17**). The dual ring closures result in a dramatic bathochromic shift in absorption (370 nm) upon going from the precursor **15** to rylene **17** (Figure 4.4b), with the distinct change in color from yellow (**15**) to green-blue (**17**) indicative of successful ring closing. Additionally, UV-Vis absorption spectroscopy reveals an absorption maximum in the near infrared region ($\lambda_{max} = 723$ nm) for **17**. This absorption shows a narrow bandgap between those of terylene diimide and quatterylene diimide derivatives, demonstrating the ability to significantly tune the electronic structure through the introduction of a π -extended core.⁸⁵

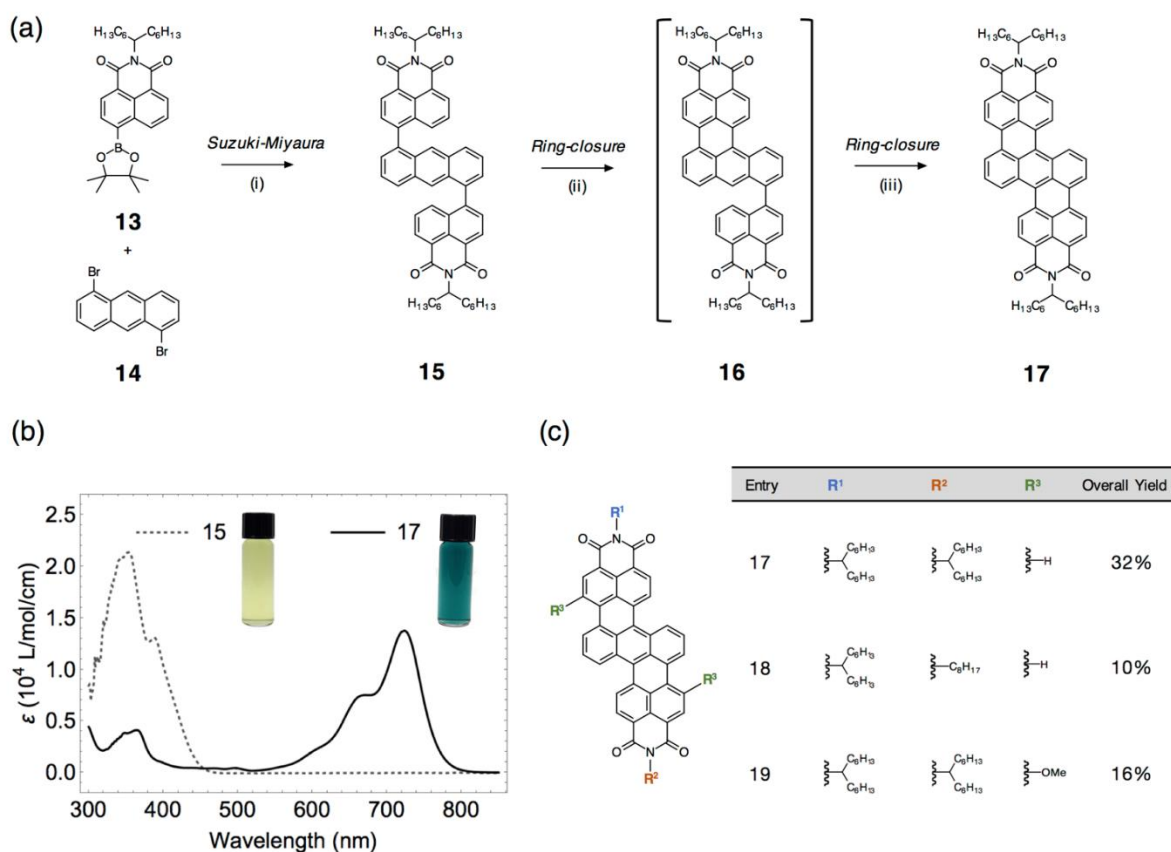


Figure 4.4 Core-extended rylenes, synthesis, and absorption. (a) Representative synthesis of **17**; (i) K_2CO_3 (aq), $Pd(PPh_3)_4$, toluene, 100 °C, 12 h, 68%; (ii) $FeCl_3$, nitromethane, DCM, 55°C, 24 h; (iii) K_2CO_3 , ethanolamine, 130 °C, 16 h, 56%. (b) Absorption spectra of **15** and **17** (100 μM in dichloromethane) and corresponding images

of solutions in vials (5 mM in dichloromethane) (c) Summary of core-extended rylene derivatives (**18–20**) synthesized with varying imide and bay substituents.

The synthesis of asymmetric extended-core rylenes was achieved in a similar fashion to that described in Figure 4.4a, however using a stepwise Suzuki–Miyaura coupling. In short, coupling compounds **13** with **14** in a 1:1 molar ratio produces a diad (**S1**), which is subsequently coupled with the borylated derivative of naphthalimide **2** to yield an asymmetric triad (**S2**) (chemical structures given in Scheme 4.2, Supplemental Results). Cyclodehydrogenative ring closing of the triad provides an asymmetric extended rylene derivative (**18**), highlighting the ability to incorporate different side chains at the imide positions for classes of larger rylenes beyond PDIs using this methodology. Moreover, the electronic properties of the higher-order rylene can be tuned with core substitutions, which was demonstrated for methoxy-substituted rylene **19**, synthesized in an analogous fashion to **17**. As observed for PDIs, methoxy substitution of extended rylenes in the bay position led to a bathochromic shift (≈ 20 nm) in absorption, which corresponds with a noticeable color change in solution, going from **17** (blue-green) to **19** (green) (Figure 4.7, Supplemental Results). Additionally, CV showed a similar increase in reduction potentials from -0.67 and -0.86 V to -0.79 and -0.96 V for **17** and **19** respectively (Figure 4.8, Supplemental Results). The asymmetric and bay-substituted core-extended rylenes showcase the modularity of this approach.

2.4 Conclusions

In summary, we have developed a strategy for the facile synthesis of asymmetric PDIs that takes advantage of modular naphthalimide units to provide increased versatility, greater atom

efficiency, and simpler purification. Using cross-coupling and base-catalyzed ring-closing, asymmetric PDIs and extended rylene derivatives can be prepared in high yields with a variety of substituents in both the imide and bay positions. This methodology provides an efficient avenue towards a wide range of novel, tunable, and functional rylene structures for utility in electronic materials applications.

2.5 Experimental

2.5.1 Materials

All reagents were purchased from Sigma Aldrich and used without further purification unless otherwise specified. 4-Bromo-1,8-naphthalic anhydride (98%) was purchased from AK Scientific and used as received. 1,5-Dibromoanthracene (97%) and 3-hydroxy-1,8-naphthalic anhydride (98%) were purchased from Spectrum Chemical and used as received. Lithium aluminum hydride (97%) and all solvents were purchased from Fisher Scientific and used as received. Aminohexanoic acid *tert*-butyl ester, 6-hexeneamine, and tridecan-7-amine were prepared according to literature procedures⁸⁶⁻⁸⁸.

2.5.2 Methods

Nuclear magnetic resonance (NMR) spectra acquired using 500 or 600 MHz spectrometers. Chemical shifts (δ) are reported in parts per million (ppm) and were measured relative to the signals for residual chloroform, dimethyl sulfoxide, or 1,1,2,2-tetrachloroethane in deuterated solvents. Mass spectrometry measurements were performed courtesy of James Pavolovich in the Mass Spectroscopy Facility at the University of California, Santa Barbara. Measurements were performed using a quadrupole/time-of-flight tandem mass spectrometer (EDI) or a time-

of-flight spectrometer (EI and FD). UV-visible spectroscopy measurements were recorded using a Shimadzu UV-3600 spectrophotometer at room temperature. Samples were tested in concentrations of ≈ 0.1 mg/mL in dichloromethane using 2 mm quartz cuvettes. Cyclic voltammetry measurements were carried out using a Bio-Logic VMP3 Potentiostat in a standard three-electrode configuration. Experiments were run in anhydrous tetrahydrofuran with 0.1 M tetrabutylammonium hexafluorophosphate (TBAF) and ≈ 0.5 mg/mL concentration of sample. After THE solution was sparged with N_2 , samples were scanned at a rate of 200 mV/s. Ferrocene was then added and the onset potentials of Fc/Fc^+ measured.

2.5.3 Synthesis

Representative Imidization

N-(2-ethylhexyl)-4-bromo-1,8-naphthalimide (**3**). A mixture of 4-bromo-1,8-naphthalic anhydride (5 g, 18.1 mmol), 2-ethyl-1-hexylamine (2.78 g, 21.7 mmol), and ethanol (100 mL) was heated at reflux under an argon atmosphere for 4 h. The solvent was then removed in vacuo and the resulting solid purified via silica gel column chromatography (eluted in 1% MeOH/DCM) to produce the product as a beige solid (5.96 g, 85%). $R_f = 0.41$ (1% MeOH/DCM); 1H NMR (500 MHz, $CDCl_3$) δ 8.66 (dd, $J = 7.3, 1.1$ Hz, 1H), 8.57 (dd, $J = 8.5, 1.1$ Hz, 1H), 8.42 (d, $J = 7.9$ Hz, 1H), 8.04 (d, $J = 7.9$ Hz, 1H), 7.85 (dd, $J = 8.5, 7.3$ Hz, 1H), 4.11 (qd, $J = 12.9, 7.3$ Hz, 2H), 1.93 (h, $J = 6.5$ Hz, 1H), 1.45 – 1.24 (m, 8H), , 0.93 (t, $J = 7.4$ Hz, 3H), 0.87 (t, $J =$ Hz, 3H) ppm; ^{13}C NMR (126 MHz, $CDCl_3$) δ 163.57, 163.55, 133.2, 132.0, 131.2, 130.6, 130.1, 129.0, 128.0, 123.2, 122.3, 40.6, 31.8, 29.3, 29.2, 28.9, 28.1, 27.1, 22.6, 14.1 ppm; HRMS (ESI-TOF) m/z : $[M + Na]^+$ Calcd for $C_{20}H_{22}BrNO_2Na$ 410.0732; Found, 410.0732.

Representative Miyaura Borylation

N-(2-ethylhexyl)-4-(4,4,5,5-tetramethyl-1,3,2-dioxaborolan-2-yl)-1,8-naphthalimide (**4**). Anhydrous *p*-dioxane (20 mL) was added to Schlenk flask under argon. *N*-(2-ethylhexyl)-4-bromo-1,8-naphthalimide (**3**, 0.33 g, 0.86 mmol), Pd(dppf)Cl₂ (54 mg, 0.07 mmol), and bis(pinacolato)diboron (325 mg, 1.28 mmol) were added to flask, followed by anhydrous potassium acetate (250 mg, 2.55 mmol). The mixture was refluxed at 100 °C for 24 hours, at which point the reaction mixture was cooled to room temperature and filtered to remove the potassium acetate. The solution was then dried *in vacuo*, and due to the instability of the product on silica gel, the resulting crude mixture used directly for the subsequent reaction.

Representative Suzuki Coupling

N-(octyl)-*N'*-(2-ethylhexyl)-4,4'-binaphthyl-1,1',8,8'-teracarboxylic diimide (**5**). The crude mixture containing *N*-(2-ethylhexyl)-4-(4,4,5,5-tetramethyl-1,3,2-dioxaborolan-2-yl)-1,8-naphthalimide (**4**) was re-dissolved into toluene (10 mL) and added to round bottom flask under argon atmosphere. *N*-(octyl)-4-bromo-1,8-naphthalimide (**2**) (334 mg, 0.86 mmol), Pd(PPh₃)₄ (32 mg, 0.03 mmol), and aqueous solution of K₂CO₃ (11 mL, 1M) were then added. The reaction mixture was refluxed at 100 °C for 12 hours and then concentrated on the rotary evaporator. The mixture was re-dissolved in dichloromethane and washed with water (3 × 20 mL). The organic layer was dried over anhydrous sodium sulfate and solvent removed under vacuum. The resulting mixture was purified using silica gel column chromatography (eluted in 6% MeOH/DCM) to give product as pale brown solid (472 mg, 67%). *R*_f = 0.37 (6% MeOH/DCM). ¹H NMR (500 MHz, CDCl₃) δ 8.74 (dd, *J* = 7.4, 1.1 Hz, 2H), 8.64 (dt, *J* = 7.1, 1.1 Hz, 2H), 7.79 (dd, *J* = 7.5, 1.8 Hz, 2H), 7.69 (ddd, *J* = 8.5, 6.4, 1.2 Hz, 2H), 7.60 (dd, *J* = 8.5, 7.2 Hz, 2H), 4.26 – 4.10 (m, 4H), 1.99 (p, *J* = 6.4 Hz, 1H), 1.82 – 1.72 (m, 2H), 1.51 –

1.22 (m, 19H), 0.95 (t, $J = 7.4$ Hz, 3H), 0.88 (q, $J = 7.0$ Hz, 5H) ppm; ^{13}C NMR (126 MHz, CDCl_3) δ 164.4, 164.2, 164.0, 163.8, 142.79, 142.75, 132.0, 131.9, 131.6, 131.5, 130.79, 130.78, 130.52, 130.46, 128.80, 128.76, 128.42, 128.39, 127.48, 127.46, 123.3, 123.2, 123.2, 123.1, 44.3, 40.7, 38.0, 31.8, 30.8, 29.3, 29.2, 28.7, 28.2, 27.2, 24.1, 23.1, 22.6, 14.10, 14.08, 10.7 ppm; HRMS (ESI-TOF) m/z : $[\text{M} + \text{Na}]^+$ Calcd for $\text{C}_{40}\text{H}_{44}\text{N}_2\text{O}_4\text{Na}$ 639.3181; Found, 639.3181.

Representative Cyclodehydrogenation

N-(octyl)-*N'*-(2-ethylhexyl)-3,4,9,10-perylene diimide (**6**). *N*-(octyl)-*N'*-(2-ethylhexyl)-4,4'-binaphthyl-1,1',8,8'-teracarboxylic diimide (**5**, 100 mg, 0.16 mmol) was dispersed in triethanolamine (8 mL) and K_2CO_3 (562 mg, 4.07 mmol) was added. The mixture was stirred at 130 °C for 24 hours under argon atmosphere. Upon cooling to room temperature, the reaction mixture was diluted with dichloromethane and washed with water (3×20 mL). The organic layer was dried over anhydrous sodium sulfate and purified by silica gel column chromatography (eluted in 2% MeOH/DCM) to yield product as dark red solid (89 mg, 89%). $R_f = 0.43$ (2% MeOH/DCM). ^1H NMR (500 MHz, CDCl_3) δ 8.65 (dd, $J = 8.0, 2.2$ Hz, 4H), 8.57 (d, $J = 8.1$ Hz, 4H), 4.23 – 4.09 (m, 4H), 1.96 (p, $J = 6.4$ Hz, 1H), 1.81 – 1.70 (m, 2H), 1.50 – 1.22 (m, 19H), 0.95 (t, $J = 7.4$ Hz, 3H), 0.88 (q, $J = 7.0$ Hz, 5H) ppm; ^{13}C NMR (126 MHz, CDCl_3) δ 190.36, 163.55, 163.16, 134.26, 134.23, 131.20, 131.13, 129.15, 126.13, 123.23, 123.21, 122.88, 122.85, 77.24, 76.99, 76.73, 44.33, 40.70, 37.97, 31.83, 30.78, 29.33, 29.23, 28.71, 28.10, 27.18, 24.09, 23.07, 22.64, 14.09, 14.08, 10.63 ppm; MS (FD): $[\text{M}]^+$ Calcd for $\text{C}_{40}\text{H}_{42}\text{N}_2\text{O}_4$ 614.31; Found, 614.29.

2.6 Supplemental Results

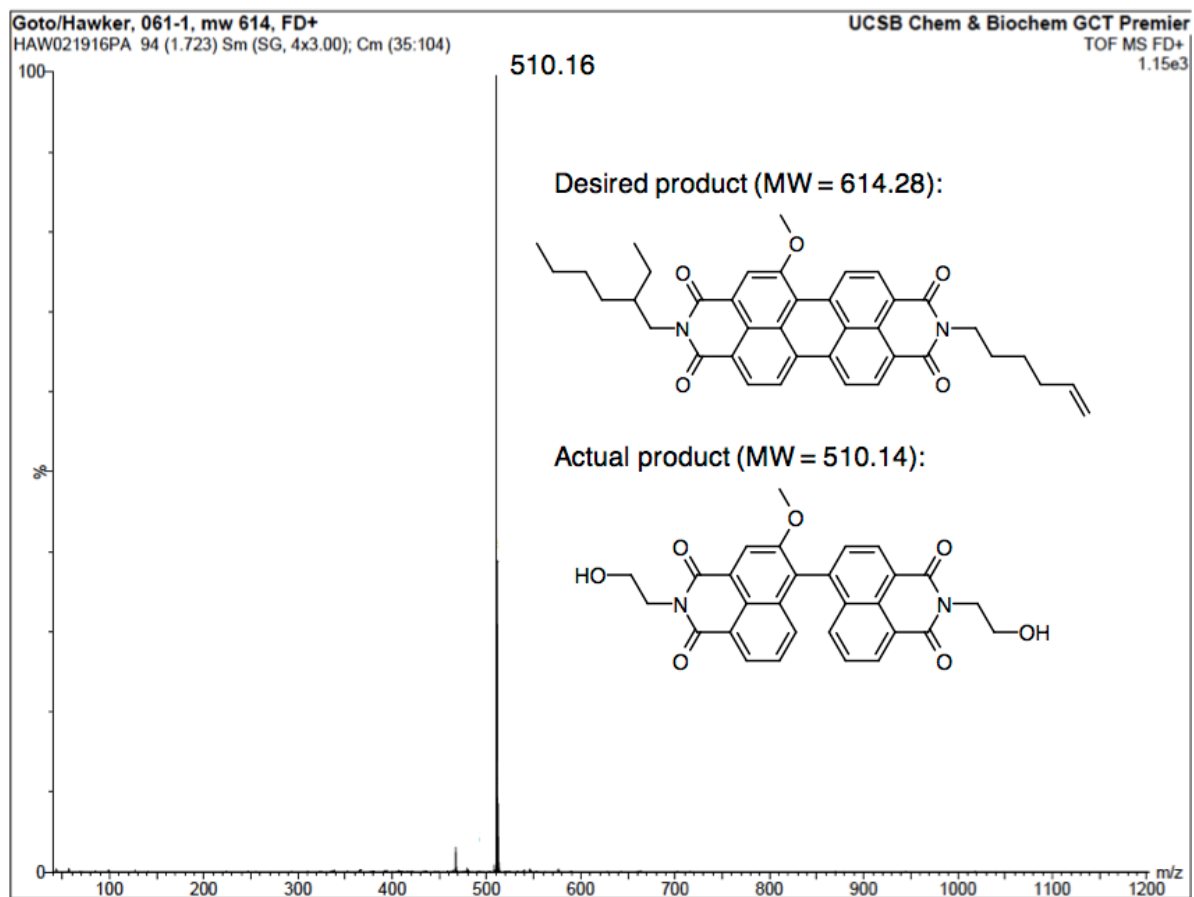


Figure 4.5 Mass spectrum showing the result of an ethanolamine-based cyclodehydrogenation to target bay-substituted PDI 12. The non-ring closed transimidated product was found.

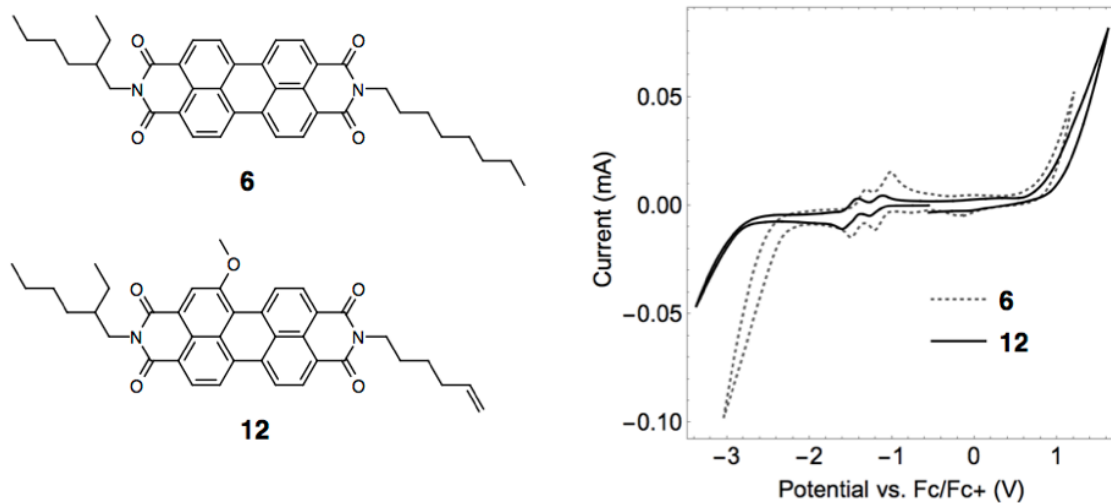
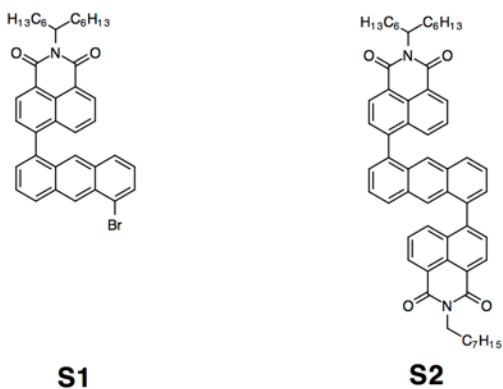


Figure 4.6 Cyclic voltammetry (200 mV/s against Fc/Fc⁺) of PDIs **6** and **12**.



Scheme 4.2 Chemical structures of mono-substituted naphthalimide-anthracene diad (**S1**) and asymmetrically substituted triad (**S2**).

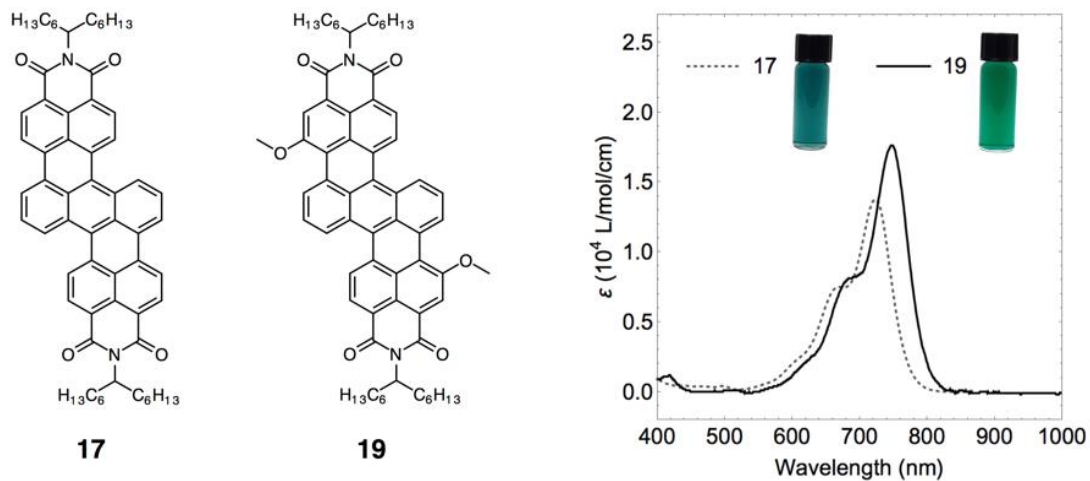


Figure 4.7 Absorption spectra (100 μM in dichloromethane) and corresponding images of **17** and **19** (5 mM in dichloromethane).

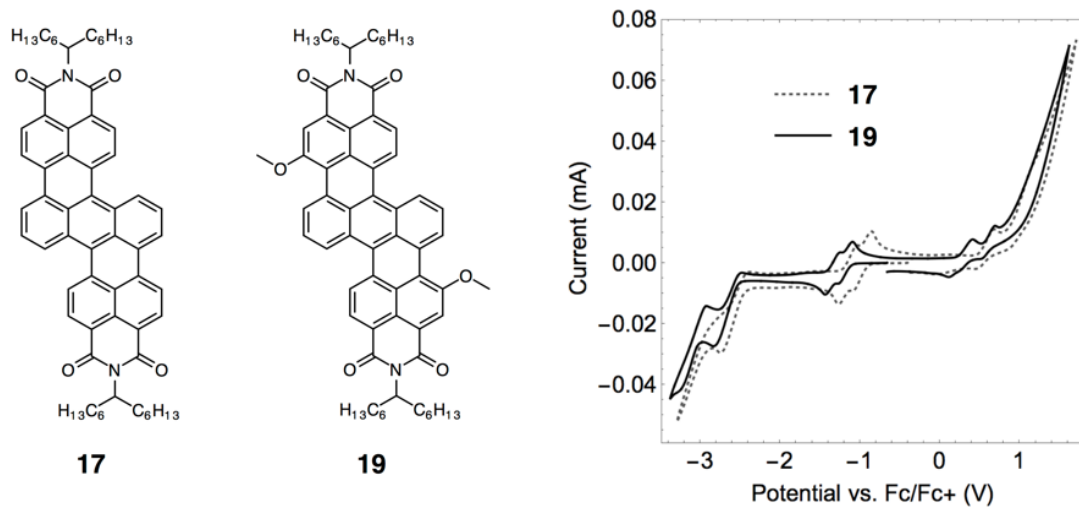


Figure 4.8 Cyclic voltammetry (200 mV/s against Fc/Fc^+) of extended rylene **17** and **19**.

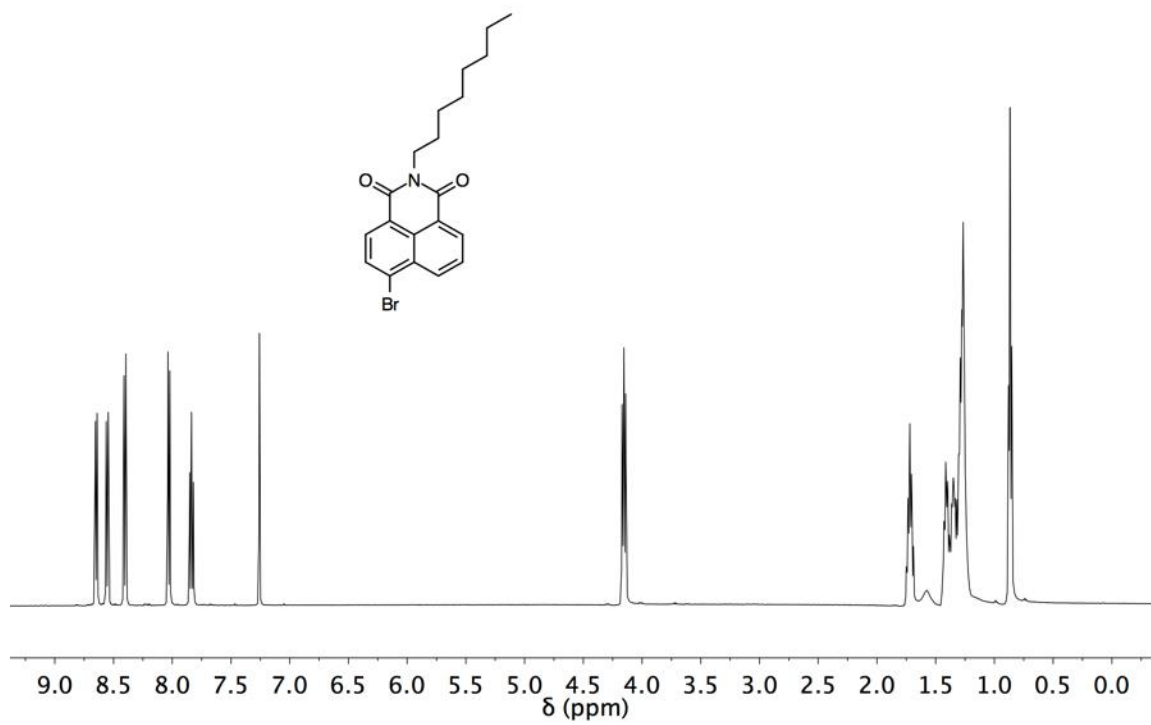


Figure 4.9 ^1H NMR spectra of compound 2 in CDCl_3 .

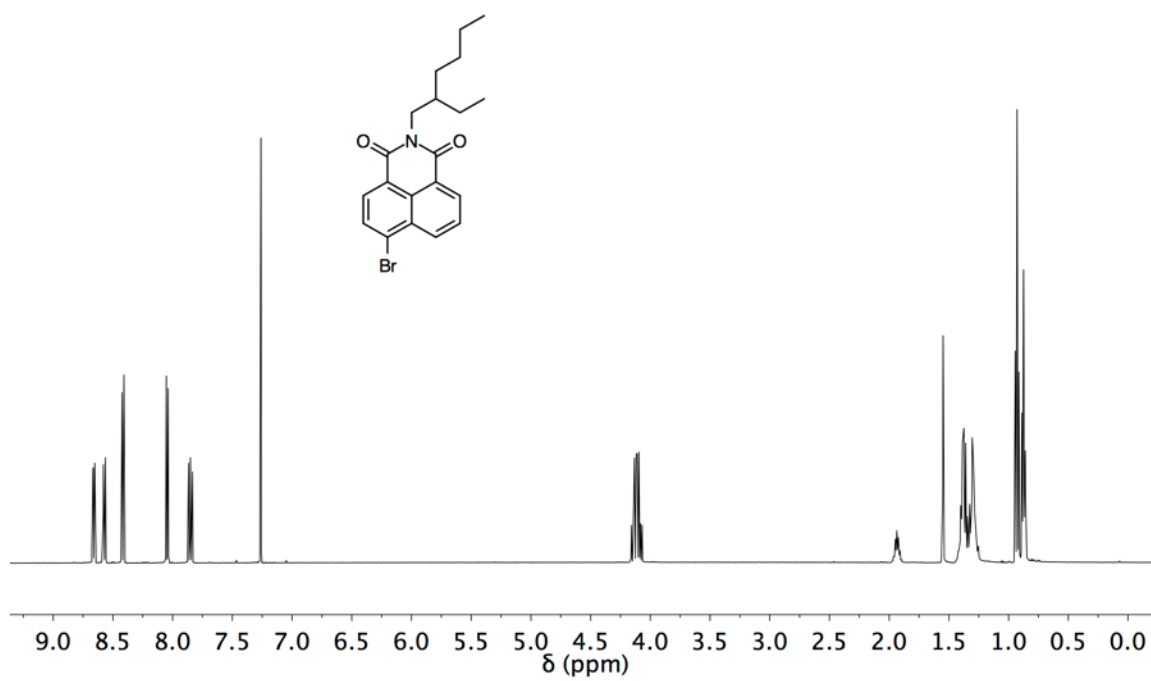


Figure 4.10 ^1H NMR spectra of compound 3 in CDCl_3 .

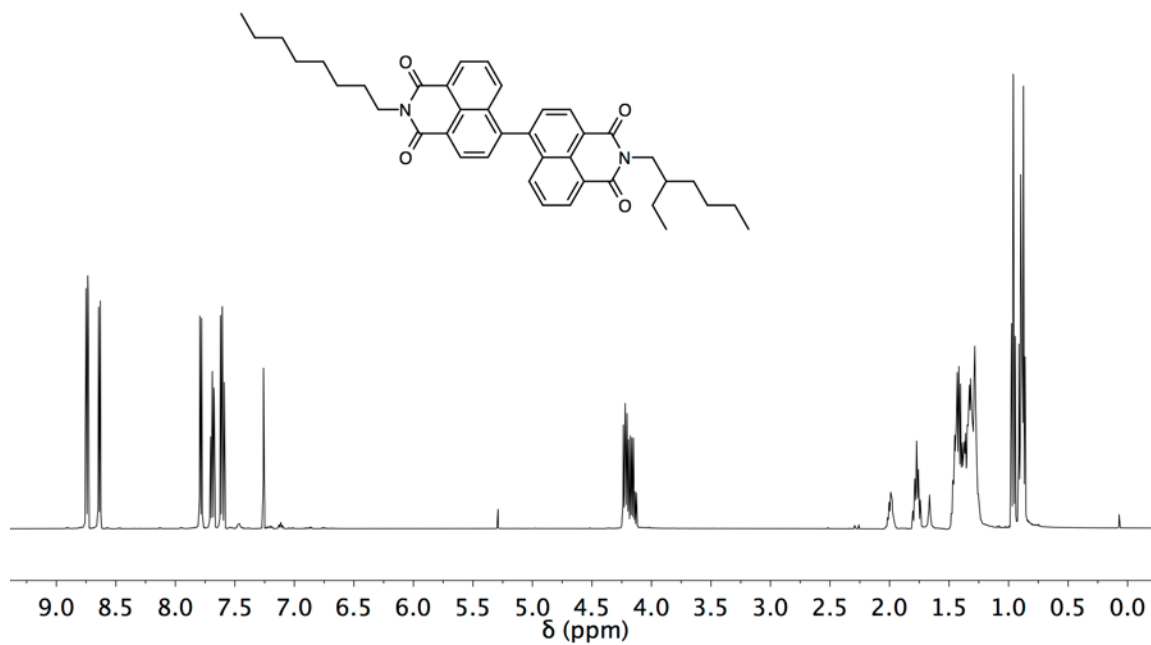


Figure 4.11 ¹H NMR spectra of compound **5** in CDCl₃.

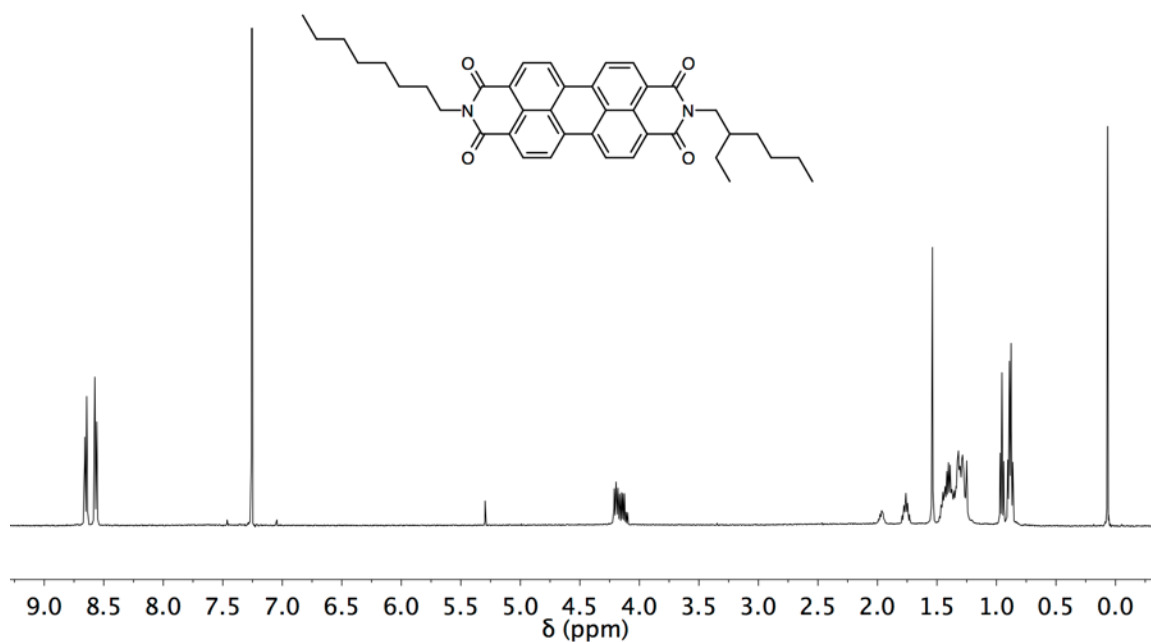


Figure 4.12 ¹H NMR spectra of compound **6** in CDCl₃.

Chapter 5

Poly(Silyl Ethers) via Borane-Catalyzed Hydrosilylation

Reprinted with permission from Sample, C. S.; Lee, S.-H.; Bates, M. W.; Ren, J. M.; Lawrence, J.; Lensch, V.; Gerbec, A.; Bates, C. M.; Li, S.; Hawker, C. J. Metal-Free Synthesis of Poly(Silyl Ether)s under Ambient Conditions. *Macromolecules* **2019**, *52*, 1993–1999.
Copyright 2019 American Chemical Society.

3.1 Abstract

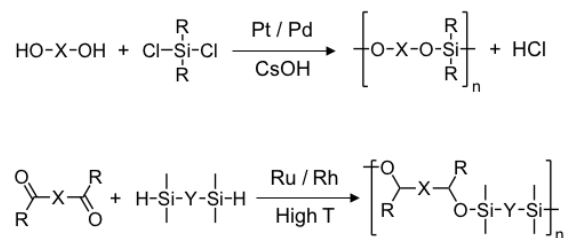
Metal-free hydrosilylation using tris(pentafluorophenyl)borane ($\text{B}(\text{C}_6\text{F}_5)_3$) as a catalyst enables the rapid polymerization of α -diketone and bis(silane) monomers under ambient conditions to give high molecular weight poly(silyl ethers) (PSEs). A wide selection of commercially available monomers bearing different backbone and side-chain functional groups are shown to be compatible with these metal-free conditions. Significantly, the thermal properties of these PSEs are highly tunable, with novel semi-crystalline materials being

obtained in a variety of cases. These PSE materials serve as a versatile platform for materials with designed degradation profiles and crystallinity.

3.2 Introduction

Poly(silyl ethers) (PSEs) are high-performance materials that, similar to poly(siloxane)s, exhibit exceptional low-temperature flexibility coupled with enhanced thermal stability. These features have led to their broad implementation as elastomers, gas-permeable membranes, and biocompatible coatings.^{20,89,90} In addition, the labile silyl ether (Si–O–C) linkages of PSEs provide susceptibility to acid-catalyzed hydrolysis, suggesting a new design motif for triggered degradation in biomedical or environmental applications^{91,92} that is particularly appealing due to increased interest in degradable materials for commodity applications.⁹³

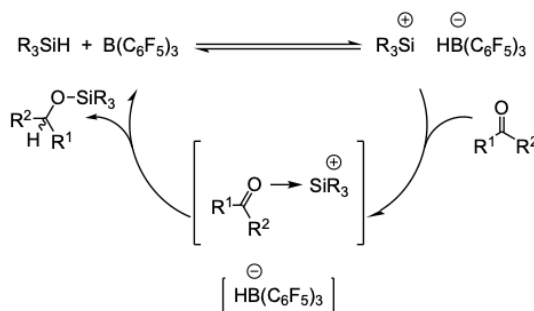
During the past decades, several strategies have been developed for the synthesis of PSEs.^{31,91,94} One commonly used approach is the condensation polymerization of diols with dihydrosilanes, dialkoxysilanes, diaminosilanes, or dihalosilanes (Scheme 5.1).⁹⁵ While high molecular weight materials are obtained, the poor atom economy⁹⁶ and production of hydrogen gas, alcohols, amines, or HX as byproducts is undesirable. Addition polymerization of cyclic ethers with dichlorosilanes or dimethyldiphenoxysilane monomers has also been demonstrated; however the range of readily available starting materials is limited leading to a lack of viable synthetic strategies.^{97–99}



Scheme 5.1 Traditional synthetic strategies for poly(silyl ethers) (PSEs), including the polycondensation of diols and difunctional silanes or transition-metal catalyzed hydrosilylation.

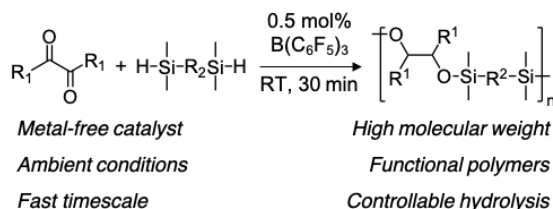
In addressing these challenges, our attention was directed towards hydrosilylation reactions involving the addition of silicon hydrides across unsaturated bonds as an attractive approach towards novel poly(silyl ethers).^{100–103} Pioneering work by Weber illustrated that poly(silyl ethers) can be prepared by hydrosilylation coupling catalyzed by transition metal complexes, including ruthenium and rhodium;^{25,27,28,30,104,105} however the reported processes suffer from harsh reaction conditions and side reactions, as well as the high cost/low abundance of Ru/Rh catalysts (Scheme 5.1). Due to these drawbacks and an increasing interest in mild, metal-free methods for the synthesis of functional polymers,¹⁰⁶ we examined the hydrosilylation of carbonyl groups catalyzed by tris(pentafluorophenyl)borane ($\text{B}(\text{C}_6\text{F}_5)_3$) in detail. Seminal work by Piers and co-workers^{33,34,107–112} has shown that $\text{B}(\text{C}_6\text{F}_5)_3$ is a water-tolerant catalyst that can be widely used in a variety of hydrosilylation coupling reactions under mild conditions.^{108–112} Unlike transition-metal catalysts that trigger the reaction by an oxidative insertion into the Si–H bond, the electron-deficient tris(pentafluorophenyl)borane ($\text{B}(\text{C}_6\text{F}_5)_3$) Lewis acid activates the Si–H bond via η -coordination leading to its addition across unsaturated groups (Scheme 5.2). Importantly, the hydrosilylation of the C=O unit in ketones, aldehydes, and esters^{113–116} occurs in high yields with low catalyst loadings. This allows for $\text{B}(\text{C}_6\text{F}_5)_3$ to be used in the

synthesis of complex structures such as functionalized carbon nanotubes,¹¹⁷ as well as for the polycondensation of dihydrosilanes with dialkoxysilanes to form polycarbosiloxanes.¹¹⁸



Scheme 5.2 Mechanism of the $B(C_6F_5)_3$ -catalyzed hydrosilylation of ketones.

Inspired by the efficiency and functional group tolerance of $B(C_6F_5)_3$, we report the synthesis of a tunable library of poly(silyl ethers) from readily available starting materials. Specifically, we demonstrate a highly efficient, scalable, and metal-free hydrosilylation polymerization using α -diketone and bis(silane) monomers (Scheme 5.3). These polymers are conveniently prepared in a single step under ambient reaction conditions using low $B(C_6F_5)_3$ loadings and short reaction times. The resultant functional polymers exhibit high structural regularity and novel thermal and semi-crystalline behavior.



Scheme 5.3 Synthetic strategy for poly(silyl ether)s (PSEs) using borane catalyzed metal-free hydrosilylation addition polymerization.

3.3 Results and Discussion

3.3.1 Small-Molecule Model Reaction

The elegant studies of Rosenberg *et al.* on borane-catalyzed hydrosilylation of both carbonyl and thiocarbonyl compounds coupled with our own investigations on $B(C_6F_5)_3$ -catalyzed side chain functionalization,^{119,120} prompted a series of small-molecule studies to define the reaction scope/optimized conditions. The reaction of benzil (α -diketone) and dimethylphenylsilane (disilane) was identified as a model small-molecule system with initial studies under ambient conditions showing that quantitative and highly efficient hydrosilylation of the α -diketone could be achieved within 30 min using only 1 mol % of the $B(C_6F_5)_3$ catalyst (Scheme 5.4). Significantly, this allows the stable silyl ether, **1**, to be produced on gram-scale from readily available starting materials with 1H NMR spectroscopy indicating the presence of *meso* and *dl* diastereomers, discernable by the distinct resonances located at 4.55 and 4.71 ppm, as well as 0.07 and 0.19 ppm, attributed to the $CH-Si-O$ and the CH_3 groups of the respective bis-silyl ether isomers (Figure 5.1). The major isomer, (4*R*,5*S*)-2,7-dimethyl-2,4,5,7-tetraphenyl-3,6-dioxo-2,7-disila-octane (ca. 80 mol %), was shown to be the *meso*-diastereomer by single-crystal X-ray diffraction with clear melting and crystallization transitions ($T_m = 90$ °C, $T_c = 30$ °C) being observed by DSC.



Scheme 5.4 Model reaction of benzil and dimethylphenylsilane.

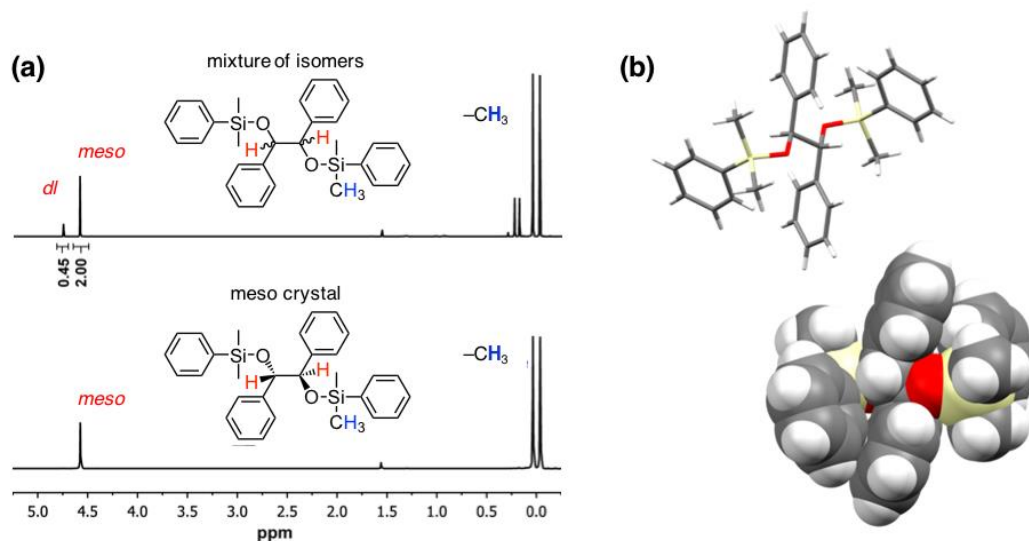


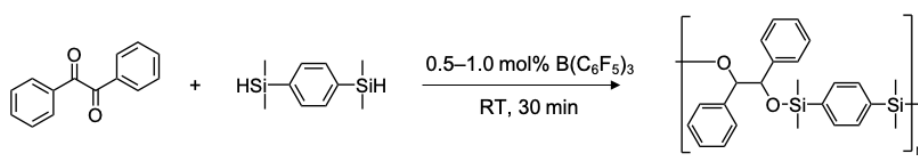
Figure 5.1 (a) ^1H NMR spectra of the diastereomer mixture of **1** (top) and the crystallized *meso*-product ((4*R*,5*S*)-2,7-dimethyl-2,4,5,7-tetraphenyl-3,6-dioxo-2,7-disilaoctane) (bottom) obtained from the model hydrosilylation reaction between benzil and dimethylphenylsilane. (b) Crystal structure of *meso*-product; the methyl and phenyl groups provide steric protection for the labile Si–O bonds.

3.3.2 Polymerization Conditions

Based on the efficiency of this metal-free hydrosilylation, we subsequently studied the reaction between benzil and 1,4-bis(dimethylsilyl)benzene as a model step-growth polymerization system with benzil acting as an A_2 monomer (Table 5.1). Significantly, low $\text{B}(\text{C}_6\text{F}_5)_3$ catalyst loading (0.5 mol %) and equimolar conditions in toluene gave the desired poly(silyl ether) as a high molecular weight product ($M_n = 55$ kDa; $D = M_w/M_n = 1.8$, entry **1b**) in $> 80\%$ yield. Varying the solvent from toluene to chloroform resulted in similar reactivity, however no polymerization was observed in either THF or NMP, presumably due to deactivation of the catalyst. Decreasing the catalyst loading to 0.25 and 0.1 mol % results in lower molecular weights, as did off-stoichiometric loading of the monomers, fully consistent with a step-growth polymerization. Interestingly, in all polymerizations a well-defined, low molecular weight component ($\approx 15\%$ yield) was observed by SEC which could be easily

purified by selective precipitation of the polymer in cold hexanes or methanol. In agreement with the step-growth process, this was identified as the cyclic dimer, which was fully characterized by NMR and mass spectrometry with the macrocyclic structure being confirmed by single crystal XRD (Figure 5.2). The formation of this cyclic byproduct could possibly be suppressed by increasing the concentration of the reaction mixture to favor intermolecular polymerization over cyclization.

Table 5.1 Optimization of the $B(C_6F_5)_3$ -catalyzed hydrosilylation polymerization.



Entry ^a	BDMSB ^b [equiv]	Solvent	Cat. [mol %]	Isolated Yield (%)	M_n^c	M_w^c	\bar{D}^c
1a	1.0	$CHCl_3$	0.5	80	26	47	1.8
1b	1.0	Toluene	0.5	80	55	98	1.8
1c	1.0	THF	0.5	0	—	—	—
1d	1.0	NMP	0.5	0	—	—	—
1e	1.0	Toluene	0.1	60	3	6	1.8
1f	1.0	Toluene	0.25	80	14	28	2.1
1g	1.0	Toluene	1.0	80	46	84	1.8
1h	0.9	Toluene	0.5	80	15	31	1.8
1i	1.1	Toluene	0.5	80	14	29	2.0

^aPolymerization conditions: benzil (1.00 mmol), 1,4-bis(dimethylsilyl)benzene, and $B(C_6F_5)_3$ in 1.0 mL of solvent. ^b1,4-bis(dimethylsilyl)benzene ^cDetermined by size-exclusion chromatography (SEC) calibrated with polystyrene standards in chloroform. Molar masses are reported in $kg\ mol^{-1}$.

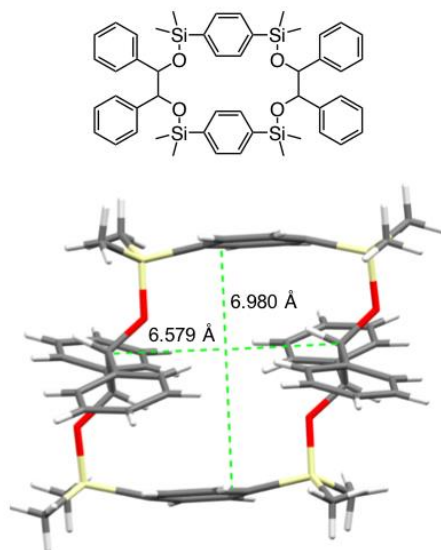


Figure 5.2 Structure and single crystal diffraction of the [2+2] cyclic product.

Characterization of the poly(silyl ether) derived from benzil and 1,4-bis(dimethylsilyl)benzene reveals a number of interesting features. As anticipated from the small-molecule model studies, hydrosilylation proceeds in a stereoselective manner resulting in a chiral backbone with $\approx 70\%$ *meso*- and $\approx 30\%$ *dl*-configuration, which is clearly shown in the relative integration of the ^1H NMR resonances at 4.55 and 4.71 ppm (Table 5.1, Entry **1b**, $M_n = 55$ kDa; Figure 5.3a). In addition, the structural regularity of the polymer is supported by well-resolved and sharp peaks in the ^{13}C and ^{29}Si NMR spectra, again a $\approx 7:3$ ratio is observed for the carbon signals of the $\text{Si}(\text{CH}_3)_2$ units and the backbone silicon atom displayed a set of two narrow ($\text{Dn}_{1/2} < 10$ Hz) resonances at 7.7 ppm (Figure 5.3b,c). As will be discussed in detail below, the thermal properties of this aromatic poly(silyl ether) are of particular interest and suggest that borane catalyzed hydrosilylation of diketones and bis(silanes) is a viable platform for stereochemically enriched backbone polymers based on readily available starting materials, opening up new application areas for poly(silyl ethers).

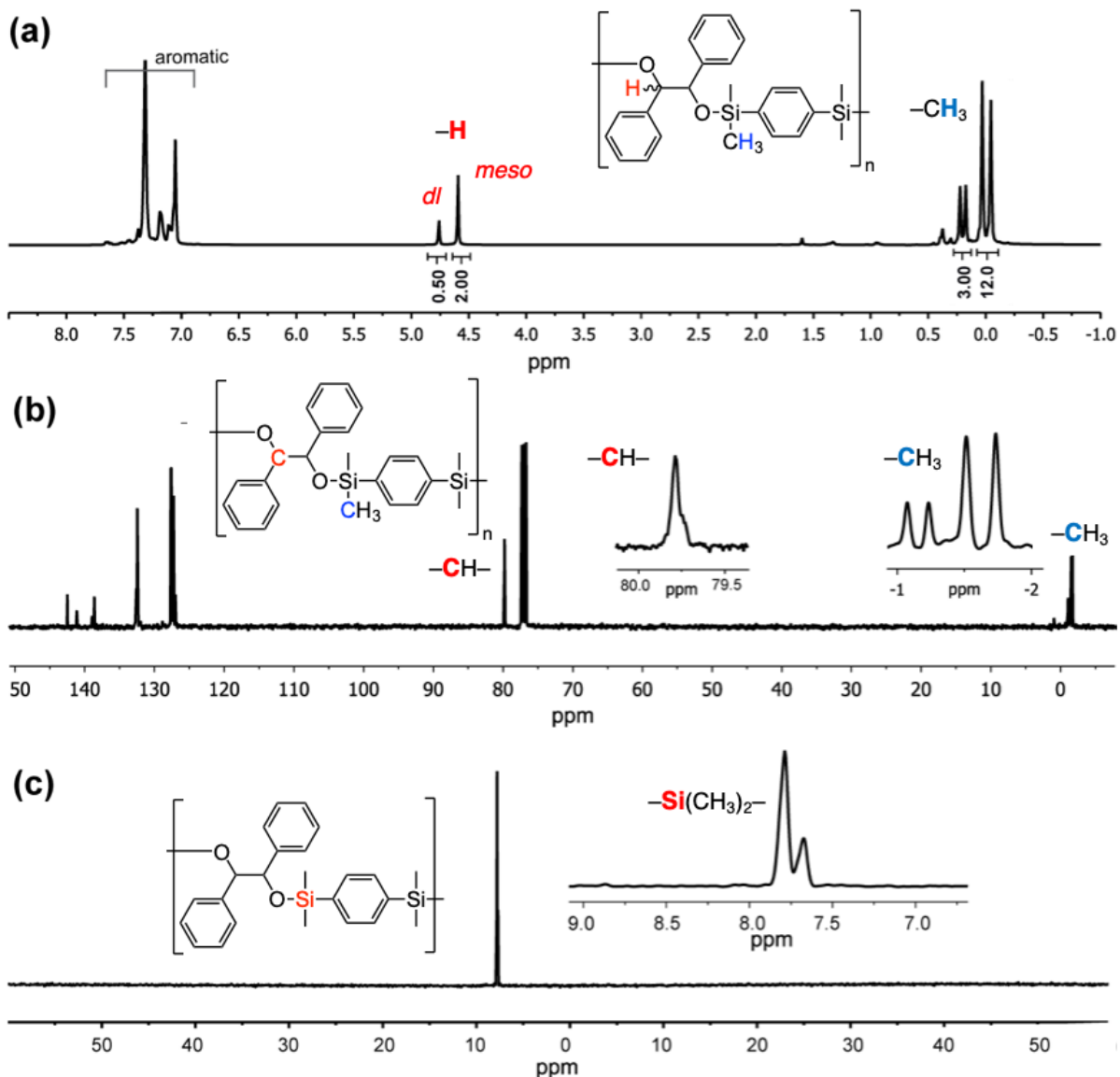


Figure 5.3 (a) ¹H, (b) ¹³C, and (c) ²⁹Si NMR spectra of model poly(silyl ether) in CDCl₃. The sharp and well-resolved peaks in (a)–(c) indicate high structural regularity of this novel PSE.

3.3.3 Expansion of Monomer Scope

The scope and functional group tolerance of this metal-free polymerization process was then investigated using a series of readily available α -diketone and bis(silane) derivatives under standard conditions (Table 5.1, Entry **1b**). Variation in the α -diketone structure was explored

by employing 1,4-bis(dimethylsilyl)benzene as a common comonomer with substitution on the benzil unit as well as exchange of the aromatic units for aliphatic groups (Table 5.2, polymers **2a–2h**). Changing the substituents from hydrogen to halogen at the benzil *para*-position did not impact polymerization efficiency, with high degrees of polymerization being produced in all cases (polymer **2a–2c**). Polymerization was also successful with cyclic, “tied-back” analogues of benzil, notably 9,10-phenanthrenequinone and acenaphthenequinone. The high reactivity of these systems shows that conjugation and steric rigidity in the monomer units does not inhibit the polyhydrosilylation reaction, although the poor solubility of the latter reduces the efficacy of polymerization. One of the attractive features of this polymerization process is the ready availability of diketones, as exemplified by the aliphatic systems that are widely used as flavoring and fragrance agents. For example, butane-2,3-dione is added to food to impart a buttery flavor, while hexane-3,4-dione is found in a variety of foods. Exchange of benzil with either butane-2,3-dione or hexane-3,4-dione was shown to also lead to the generation of high molecular weight polymers, with the aliphatic repeat units imparting increased solubility when compared to the benzil-derived materials.

Table 5.2 Preparation of PSEs from α -diketones and disilanes.

Polymer ^a	R ¹	R ²	M_n^b	\bar{D}^b	[<i>meso</i>]:[<i>dl</i>] ^c	T_g^d (°C)	T_{d5}^e (°C)
2a			55.0	1.8	70:30	40 (T_m 175)	415
2b			40.0	2.0	70:30	50 (T_m 160)	380
2c			48.2	1.8	70:30	80 (T_m 120)	380
2d			14.1	2.1	60:40	-2	195
2e			20.7	1.7	50:50	70	335
2f			8.0	1.5	–	30	285
2g			30.3	1.7	70:30	-30	250
2h			27.3	2.7	70:30	-25 (T_m 120)	310
2i			2.6	1.2	–	-20 (T_m 65)	310
2j			7.0	1.5	–	-15 (T_m 95)	330
2k ^g			12.3	2.2	85:14	–	340

^aPolymerization conditions: 1 M of each monomer with 0.5 mol % B(C₆F₅)₃ in toluene. ^b M_n determined by size exclusion chromatography (SEC) calibrated with polystyrene standards in chloroform. Molar masses are in kg mol⁻¹. ^cRatio of [*meso*]:[*dl*] determined by ¹H NMR. ^dMelting and glass transition temperatures (T_m and T_g , respectively) were measured via differential scanning calorimetry (DSC). ^eThermal decomposition temperatures (T_{d5}) were measured by thermogravimetric analysis (TGA) and indicate the temperature at 5% mass-loss under nitrogen. ^fPolymerization run in chloroform instead of toluene due to poor solubility of acenaphthenequinone. ^gMolar mass of siloxane linker, $M_n = 500$ g mol⁻¹.

Substitutions of the bis(silane) monomer were then examined using benzil as a common comonomer. In these systems, high conversions were observed, but the resulting molecular weights were lower when compared to the phenylene-bridged bis(silane) monomer. For the ethylene-bridged and oxo-bis(silane) derivatives, polystyrene-equivalent molecular weights

were less than 10,000 g/mol with hydrogen terminated polydimethylsiloxane macromonomers affording oligomers (Table 5.2, polymers **2i–k**). If the mechanism of the $B(C_6F_5)_3$ -mediated α -diketone hydrosilylation reaction is considered (see Scheme 5.2), it is postulated that stabilization of the β -silylium intermediate is critical for attaining high degrees of polymerization with aryl-bridged silanes offering higher reactivity as well as improved sterics for formation of the silylium cation, therefore resulting in higher molar mass materials.

3.3.4 Physical and Thermal Properties

The synthetic versatility inherent in these metal-free systems allows structure/property relationships to be developed based on a poly(silyl ether) backbone. As expected, thermal stability for these materials is high as exemplified by aromatic systems based on benzil and 1,4-bis(dimethylsilyl)benzene where increased thermal decomposition temperatures are observed when compared to traditional siloxanes (**2a–c**, $T_{d5,N_2} > 380$ °C). Similarly, the glass transition temperature could be varied from ≈ -30 °C to ≈ 80 °C by selecting the appropriate side chain groups (derived from the diketone) and the backbone linker unit (derived from the bis(silane)). Surprisingly, a wide range of these materials proved to be semi-crystalline in analogy with engineering plastics such as high-density polyethylene and polylactide leading to a rich array of melting/crystallization temperatures and thermal behavior being observed (Figure 5.4). Moreover, cold crystallization on heating is apparent for phenylene bridged poly(silyl ether)s with the benzil-based system, **2a**, showing a T_c of 135 °C and a T_m of 185 °C. Replacement of the freely rotating phenyl rings in **2a** with a rigid phenanthrene unit leads to an increase in the glass transition temperature but no observable T_c or T_m in the measurement window. This absence of crystallinity may be due to the stereochemically random nature of the backbone for **2e**. In contrast, the alkyl-substituted, hexane-3,4-dione derivative, **2h**, was

observed to have sharp transitions with the T_c being 30 °C and the T_m being 120 °C. For the benzil-based polymer with ethylene linker unit, **2i**, crystallization was observed on cooling with multiple melting transitions. It should be noted that all semi-crystalline behavior was further supported by sharp, well-defined maxima observed by XRD (see supporting information) which illustrates the utility of this polymerization strategy for producing libraries of semi-crystalline thermoplastics based on readily available poly(silyl ether) building blocks.

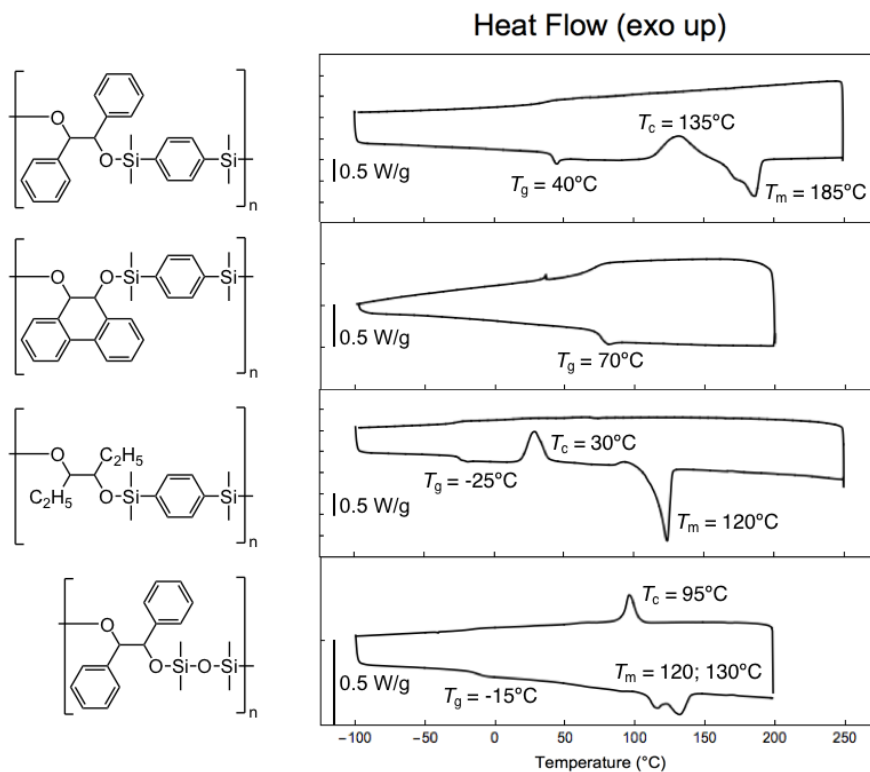


Figure 5.4 DSC chromatograms of selected PSEs **2a**, **2e**, **2h**, and **2i** on the second heat and cool cycle at a rate of 10 °C min⁻¹. The phenylene bridged **2a** and **2h** exhibit cold crystallization peaks during heating (T_c = 135 and 30 °C, respectively), while **2i** displays exothermic crystallization on cooling (T_c = 95 °C). The phenanthrene-based **2e** shows no crystallization in the temperature window examined.

3.3.5 Hydrolysis

PSEs are known for their potential to undergo hydrolysis due to the nucleophilically labile Si–O–C bonds in the backbone. In investigating the degradability of the polymers presented here, we selected four representative examples, the bis(silyl)phenylene-based polymers **2a** (–H substituted), **2c** (–Br), and **2d** (–CH₃), as well as the siloxane polymer **2j**. After dissolving these polymers in CHCl₃ solutions containing either methanol (80/20 (v/v)), TEA (20 mM), or HCl (1 mM), alcoholysis and hydrolysis were monitored as a function of time via changes in the relative molar mass by SEC analysis. The silphenylene-containing polymers **2a**, **2c** and **2d** proved very stable against alcoholysis, showing no change in molecular weight after an extended period (Figure 5.5). In contrast, the siloxane-based copolymer **2j** underwent methanolysis under the same reaction conditions, as indicated by a two-fold molecular weight decrease after 15 days. Significantly, in the presence of triethylamine, TEA, both the silphenylene copolymer **2a** and siloxane copolymer **2j** are stable, with no apparent change in molar mass over the same time period. As expected, these materials did prove to be susceptible to acid-catalyzed hydrolysis, exhibiting complete degradation for the poly(siloxane) derivative **2j** within 12 hours and for the phenylene derivative over 5+ days. This tunable degradation of **2j** relative to the silphenylene polymer **2a** is attributed to decreased steric hindrance and electronic nature of the Si–O bonds. In all cases, the degradation products were isolated and characterized by ¹H NMR and gas chromatography-mass spectrometry (GC-MS) measurements and for **2a** shown to be consistent with hydrolysis of the silyl ether backbone, yielding hydrobenzoin and phenylsilanediol (Figure 5.5a). The results demonstrate the further tunability of the properties of these PSEs with the observed acid-promoted degradation providing a new platform for the construction of responsive polymeric Si-based materials.

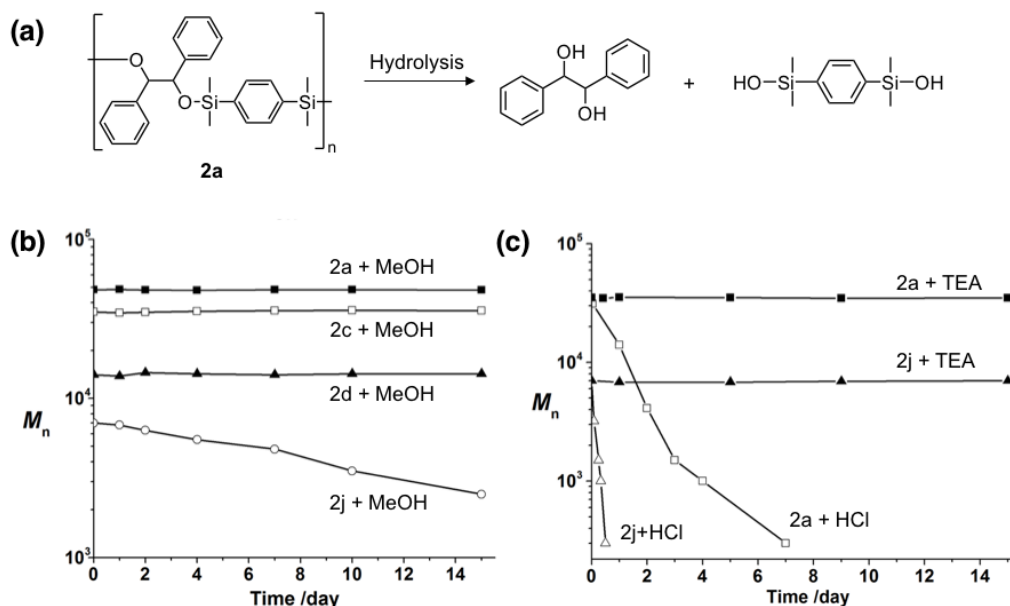


Figure 5.5 (a) Representative degradation behavior of PSEs **2a**. Number-average molar mass of PSE samples estimated via SEC as a function of time after exposure to (b) $\text{CHCl}_3/\text{MeOH}$ mixture (80/20, v/v) or (c) CHCl_3/TEA (20 mM) or CHCl_3/HCl (1 mM).

3.4 Conclusions

In conclusion, the step-growth polymerization of α -diketone and disilane monomers was successfully demonstrated using the Lewis acid catalyst, $\text{B}(\text{C}_6\text{F}_5)_3$. A wide variety of commercially available monomers, including benzil and other alkyl substituted α -diketones, could be coupled with bis-silanes to produce a library of functionalized semi-crystalline polymers with high molar mass, tunable thermal properties, and degradable Si–O–C backbones. Further development of this facile metal-free polyhydrosilylation chemistry and expansion to other Lewis acids, copolymers, and PSE-based thermosets are underway.

3.5 Experimental

3.5.1 Materials

Benzil (98%), 4,4'-difluorobenzil (98%), 4,4'-dibromobenzil (98%), 4,4'-dimethylbenzil (97%), dimethylphenylsilane (> 98%), 1,1,3,3-tetramethyldisiloxane (97%), 1,1,3,3,5,5-hexamethyltrisiloxane (95%), 1,2-bis(dimethylsilyl)ethane (> 97%), tris(pentafluorophenyl)borane (95%), chloroform (99% anhydrous), tetrahydrofuran (> 99%), and N-methyl-2-pyrrolidinone (> 98.5%) were used as received from Sigma-Aldrich. 2,3-Butanedione (97%, Sigma), 3,4-hexanedione (95%, Sigma), and 1,4-bis(dimethylsilyl)benzene (97%, Gelest) were dried over CaH₂ and distilled before use. Toluene was distilled from sodium benzophenone prior to use.

3.5.2 Methods

Nuclear magnetic resonance (NMR) measurements were performed using Varian Unity Inova 500 and 600 MHz instruments. All samples were dissolved in CDCl₃ or DMSO-d₆, and chemical shifts (δ) are reported in ppm relative to the residual proton signal of the deuterated solvent as appropriate. Mass spectrometry was performed on a Micromass QTOF2 quadrupole/time-of-flight tandem mass spectrometer (ESI) or a Waters GCT Premier time-of-flight mass spectrometer (EI and FD). Infrared (IR) spectra were recorded on a Thermo Nicolet iS10 Fourier-transform infrared (FTIR) spectrometer with a Smart Diamond attenuated total reflectance (ATR) sampling accessory. Size-exclusion chromatography (SEC) was performed on a Waters 2695 Separation Module equipped with a Waters 2414 refractive index detector and Waters 2996 Photodiode Array detector eluting with 0.25% triethylamine in chloroform. Molar masses were estimated relative to polystyrene standards. Differential scanning

calorimetry (DSC) was performed on a TA Instruments Q2000 DSC system at a heating rate of 10 °C/min under a nitrogen atmosphere. Thermal stability was evaluated using a TA Discovery Thermo-Gravimetric Analyzer with a heating rate of 10 °C/min under a nitrogen or air atmosphere. Single-crystal X-ray diffraction (XRD) data acquisition was performed on a Bruker Kappa APEX II CCD diffractometer with graphite-monochromatized Mo K α radiation ($\lambda = 0.7107 \text{ \AA}$) at $T = 100 \pm 2 \text{ K}$. Data were collected using an ω scan width of 0.588° and 3 axes with exposure times of 15 s and a fixed sample-to-detector distance of 60 mm. X-ray data collection was monitored by the APEX2 program. Data were corrected for Lorentz, polarization, and absorption effects using SAINT and SADABS. SHELXTL was used for structure solution and full matrix least-squares refinement on F2. All the H-atoms were placed in geometrically idealized position and constrained to ride on their parent atoms.

3.5.3 Synthesis

Model Small-Molecule Reaction

In a 20 mL glass vial equipped with a Teflon coated stir bar, dimethylphenylsilane (2.78 g, 20.0 mmol) was added to a solution of B(C₆F₅)₃ (25.6 mg, 0.05 mmol) in chloroform (5.0 mL) and the resulting solution stirred briefly. Benzil (2.10 g, 10.0 mmol) was then added slowly. The reaction mixture was stirred at room temperature for 30 min. The obtained solution of diastereomers was investigated by ¹H NMR, after which the chloroform was evaporated at room temperature to generate suitable crystals for single-crystal X-ray diffraction. ¹H NMR (400 MHz, CDCl₃) δ 7.45 – 7.00 (m, Ar), 4.70 (s, dl-OCHPh), 4.50 (s, meso-OCHPh), 0.16 and –0.04 (d, $J = 16.0$, –Si(CH₃)₂–). ¹³C NMR (100 MHz, CDCl₃) δ 142.5, 141.2, 139.5, 137.5, 133.6, 133.5, 129.3, 129.2, 127.6, 127.5, 127.3, 127.2, 127.0, 79.8, –1.0, –1.4, –1.5, –1.8. ²⁹Si

NMR (79.5 MHz, CDCl₃) δ 7.9, 7.6. MS (ESI+) calcd for C₃₀H₃₄O₂Si₂⁺ [M + H⁺] 483.21, found 483.21. FTIR ν_{\max} (cm⁻¹): 2950, 2850, 1750, 1620, 1550, 1275, 1110.

Representative Polymer Synthesis

In a 10 mL glass tube equipped with a Teflon coated stir bar, 1,4-bis(dimethylsilyl)benzene (194 mg, 1.00 mmol) was added to a solution of B(C₆F₅)₃ (2.56 mg, 0.005 mmol) in toluene (1.0 mL) and the resulting solution was stirred briefly. Benzil (210 mg, 1.00 mmol) was then added. The reaction mixture was stirred at room temperature for 30 min. The resulting mixture was diluted with 2.0 mL of chloroform, passed through a neutral alumina filter, and precipitated into cold hexanes. The final precipitate was isolated and dried in a vacuum oven to give the poly(silyl ether), **2a**. ¹H NMR (600 MHz, CDCl₃) δ 7.37 – 6.95 (m, Ar), 4.73 (d, J = 5.1 Hz, *dl*-OCHPh), 4.56 (s, *meso*-OCHPh), 0.41 and -0.16 (m, -Si(CH₃)₂-). ¹³C NMR (151 MHz, CDCl₃) δ 142.66, 142.63, 141.28, 138.80, 132.83, 132.74, 132.69, 132.60, 132.57, 127.84, 127.71, 127.61, 127.41, 127.33, 127.14, 79.98, 1.08, -1.08, -1.33, -1.35, -1.37, -1.57. ²⁹Si NMR (119 MHz, CDCl₃) δ 7.80 (d, J = 4.1 Hz), 7.69 (d, J = 5.1 Hz). FTIR ν_{\max} (cm⁻¹): 3065, 3034, 2957, 1493, 1452, 1380, 1251, 1200, 1136, 1100, 1069, 1027, 891, 844, 822, 778, 699, 664, 588, 560, 545. SEC M_n = 35.0 kg/mol, M_w = 70.5 kg/mol, M_w/M_n = 2.0. TGA $T_{d5,N2}$ = 415 °C. DSC T_g = 43 °C, T_c = 132 °C, T_m = 187 °C.

3.5 Supplemental Results

Crystallography

Table 5.3 Crystallographic data and refinement parameters for model small molecule (see Figure 5.1 for structure) and [2+2] cyclic product (see Figure 5.2 for structure).

	<i>Meso</i> -silyl ether	[2+2] cyclic product
Chemical formula	C ₃₀ H ₃₄ O ₂ Si ₂	C ₄₈ H ₅₆ O ₄ Si ₄
Molar mass	482.75	809.28
Temp (K)	100(2)	100(2)
Crystal system	Triclinic	Triclinic
Space group	P-1	P-1
<i>a</i> (Å)	16.051(3)	9.976(2)
<i>b</i> (Å)	20.072(3)	10.686(2)
<i>c</i> (Å)	20.123(3)	11.503(2)
α (°)	79.685(3)	100.497(5)
β (°)	77.242(3)	90.836(5)
γ (°)	79.172(3)	108.275(5)
<i>V</i> (Å ³)	6146.3(17)	1141.6(4)
<i>Z</i>	9	1
F(000)	2322	432
<i>D</i> _{cal} (g/cm ³)	1.174	1.177
<i>R</i> _{int}	0.0596	0.0316
GOF (on F ²)	0.979	1.029
<i>R</i> ₁ [<i>I</i> > 2 σ (<i>I</i>)] ^a	0.0694	0.0729
<i>wR</i> ₂ [<i>I</i> > 2 σ (<i>I</i>)] ^b	0.2094	0.1800

$${}^a R_1 = \frac{\sum ||F_o| - |F_c||}{\sum |F_o|}, \quad {}^b wR_2 = [\frac{\sum w(F_o^2 - F_c^2)^2}{\sum w(F_o^2)^2}]^{1/2}.$$

Polymer X-Ray Diffraction

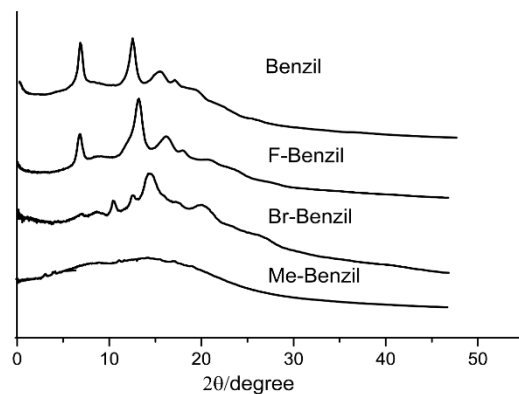


Figure 5.6 XRD measurement of polymers **2a–2d**.

Hydrolysis Analysis

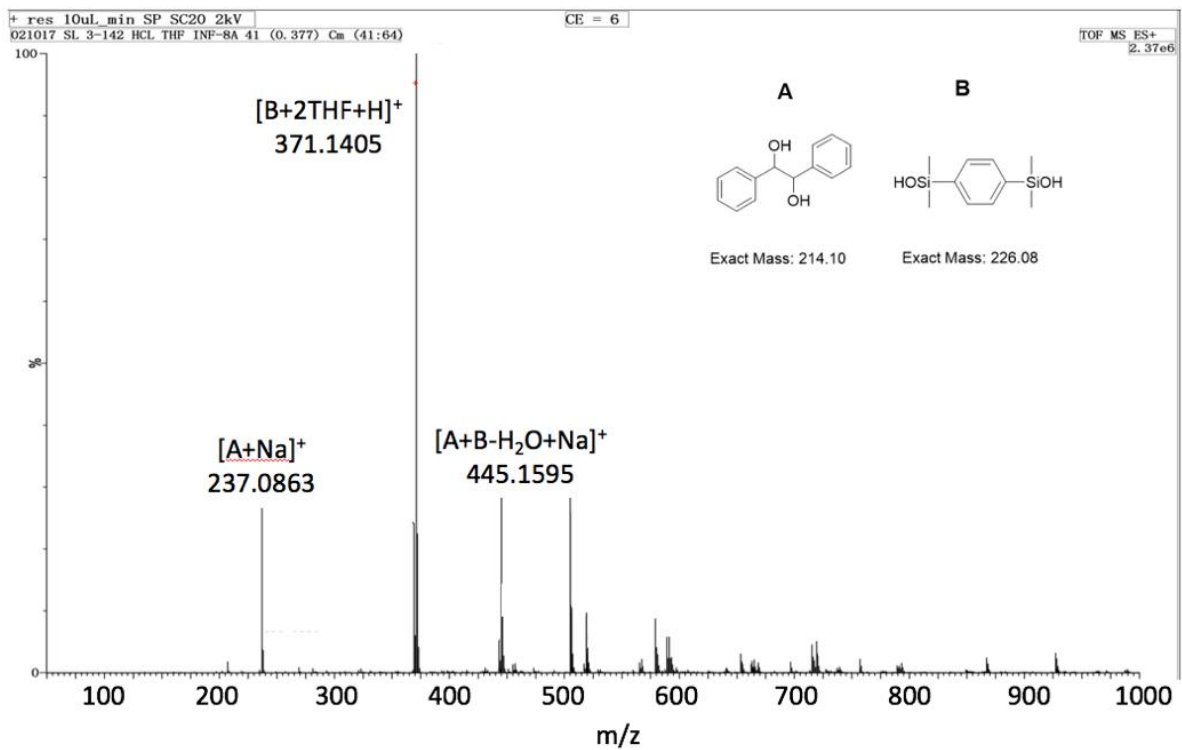


Figure 5.7 Mass spectroscopy analysis of the residue produced from hydrolysis of polymer **3a**.

Chapter 6

Metal-Free Vulcanization of Silicone Networks

Reprinted with permission from Sample, C. S.; Lee, S.-H.; Li, S.; Bates, M. W.; Lensch, V.; Versaw, B. A.; Bates, C. M.; Hawker, C. J. Metal-Free Room-Temperature Vulcanization of Silicones via Borane Hydrosilylation. *Macromolecules* **2019**, *52*, 7244–7250. Copyright 2019 American Chemical Society.

4.1 Abstract

Vulcanization of silicone networks from commercially available linear poly(dimethyl-*co*-methylhydro)siloxane (PMHS) and α -diketones was achieved using metal-free borane hydrosilylation at room temperature. The Lewis acid catalyst, tris(pentafluorophenyl)borane ($B(C_6F_5)_3$), efficiently crosslinked PMHS at minimal catalyst loadings (200–1000 ppm) to produce polymer networks with mechanical properties, thermal stability, and optical clarity rivaling that achieved from traditional platinum catalysis. Variation of the starting PMHS

structure is shown to influence the final characteristics of the network. Increasing the molar mass of PMHS results in a higher thermal decomposition temperature while increasing mole fractions of Si–H moieties along the backbone increases crosslink density and the attendant Shore hardness. The degradation behavior of the networks was investigated, with borane-vulcanized samples showing rapid dissolution upon exposure to acid and high stability to neutral and basic conditions. Functional networks bearing halide and vinyl groups were also prepared via a preliminary reaction of PMHS with an appropriate monoketone, providing a general and versatile strategy for network derivatization with the potential for post-vulcanization functionalization being subsequently demonstrated via thiol–ene click chemistry.

4.2 Introduction

Silicone networks, containing polysiloxane backbones of repeating Si–O bonds, are widely used engineering materials due to their high thermal, chemical, and light stability, which can be combined with effective thermal and electrical insulation, and tailorable mechanical properties. These beneficial attributes result in silicones being widely used industrially as sealants, coatings, electronic encapsulants, as well as in a range of biomedical devices.^{121–129}

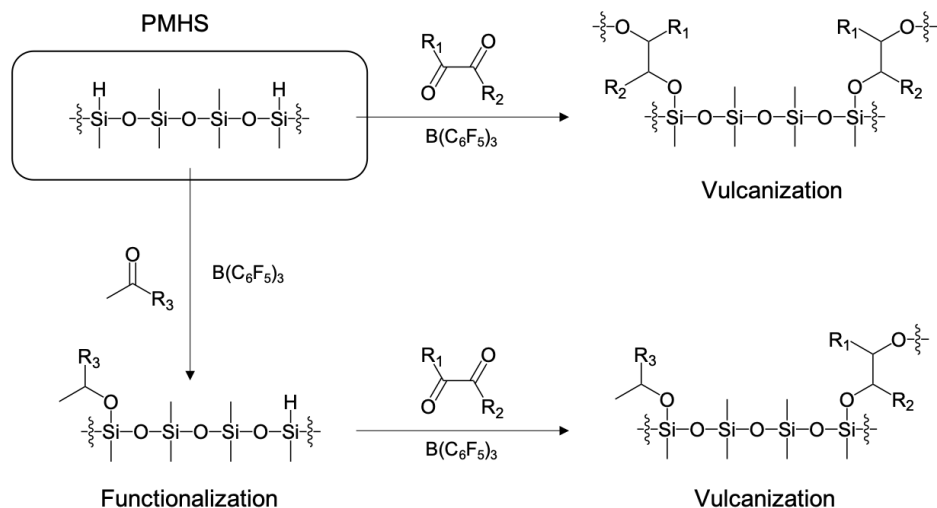
The increasing demand for silicone networks has consequently motivated the development of various curing strategies, which include peroxides and tin-catalyzed condensation chemistries. However, due to the high temperatures required for the former and the toxicity of the latter, modern vulcanization processes are primarily based on platinum-catalyzed addition.¹³⁰ While effective in crosslinking hydrosiloxanes via olefin hydrosilylation, the cost and scarcity of platinum presents a significant future challenge. Current silicone production consumes over five metric tons of platinum each year,¹⁰³ which represents $\approx 5\%$ of global

production. Additionally, the presence of residual Pt or Sn in crosslinked silicones can have deleterious effects in electronic, optical, and biological applications.

As a result, there is substantial interest in vulcanization strategies that do not require precious metal or even, following recent trends in polymer science,^{131–133} that are metal-free.^{134–138} A promising system for metal-free crosslinking of silicones is the Lewis acid, tris(pentafluorophenyl)borane ($\text{B}(\text{C}_6\text{F}_5)_3$), which can catalyze hydrosilylation via η^1 -coordinated activation of Si–H bonds. Originally developed by Piers and Parks for the hydrosilylation of aldehydes, ketones, and esters,³⁴ it has been further extended to amides,¹³⁹ olefins,^{140,141} quinolines,¹⁴² and nitriles.¹⁴³ While previous work has focused on small-molecule transformations, $\text{B}(\text{C}_6\text{F}_5)_3$ -catalyzed hydrosilylation has also been employed in polymer chemistry to produce a variety of Si–O-containing polymers, including polysiloxanes via the oligomerization of dihydrosilanes,^{144,145} poly(silphenylenesiloxane)s via the polycondensation of dihydrosilanes and dialkoxysilanes or dihydroxysilanes^{118,146}, and poly(silyl ethers) via the polycondensation of dihydrosilanes and dihydroxysilanes,¹⁴⁷ dienes,¹⁰⁸ or diketones.² The use of $\text{B}(\text{C}_6\text{F}_5)_3$ in vulcanization, however, has been limited; previous examples are based on the reaction of hydrosilanes with alkoxysilanes or other non-atom-efficient partners,^{148–152} with the evolved gaseous byproducts used to produce foams or removed prior to full cure.

In this work, the borane-catalyzed hydrosilylation of commercially available α -diketones and linear siloxanes is shown to lead to rapid, efficient vulcanization of silicones with no byproducts (Scheme 6.1). In this approach, catalytic activation of the Si–H bonds of commercial poly(dimethyl-*co*-methylhydro)siloxane (PMHS)—available in a range of molecular weights and hydrosilane contents—results in their efficient crosslinking with α -diketones, a class of molecules manufactured on a large scale as various flavor and fragrance

ingredients. Additionally, this hydrosilylation reaction leads to networks containing acid-labile C–O–Si linkages, allowing degradability to be tuned and environmental impact minimized.¹⁵³



Scheme 6.1 Vulcanization of silicone networks via borane-catalyzed hydrosilylation of commercially available α -diketones with polymethylhydrosiloxanes. Routes to both crosslinked (top row) and functionalized networks (bottom row) are shown.

Additionally, sequential reaction of PMHS with functionalized monoketones followed by α -diketone crosslinking can be used to introduce secondary functionality (bottom row, Scheme 6.1) into the final silicone network. In this process, a fraction of the initial Si–H bonds are first reacted to yield a functional PMHS derivative, with the orthogonal nature of B(C₆F₅)₃ allowing for the formation of networks with reactive halide and vinyl groups. The latter is of particular interest due the incompatibility of vinyl groups with traditional Pt-catalysts and the synthetic versatility of thiol–ene click chemistry for the introduction of reactive functionalities.

4.3 Results and Discussion

4.3.1 Development of Vulcanization

In parallel to the simplicity of traditional Pt-catalyzed procedures, silicone vulcanization via borane-catalyzed hydrosilylation is based on commercially available starting materials and proceeds under solvent-free conditions. To illustrate this chemistry, the starting materials, PMHS, α -diketone, and $B(C_6F_5)_3$, were collectively mixed and solubilized under ambient conditions. After casting into the desired mold and degassing under reduced pressure in a vacuum oven, curing occurs at room temperature.

4.3.2 Varied Crosslinker Scope

Using this procedure, a library of silicone networks was initially synthesized based on linear PMHS (molecular weight of 6 kDa and Si–H incorporation of 8%) and various α -diketones with the networks being characterized thermally and mechanically, as shown in Table 6.1. Rapid curing is observed with 2,3-butanedione (Table 6.1, Entry 1), and increasing the steric bulk of the crosslinker to 3,4-hexanedione (Table 6.1, Entry 2) did not increase the cure time significantly.¹⁵⁴ Vulcanization was also successful with the aryl-substituted 1-phenyl-1,2-propanedione (Table 6.1, Entry 3), however in this case cure time was extended due to the reduced miscibility of PMHS and 1-phenyl-1,2-propanedione. Significantly, the nature of the α -diketone was observed to have little effect on the thermal decomposition temperature ($T_{d5, \text{air}} \approx 320\text{--}330^\circ\text{C}$ for all samples) and hardness (60–75 Shore OO), illustrating that thermal and mechanical properties are largely independent of crosslinker chemical identity, likely due to the limited interaction of crosslinker side groups with the primary network.

Table 6.1 Silicone networks synthesized from PMHS (6 kDa, 8% Si-H) via borane-catalyzed hydrosilylation of α -diketones and the corresponding network prepared by Pt-catalyzed hydrosilylation of the olefin divinyltetramethyldisiloxane using Karstedt's catalyst.

Catalyst: $B(C_6F_5)_3$

MW = 6 kDa, % Si-H = 8

Entry	Crosslinker	Cat. loading (ppm)	Gelation time (hr)	$T_{d5,air}$ (°C)	Hardness (Shore OO)
1		500	2	330	60 +/- 1
2		500	4	330	70 +/- 1
3		1000	24	320	67 +/- 1

Catalyst: Pt

MW = 6 kDa, % Si-H = 8

4		125	24	360	77 +/- 1
---	--	-----	----	-----	----------

Due to the utility of polymethylhydrosiloxanes in both borane- and platinum-catalyzed hydrosilylation reactions, control networks based on the same polymeric building block could be prepared from equivalent PMHS (6 kDa, 8% Si-H) using the traditional Karstedt's catalyst and the small-molecule crosslinker 1,3-divinyltetramethyldisiloxane (Table 6.1, Entry 4). In this system, cure times depend substantially on catalyst loading, with the lowest loading (125 ppm) achieving gelation within 24 h. While higher Pt-loadings accelerated vulcanization (e.g., 1 h at 500 ppm), the increased metal concentration results in significant coloration as shown in Figure 6.1. Yellowing of the Pt-catalyzed networks prepared at room temperature was apparent at all loadings; attempts to further reduce catalyst amount to yield a colorless network

were offset by necessary increases in cure temperature to promote vulcanization. In direct contrast, the metal-free borane strategy produced optically transparent materials at room temperature, regardless of catalyst loading.

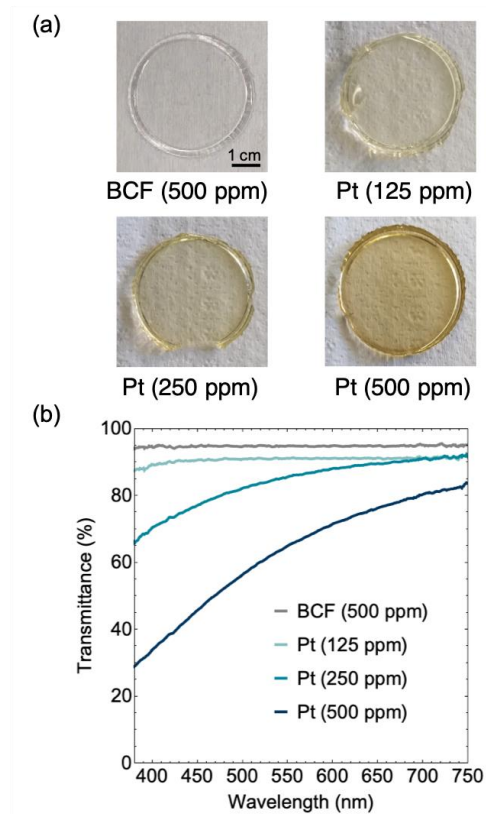
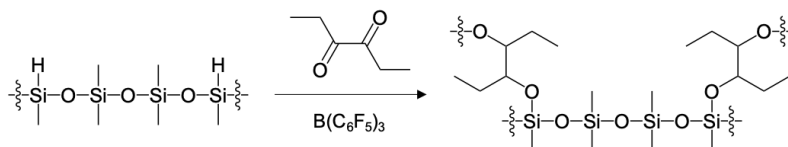


Figure 6.1 Optical properties shown via (a) images of a borane-catalyzed network (Table 6.1, Entry 1) and platinum-catalyzed networks formed using 125, 250, and 500 ppm Karstedt's catalyst and (b) UV-Vis transmittance spectra obtained for the corresponding 1 mm thick samples.

4.3.3 Varied Prepolymer Scope

In analogy with platinum systems, Si-H containing copolymers are commercially available in a variety of molecular weights and Si-H contents, enabling control over both the PMHS backbone length and the crosslink density. This allows further tailoring of material properties through increasing the backbone length and mole percent of Si-H units along the backbone.

For example, increasing the molecular weight from 6 kDa to 60 kDa while maintaining a similar Si–H content (Table 6.2, Entries 1 and 2) increases the thermal stability, likely due to a smaller fraction of weaker C–O–Si bonds relative to the more stable siloxane backbone motif. However, the increased backbone length results in little change in Shore hardness due to the dominant effect of the crosslink density on mechanical properties, although the increased viscosity of the higher molar mass precursor leads to longer cure times. Low molar mass PMHS (2 kDa) (Table 6.2, Entry 3) undergoes coupling, however the low Si–H content ($\leq 3\%$ Si–H) and limited number of groups per backbone (≈ 2 to 3) leads only to a branched structure and does not produce sufficient crosslinks per chain to achieve gelation. Vulcanization is possible at 7% Si–H (Table 6.2, Entry 4), with weakly crosslinked materials being obtained, while stronger gels are prepared at higher levels of Si–H incorporation and consequently higher crosslink density (Table 6.2, Entries 5 and 6). This increase in crosslinking results in an increase in Shore hardness.

Table 6.2 Silicone networks synthesized with varying PMHS starting materials.

Entry	PMHS	MW (kDa)	Si-H (mol%)	Cat. loading (ppm)	Gelation time (hr)	T _{d5,air} (°C)	Hardness (Shore OO)
1	HMS-082	6	8	500	4	330	70 +/- 1
2	HMS-064	60	6	600	6	350	75 +/- 2
3*	HMS-031	2	3	—	—	—	—
4	HMS-071	2	7	500	4	290	28 +/- 1
5	HMS-151	2	15	250	6	290	68 +/- 2
6	HMS-301	2	30	200	8	270	85 +/- 2

*No vulcanization at any catalyst loading from 250 to 1000 ppm due to insufficient cross-linking points per chain.

4.3.4 Hydrolysis

Based on the $B(C_6F_5)_3$ -catalyzed carbonyl addition chemistry, the resulting Si–O–C linkages are less stable hydrolytically when compared to traditional Pt-cured silicones, which is of great interest due to the growing demand for degradable materials with shorter environmental residence times. To compare the degradation behavior of the borane-vulcanized networks with the platinum analogues, samples of PMHS (6 kDa, 8% Si–H) crosslinked with either hexanedione (Table 6.1, Entry 2) or divinyltetramethyldisiloxane (Table 6.1, Entry 4) were weighed and then immersed in chloroform solutions containing methanol (80/20 (v/v)), triethylamine (TEA, 20 mM), or HCl (1 mM). Neither the $B(C_6F_5)_3$ - or the Pt-vulcanized samples exposed to methanol or TEA showed appreciable mass loss over the course of two weeks. However, while the platinum sample immersed in HCl solution remained intact over

that same period, the $B(C_6F_5)_3$ sample dissolved completely within 24 hours. Evaporation of the chloroform revealed a viscous oil that 1H NMR (Figure 6.5, Supplemental Results) confirmed to be the hydrolysis products, poly(dimethyl-*co*-methylhydroxy)siloxane and 3,4-hexanediol (Figure 6.2a). Further size-exclusion chromatography showed the molecular weight of the post-hydrolysis product to be less than that of the starting material, evidence that not only did the silyl ether linkages break down but the siloxane backbone itself is degrading during network cleavage. This decrease in molecular weight is also observed for linear PMHS exposed to acidic conditions (Figure 6.6, Supplemental Results), while the relative stability of the backbone of the Pt-vulcanized sample is attributed to the poor swelling of the network with solvent, reducing the exposure of the siloxane backbone to acid relative to the fully dissolved chains. Thus, while some degradation may initially occur, it takes longer for the network to lose full integrity; indeed, the Pt-catalyzed samples eventually dissolve after one month in the 1 mM HCl solution.

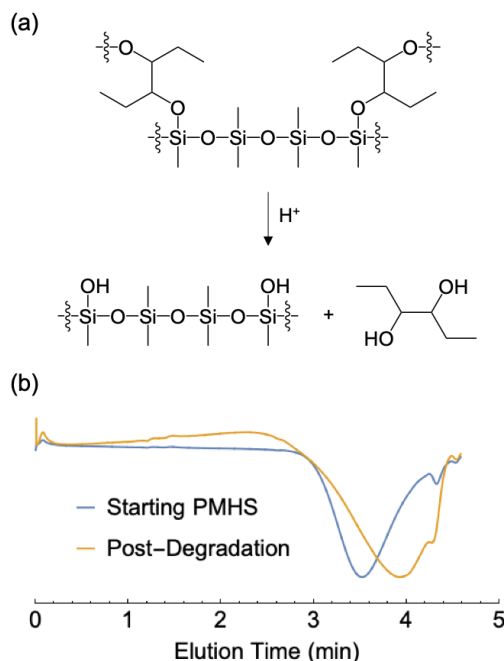


Figure 6.2 (a) Scheme of hydrolysis of borane-catalyzed PMHS network and (b) size-exclusion chromatograms showing the elution profiles of the starting PMHS (6 kDa, 8% Si-H) and the crude product after network degradation. The differential refractive index signals are negative due to the lower refractive index of polysiloxanes relative to the eluent (chloroform).

5.3.5 Introduction of Functionality

In addition to efficiently catalyzing the room temperature, metal-free vulcanization of silicone elastomers, the tolerance of $B(C_6F_5)_3$ towards functional groups incompatible with traditional vulcanization chemistry (i.e., halide or vinyl groups under Pt-catalysis) enables the synthesis of reactive silicone networks via initial coupling of PMHS with functional monoketones. It should be noted that preliminary coupling of the monoketone with PMHS necessitates a higher catalyst loading (1000 ppm) due to the decreased reactivity of monoketones when compared to the vicinal diketones described above. In this process, PMHS, monoketone, and $B(C_6F_5)_3$ are stirred overnight to give the functional PMHS and then passed through neutral alumina to remove residual catalyst. This gives the desired functional polymer

with no further purification required. A representative example of this reaction is shown in Figure 6.3a, where reaction of PMHS with 0.5 equivalents of 5-chloro-2-pentanone introduces chloride-containing side chains along the siloxane backbone. From ^1H NMR analysis (Figure 6.3b), copolymer functionalization was shown to be near quantitative when targeting partial substitution with the product having 15 mol % of substituted chloropentyl units and 15 mol % of remaining Si–H units compared to the starting PMHS polymer (30 mol % of Si–H units). Supporting experiments using PMHS consisting of 99% hydrosilane backbone (99% Si–H), and excess monoketone indicate that maximum functionalization density is limited to 50% incorporation, likely due to steric hindrance that prevents higher levels of incorporation.

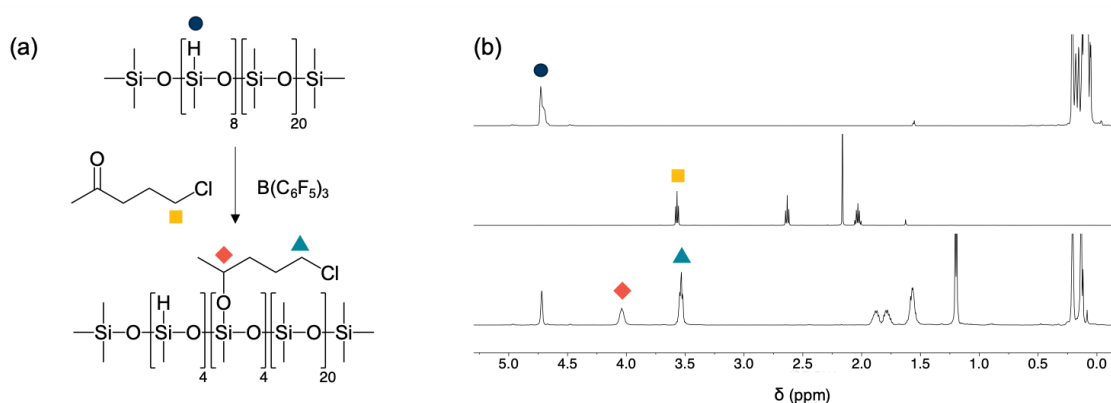
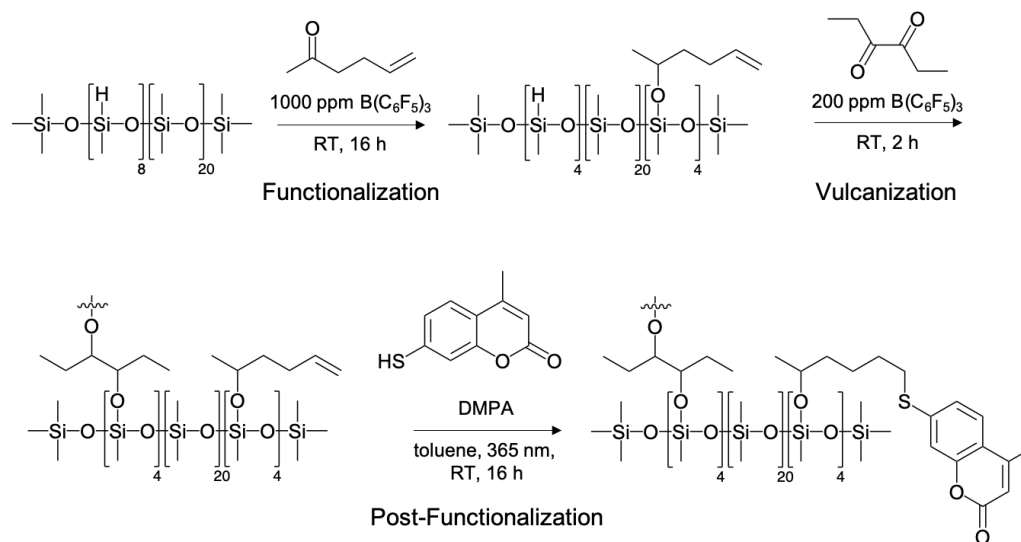


Figure 6.3 (a) Representative synthesis of functionalized PMHS derivatives via reaction with a substituted monoketone (5-chloro-2-pentanone) with (b) ^1H NMR showing the appearance of a proton adjacent to the silyl ether as well as preservation of the chloride group.

The ability to tune the level of functionalization then allows remaining hydrosilane groups to be crosslinked using 3,4-hexanedione at 200 ppm $\text{B}(\text{C}_6\text{F}_5)_3$ via the same procedure described for pristine PMHS. In addition to halide substituents, this process can alternatively employ 5-hexen-2-one to introduce pendant vinyl groups into a silicone network (Scheme 6.2). Such functionality is not accessible via traditional Pt-catalyzed hydrosilylation due to the reactivity of alkenes under Pt catalysis. We note that while $\text{B}(\text{C}_6\text{F}_5)_3$ can catalyze the hydrosilylation of

alkenes, the catalyst loadings necessary to promote reaction at the carbonyl (0.1 mol %) are significantly lower than that required for vinyl hydrosilylation (5 mol %), allowing for orthogonal reactivity.⁹⁴ The tolerance of $B(C_6F_5)_3$ towards alkenes was confirmed by 1H NMR of the vinyl-functionalized polymer (Figure 6.7, Supplemental Results).



Scheme 6.2 Multi-step synthesis of functional silicone networks via initial reaction with 5-hexen-2-one, crosslinking with 3,4-hexanedione, and thiol–ene click coupling with 7-mercapto-4-methylcoumarin.

The inclusion of alkenes in borane-catalyzed silicone networks permits additional post-vulcanization modification via reactions such as thiol–ene click coupling. To demonstrate this, a vinyl-functionalized network was swollen with a solution containing the fluorophore 7-mercapto-4-methylcoumarin and the photocatalyst dimethoxy-2-phenylacetophenone in toluene. After exposure to 365 nm light, Soxhlet extraction with acetone was used to remove any unreacted coumarin, and the network was thoroughly dried under vacuum. Figure 6.4a shows that the extracted network remains mechanically robust and is also fluorescent under UV irradiation indicating covalent attachment of the fluorophore. As a control experiment, thiol–ene addition to a network derived from unmodified PMHS does not fluoresce following

Soxhlet extraction (Figure 6.4b), supporting our conclusion that the fluorescent network is a product of covalent coupling via the reactive alkene unit rather than non-specific absorption.

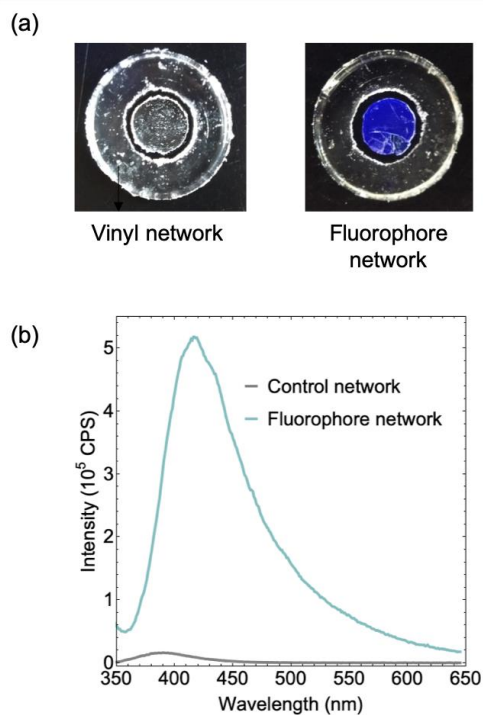


Figure 6.4 (a) Images of vinyl-functionalized network before (left) and after (right) thiol–ene click with 7-mercapto-4-methylcoumarin under 365 nm irradiation. The center disk has undergone thiol–ene click while the outer ring is an unreacted control sample. (b) Fluorescence spectra of the coumarin-containing network as well as the undecorated control.

4.4 Conclusions

The metal-free room-temperature vulcanization of silicones is demonstrated to be a simple, yet versatile process using borane-catalyzed hydrosilylation. These crosslinked networks have mechanical, thermal, and optical properties rivaling those obtained via industry-standard Pt catalysis with a significant enhancement in cure time and optical transparency. Various combinations of commercial α -diketone and PMHS starting materials can furnish mechanically tailorable networks, and the silyl ether bonds contained within these networks allow for

triggerable degradation upon exposure to acid. Moreover, these networks can be further functionalized through a two-step strategy involving initial reaction of PMHS with a substituted monoketone followed by $B(C_6F_5)_3$ -catalyzed crosslinking. In comparison with Pt-based systems, $B(C_6F_5)_3$ offers a room temperature, metal-free approach to synthesizing wide range of silicone networks.

4.5 Experimental

4.5.1 Materials

Tris(pentafluorophenyl)borane was purchased from TCI America, dried by saturating with chlorotrimethylsilane, and sublimed under reduced pressure. Methylhydrosiloxane-dimethylsiloxane copolymers (HMS-031, -064, -071, -082, -151, -301) and Karstedt's catalyst (2% Pt in xylene) were obtained from Gelest and used as received. 2,3-Butanedione, 3,4-hexanedione, 1-phenyl-1,2-propanedione, 5-hexen-2-one, 5-chloro-2-pentanone, and 1,3-divinyltetramethyldisiloxane were purchased from Sigma Aldrich. Diketones were dried over CaH_2 and distilled under reduced pressure before use.

4.5.2 Methods

Thermal gravimetric analysis (TGA) was performed under air using a TA Discovery thermogravimetric analyzer at a heating rate of 10 °C/min and 8–12 mg of sample in an alumina sample cup atop a platinum or ceramic hanging pan. Shore hardness measurements were taken using a Rex Model 1600 Type OO durometer on samples measuring ≥ 7 mm in thickness according to ASTM D2240. Reported hardness values are the average of three measurements. UV-Vis analysis was performed on a Shimadzu UV-3600 UV-Vis-NIR spectrophotometer

equipped with an integrating sphere. Visible light (380–750 nm) transmission measurements were taken on 1 mm thick samples. Nuclear magnetic resonance (NMR) measurements were performed using Varian Unity Inova 500 and 600 MHz instruments. All samples were dissolved in CDCl_3 and chemical shifts (δ) are reported in ppm relative to residual protic chloroform. Size-exclusion chromatography (SEC) was performed on a Waters Acquity Advanced Polymer Characterization (APC) System equipped with three Waters Acquity APC XT columns (45, 200, and 450 pore sizes), a Waters Acquity UPLC refractive index detector, and Waters Acquity UPLC Photodiode Array detector eluting with 0.25% triethylamine in chloroform at a flow rate of 0.5 mL/min. Fluorescence analysis employed a Horiba FluoroMax-4 fluorimeter. Samples (0.5 mm thick) were excited at a wavelength of 330 nm and the emission spectra recorded from 345–645 nm.

4.5.3 Synthesis

Representative Procedure for $\text{B}(\text{C}_6\text{F}_5)_3$ -Catalyzed Vulcanization of PMHS (HMS-082)

HMS-082 (2.00 g, 2.16 mmol equivalents of Si–H) and 2,3-butanedione (90 μL , 1.03 mmol) were added to a 20 mL scintillation vial and vortexed until homogeneous. A 0.1 M $\text{B}(\text{C}_6\text{F}_5)_3$ solution in 2,3-butanedione (5.0 μL , 0.5 μmol catalyst, 0.06 mmol diketone) was added and thoroughly mixed via vortex. The mixture was then transferred to a 4 cm diameter aluminum weigh dish and placed in a vacuum oven containing calcium sulfate (DrieriteTM) and equipped with an argon inlet. The vacuum oven was evacuated and flushed with argon three times before reduction to ≈ 400 mmHg to remove any bubbles. After 2 h, the vacuum oven was refilled with argon, and samples were checked periodically to monitor vulcanization over 24 h.

Representative Procedure for Pt-Catalyzed Vulcanization of PMHS (HMS-082)

HMS-082 (2.00 g, 2.16 mmol equivalents of Si-H) and 1,3-divinyltetramethyldisiloxane (274 μ L, 1.19 mmol) to a 20 mL scintillation vial and thoroughly mixed via vortex. Karstedt's catalyst (17 μ L, 0.34 μ mol, 2% Pt in xylenes) was added and the solution vortexed. The solution was then transferred to a 4 cm diameter aluminum weigh dish and placed in a vacuum oven containing DrieriteTM and equipped with an argon inlet. The pressure inside the vacuum oven was reduced and purged with argon three times before evacuation to \approx 400 mmHg. After 2 h under static vacuum, the oven was refilled with argon as the samples cured for an additional 22 h.

Synthesis of HMS-chloro

In a 25 mL round-bottom flask, HMS-301 (5.00 g, 20.4 mmol Si-H) and 5-chloro-2-pentanone (970 μ L, 8.5 mmol) were combined and stirred for one minute. A 0.1 M B(C₆F₅)₃ solution in 5-chloro-2-pentanone (194 μ L, 20 μ mol catalyst, 1.7 mmol ketone) was added and stirred at 50°C for 3 h. The mixture was passed through a neutral alumina plug to remove residual catalyst and give HMS-chloro as a viscous oil (5.79 g, 93% yield). ¹H NMR (CDCl₃, 500 MHz): δ 4.76 (s, -O-SiH(CH₃)-O-), 4.03 (m, -O-CH(CH₃)-CH₂-), 1.96-1.72 (m, -CH₂-CH₂-Cl), 1.57 (m, -CH(CH₃)-CH₂-CH₂-), 1.18 (d, J = 6.2, -O-CH(CH₃)-CH₂-), 0.24-0.03 (m, -SiR(CH₃)-). ¹³C NMR (CDCl₃, 125 MHz): δ 71 (-O-CH(CH₃)-CH₂-), 48 (-CH₂-CH₂-Cl), 40 (-CH₂-CH₂-Cl), 32 (-CH(CH₃)-CH₂-CH₂-), 27 (-O-CH(CH₃)-CH₂-), 4.2 (-SiR(CH₃)-).

Synthesis of HMS-vinyl

In a 25 mL round-bottom flask, HMS-301 (5.00 g, 20.4 mmol Si-H) and 5-hexen-2-one (985 μ L, 8.5 mmol) were combined and stirred for one minute. A 0.1 M $B(C_6F_5)_3$ solution in 5-hexen-2-one (200 μ L, 20 μ mol catalyst, 1.7 mmol ketone) was added and followed by stirring at room temperature for 16 h. The mixture was passed through a neutral alumina plug to remove residual catalyst and give HMS-vinyl as a viscous oil (5.70 g, 95% yield). 1H NMR ($CDCl_3$, 500 MHz): δ 5.80 (m, $-CH_2-CH=CH_2$), 4.96 (dd, $J = 38, 10$ Hz, $-CH=CH_2$), 4.72 (s, $-O-SiH(CH_3)-O-$), 4.01 (m, $-O-CH(CH_3)-CH_2-$), 2.19–2.00 (m, $-CH_2-CH=CH_2$), 1.62–1.43 (m, $-CH(CH_3)-CH_2-CH_2-$), 1.18 (d, $J = 6.1$, $-O-CH(CH_3)-CH_2-$), 0.25–0.05 (m, $-SiR(CH_3)-$). ^{13}C NMR ($CDCl_3$, 125 MHz): δ 142 ($-CH_2-CH=CH_2$), 118 ($-CH=CH_2$), 72 ($-O-CH(CH_3)-CH_2-$), 42 ($-CH_2-CH=CH_2$), 34 ($-CH(CH_3)-CH_2-CH_2-$), 27 ($-O-CH(CH_3)-CH_2-$), 4.5 ($-SiR(CH_3)-$).

Representative Vulcanization of Functional PMHS (HMS-vinyl)

HMS-vinyl (500 mg, 1.3 mmol equivalents of Si-H) and 3,4-hexanedione (70 μ L, 0.58 mmol) were added to a 4 mL single-dram glass vial. The mixture was vortexed until homogeneous and then 8 μ L of a 0.1 M solution of $B(C_6F_5)_3$ in 3,4-hexanedione (0.8 μ mol catalyst, 0.07 mmol ketone) was added. After vortexing again, the vial was placed in a vacuum oven containing DrieriteTM and equipped with an argon inlet. The oven was evacuated and refilled with argon three times before evacuation to ≈ 400 mmHg. The sample vulcanized for 2 h under static vacuum.

4.6. Supplemental Results

4.6.1 Hydrolysis Analysis

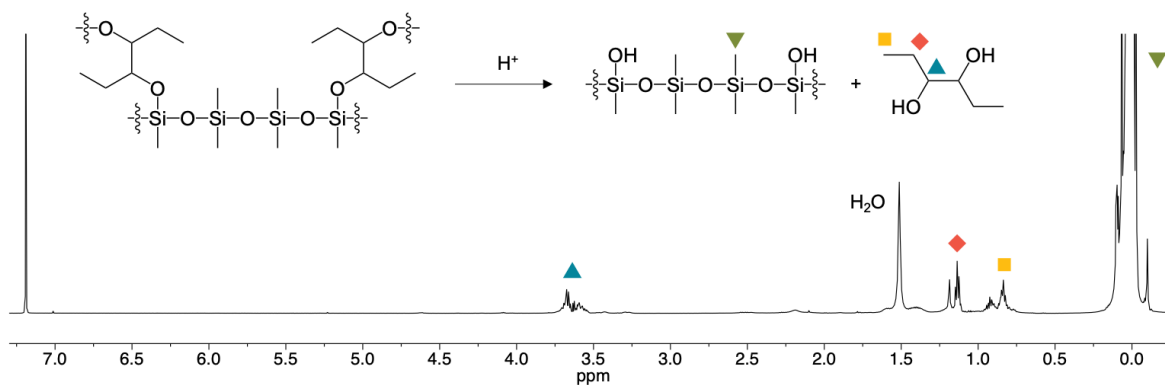


Figure 6.5 Scheme of hydrolysis and ¹H NMR of resulting product.

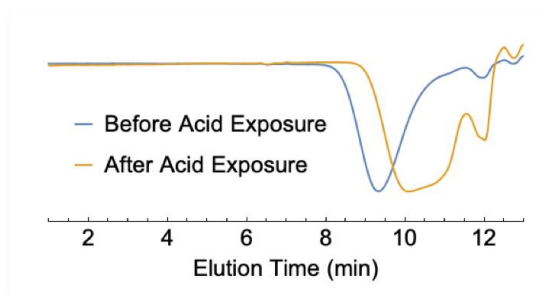


Figure 6.6 Size-exclusion chromatograms showing the elution profiles of linear PMHS (6 kDa, 8% Si-H) before and after dissolution in chloroform containing 1 mM HCl for 24 h.

4.6.2 Functionalization of PMHS

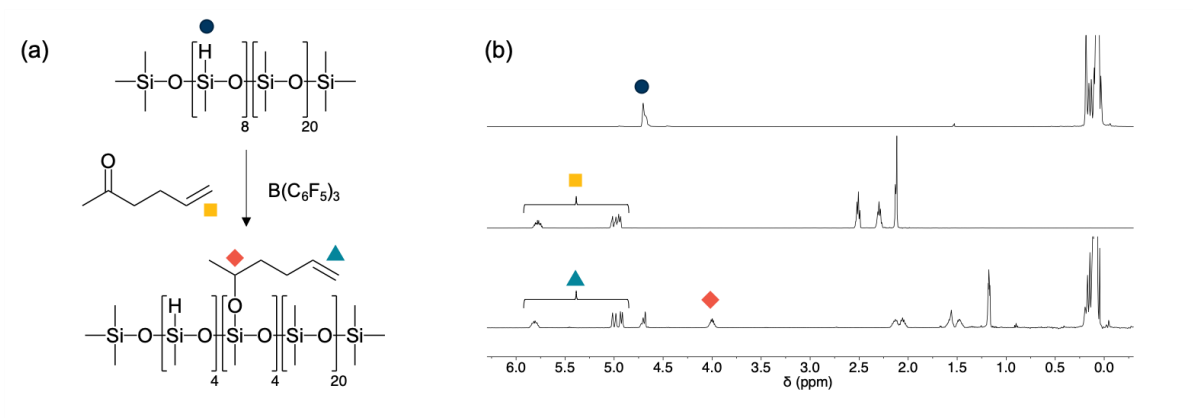


Figure 6.7 (a) Synthesis of functionalized PMHS derivatives via reaction with 5-hexen-2-one and (b) 1H NMR showing the appearance of a proton adjacent to the silyl ether as well as preservation of the vinyl group.

Chapter 7

3D Printing of Boronic-Ester Vitrimers

5.1 Abstract

As 3D printing increases in prominence, so too does the need for strategies to improve its sustainability. In the case of vat polymerization techniques such as stereolithography (SLA) and dynamic light processing (DLP), there is a shortage of ways to prevent the thermoset parts generated from ending up as polymer waste. In this work we present the development of a facile approach towards the inclusion of dynamic covalent bonds into 3D-printing resins for vat polymerization. In particular, the thiol-ene curing of resins containing boronic ester moieties is demonstrated, and the dynamic character and reprocessability of the resultant 3D-printed parts is shown. Furthermore, the effect of dilution with non-dynamic monomers is investigated, revealing that the relaxation kinetics can to be controlled across multiple timescales.

5.2 Introduction

Additive manufacturing, or 3D printing, of polymeric materials is undergoing a massive upswing in development and implementation, with the ability to generate intricate three-dimensional structures enabling applications in industry, biomedicine, construction, and many others.^{41,42,155–157} With that increase in use comes the challenge facing plastics manufacturing at all levels: the generation of large quantities of waste. In the case of 3D printing, the fate of that waste depends on the strategy employed. Fused filament fabrication (FFF), which relies on the thermal extrusion of filaments made from thermoplastic polymers, has an inherent degree of recyclability, even to the point of allowing for a closed-loop system via reprocessing of parts into filament.¹⁵⁸ However, a growing segment of the additive manufacturing market, especially on the industrial scale, consists of photocured vat polymerization strategies such as stereolithography (SLA) and dynamic light processing (DLP).¹⁵⁹ While these techniques are increasingly popular due to their high degree of accuracy, relative rapidity, and flexibility of material choice, the primary focus of sustainability research has been on producing resins from more renewable sources.^{160–162} Once printed, the thermosets generated by vat polymerization techniques are structurally nonreconfigurable and therefore face poor end-of-life outcomes.

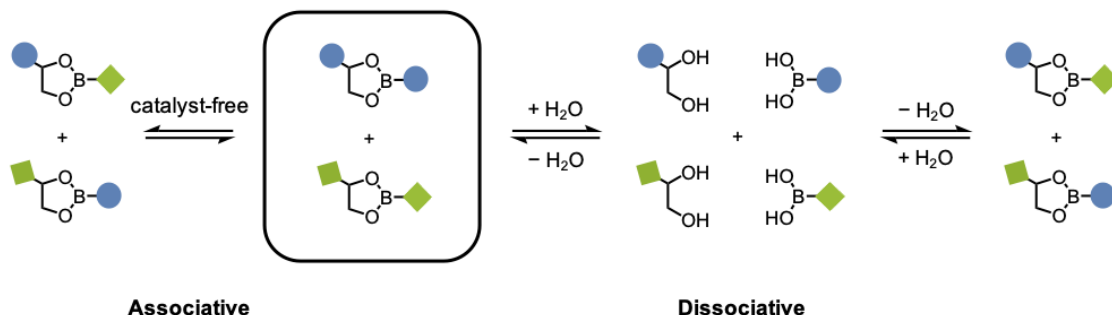
One promising strategy for overcoming the non-recyclable nature of thermosets lies in the field of covalent adaptable networks (CANs). These networks combine the fully crosslinked structure of traditional thermosets with the potential for reconfiguration provided by the inclusion of dynamic covalent bonds. The term “vitriimer” was coined by Leibler and coworkers in 2011 to describe a particular subset of CANs that undergo associate exchange, maintaining network structure during thermal processing.⁴⁴ While this system took advantage of transesterification for the exchange, the field has broadened to include olefins,⁴⁶ urethanes,⁴⁷

vinylogous urethanes,⁴⁸ triazoles,⁴⁹ thioethers,⁵⁰ and others. While mechanistically different, these CANs share qualities of self-healing, the ability to relax stress, and potential for reprocessability.

Despite the wide and ever-growing range of research into CANs and the associated dynamic covalent chemistry, their application in the field of vat polymerization 3D printing has so far been limited. Ge, Dunn, and coworkers recently reported the UV-cured 3D printing of vitrimers that take advantage of constituent ester and hydroxyl functionalities to reconfigure via transesterification, analogous to Leibler's original study.¹⁶³ This work was an elegant demonstration of the potential afforded by the inclusion of dynamic covalent moieties into 3D-printed parts, showing not only the repair of damaged prints but also the ability of end-of-lifetime objects to be remolded into entirely new forms. However, transesterification is an energetically disfavored transformation, requiring the addition of catalysts such as tin or zinc that can leach out over time, as well as high temperatures that can induce unwanted degradation of the bulk material. Therefore, just as the scope of CANs includes chemistries beyond transesterification, so too can the field of 3D-printed vitrimers benefit from the introduction of new dynamic exchange processes, including those with no need for catalyst or highly elevated temperatures.

To that end, we turn in this work to the exchange of boronate esters, or dioxaborolanes, which can undergo exchange via both associative and dissociative pathways (Scheme 7.1).⁵¹ Dioxaborolane metathesis has recently been shown to be a potent force for dynamic exchange at temperatures as low as 60 °C,⁵³ and inducing boronate ester hydrolysis by selective wetting lowers the barrier for self-healing to below room temperature.⁵² Furthermore, the tolerance of boronate esters towards radicals makes them an attractive candidate for the photocuring

strategies used in vat polymerization, with boronate-containing vitrimers having been prepared via controlled-radical polymerization and thiol–ene click reactions.^{53,54}



Scheme 7.1 Schematic of boronate exchange, showing associative and dissociative pathways.

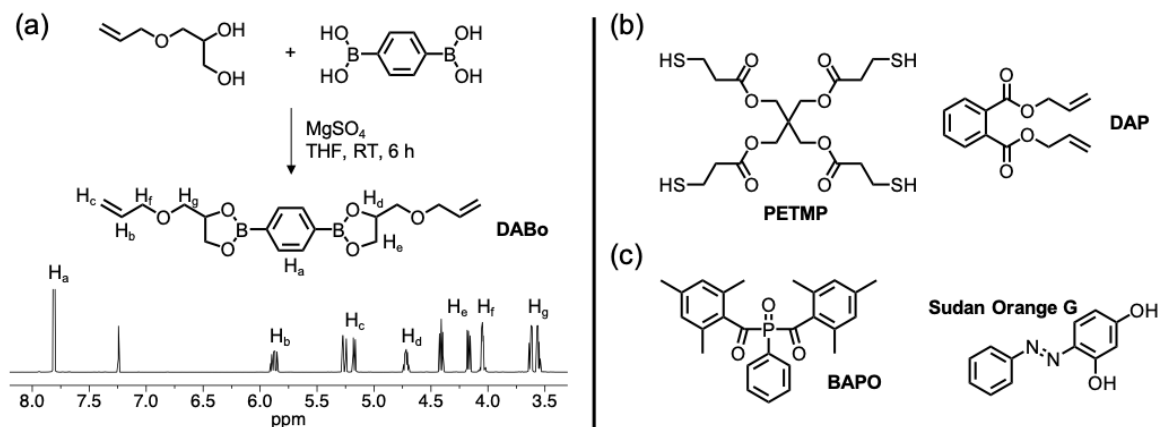
Here we present the development of a thiol–ene vat polymerization strategy towards the 3D printing of boronate CANs. The vitrimeric character of the resultant parts arises from inclusion of a readily accessible allylic monomer containing boronate ester moieties, and by varying the degree of incorporation of this dynamic monomer relative to non-dynamic allyl counterparts, the relaxation rate of the resultant materials can be tuned. The parts printed using this resin show rapid stress relaxation, as well as room-temperature self-healing.

5.3 Results and Discussion

5.3.1 Resin Formulation

In the design of a resin for 3D printing vitrimers, the key element is the inclusion of a dynamic covalent bond. To that end, a synthetic strategy for a monomer containing the desired boronate ester moiety was necessary. Condensation of boronic acids with 1,2-diols provides a facile route to boronate esters, and 1,4-phenylenediboronic acid was selected as substrate to

target a monomer with symmetric reactivity on both sides. Synthetic routes to both dithiol (via 1-thioglycerol) and diallyl (via 3-allyloxy-1,2-propanediol) monomers were investigated, but the diallyl boronate (DABo) was chosen for this study due to its improved solubility in other resin components. The synthesis of DABo is shown in Scheme 7.2a, with stirring over an excess of drying agent giving the product in >80% yield with minimal purification. The low cost of 3-allyloxy-1,2-propanediol and ease of synthesis makes this approach well-suited for 3D-printing applications, which require the use of substantial quantities of resin to generate large parts. Moreover, the moderate reactivity of the allyl ether functionality strikes a balance between being low enough to improve shelf-stability but high enough to give good reactivity when initiated; allyl ethers also lack the homopolymerization tendency of (meth)acrylate systems.¹⁶⁴



Scheme 7.2 (a) Synthesis and ¹H NMR of diallyl boronate (DABo). Higher resolution ¹H NMR and ¹³C NMR are found in Figure 7.7 (Supplemental Results). (b) Structures of additional monomers, pentaerythritol tetrakis(3-mercaptopropionate) (PETMP) and diallyl phthalate (DAP). (c) Structures of initiator (phenylbis(2,4,6-trimethylbenzoyl)phosphine oxide, BAPO) and absorber (Sudan Orange G).

To partner with the difunctional allylic monomer, the requirements for the thiol monomer were that it have functionality >2 to allow for network generation, blend well with the DABo

monomer, and be inexpensively commercially available. The tetrafunctional thiol pentaerythritol tetrakis(3-mercaptopropionate) (PETMP, Scheme 7.2b) satisfies all of these criteria, with a fully liquid resin found to form when mixed with stoichiometric quantities of DABO. An additional benefit of PETMP is that its low volatility results in a much less odoriferous resin than those containing smaller and less hydrogen-bonded thiols. Furthermore, diallyl phthalate (DAP, Scheme 7.2b) was chosen as a reactive diluent to give control over the concentration of boronate ester bonds. The effect of this dilution on mechanical properties is discussed in a later section.

Beyond monomer selection, another central aspect of resin formulation for vat polymerization is the choice of photoinitiator, which gives spatiotemporal control over the curing and must absorb in the printer's wavelength range. The output of the projector used in this study is limited to the visible range (in particular, 425–750 nm);¹⁶⁵ thus phenylbis(2,4,6-trimethylbenzoyl)phosphine oxide (bisacyl phosphine oxide or BAPO, Scheme 7.2c) was selected due to its ability to absorb blue wavelengths. To minimize unwanted polymerization outside of illuminated areas, it is typical to include a protective dye whose absorbance overlaps with the photoinitiator. Sudan Orange G has been successfully paired with BAPO in previous work,¹⁶⁶ and UV-vis measurements demonstrate that it shows high attenuation in the wavelength range of interest (Figure 7.8, Supplemental Results). Finally, the inhibitors 2,6-di-*tert*-butyl-4-methylphenol (BHT) and phenylphosphonic acid (PPA) were included, as those have been found to greatly extend the shelf-life of thiol–ene resins by quenching adventitious radical reactions and nucleophilic addition, respectively.¹⁶⁷ The complete resin formulation containing all of these components is shown in Table 7.2 (Supplemental Results).

5.3.2 Varied Concentration of Boronate

As commented upon in the discussion of resin formulation, the ability to incorporate a non-dynamic allylic monomer (DAP) allows for control over the concentration of dynamic bonds within the final material, ranging from each crosslink containing a boronate ester moiety (100% DABo) to no boronate esters present (0% DABo). To investigate the effect that this concentration has on vitrimeric character and to determine which ratio of DABo/DAP to print, resins were prepared with 100%, 75%, 50%, 25%, and 0% DABo as the allyl monomer. These resins were subsequently mold-cast and cured via irradiation with 405 nm light, giving highly crosslinked elastomers with glass transitions temperatures all near 0 °C (Figure 7.9, Supplemental Results).

These samples were cast into 8 mm disks to allow for rheological testing, and the frequency sweeps for representative samples are shown in Figure 7.1. The sample containing no boronate moieties (0% DABo) behaves as expected for a traditional thermoset, with both the storage and loss moduli approaching plateaus at low frequencies. However, as the incorporation of DABo increases, there are a few notable differences. First is the increase in plateau modulus, from $G' = 420$ kPa for 0% to 1.65 MPa for 100% DABo. While this is possibly due to differences in crosslinking efficiency between DABo and DAP, the similarity between 0% and 50% compared with the large increase from 50% to 100% implies that some critical concentration of the boronate monomer is required. Combined with the observed crystalline nature of DABo in its monomeric form, we suspect that the increased stiffness is due to secondary interactions such as π - π stacking between the phenylene units. Further investigation is necessary to support this hypothesis. The more important difference between the frequency-dependent behavior of the 0% and 100% DABo samples is seen in the loss modulus. Instead

of a monotonic decrease or plateau at low frequencies, the G'' curve of the 100% DABo sample begins to increase, approaching the storage modulus. This increasing viscous behavior at lower frequencies suggests the possibility for corresponding relaxation behavior at longer time scales.

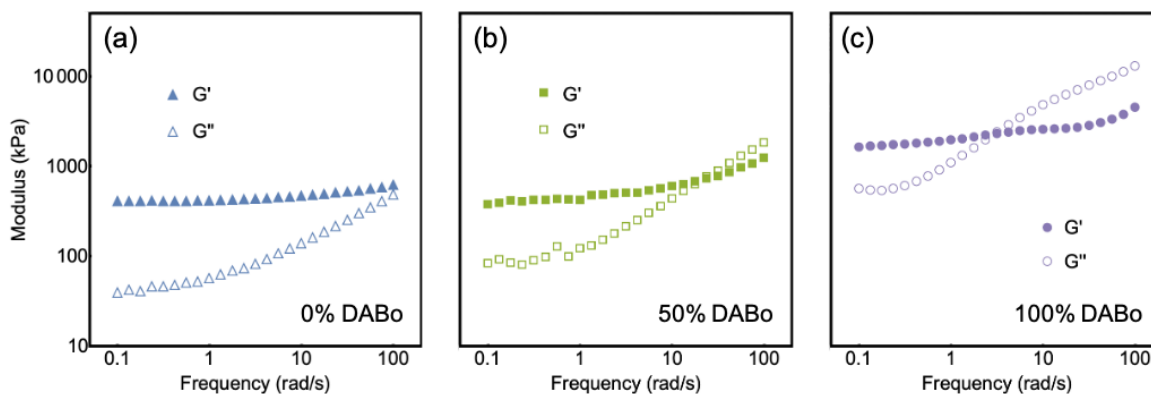


Figure 7.1 Frequency sweeps at room temperature of samples cast using resins containing, as allyl monomers, (a) 100% DABo and 0% DAP, (b) 50% DABo and 50% DAP, and (c) 0% DABo and 100% DAP.

The full extent of these differences between the fully dynamic and fully non-dynamic networks, and the behavior of the intermediate samples, can be more directly observed via stress relaxation experiments (Figure 7.2). As with the frequency sweeps, the 0% DABo sample exhibits the expected behavior of a highly crosslinked elastomer, with some stress relaxed due to network mobility but the majority (> 90%) maintained. The introduction of 25% DABo leads to a substantial drop in residual stress due to the presence of exchangeable boronate esters, but full network rearrangement is prohibited due to the presence of a percolating non-dynamic network formed from PETMP and DAP. The 50%/50% DABo/DAP represents the theoretical lower limit of non-dynamic percolation,^{168,169} but imperfect conversion and network defects interrupt this connectivity, resulting in full stress relaxation.

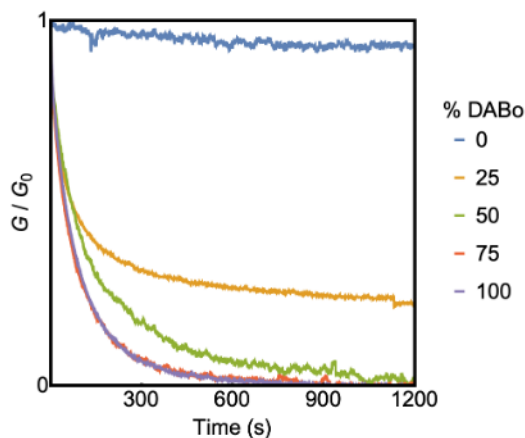


Figure 7.2 Stress relaxation at room temperature of cast samples containing different proportions of allyl monomers. The percentage of DABo is shown, with the remainder being DAP.

Of particular interest is the stress relaxation behavior of the 75% DABo sample, which is both more rapid than the 50% sample and essentially indistinguishable from the 100% sample. A similar trend was recently observed in poly(alkylurea-*co*-urethane) networks, in which samples containing 100%, 80%, and 60% dynamic alkylurea bonds (relative to total alkylurea/urethane incorporation) showed minimal differences in relaxation time.¹⁷⁰ While the increasing proportion of non-dynamic network leads to a higher degree of entanglement, thereby slowing relaxation, Rowan and co-authors found that the rate-limiting step for their percolating dynamic networks was the bond exchange itself. The evidence presented here suggests that the boronate-based systems behave similarly. The outlier is the 50% DABo sample, which exhibits full network rearrangement but does so at extended timescales relative to the more boronate-rich networks. We attribute this intermediate behavior to the greater degree of extended, non-dynamic polymers and sub-networks, which, while not connected enough to fully percolate, introduce substantial enough entanglements that diffusion begins to

compete with the bond exchange process. Due to this combination of full stress relaxation with reduced potential for creep, we selected the 50% DABo formulation for printing.

5.3.3 3D Printing of Boronate Resins

To test the performance of these resins in 3D printing, a DLP-based strategy was used to print disks with both 0% and 50% DABo resins (the latter is shown Figure 7.3a). Both samples exhibited good fidelity after 17 layers of printing. The choice of part geometry allowed for rheological testing, with frequency sweeps largely showing similar trends to the mold-cast samples (Figure 7.10, Supplemental Results). The plateau moduli of the printed samples were lower than their mold-cast counterparts, which suggests lower crosslinking density that is likely due to the presence of the Sudan dye hindering full conversion.

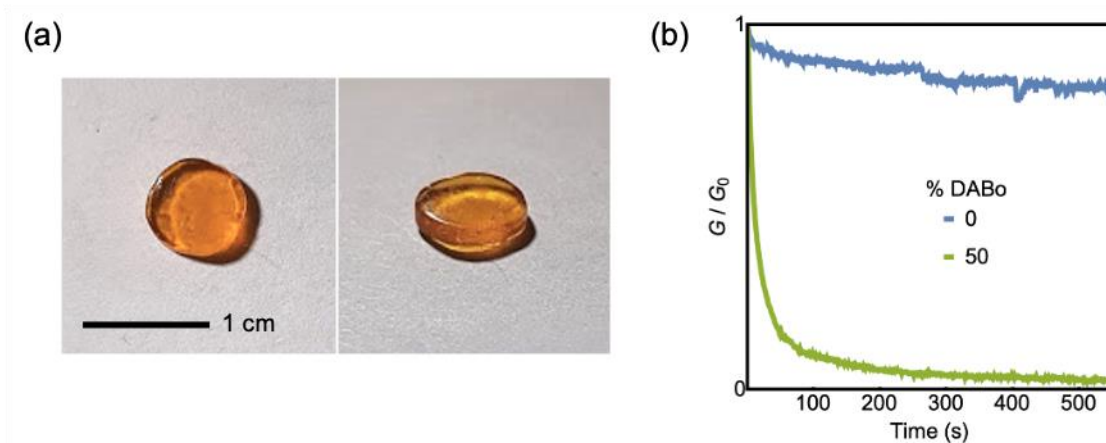


Figure 7.3 (a) Image of printed rheology disk (50% DABo) and (b) stress relaxation of printed samples at room temperature.

The stress relaxation results closely correspond with the trends observed in frequency sweeps. Overall, the behavior remains the same between mold-cast and printed samples; 0% DABo shows some stress relaxation but substantial stress remains, while the stress in the 50% sample dissipates nearly entirely (due to its presence at the cusp of the non-dynamic and

dynamic regimes, small fluctuations can lead to slight differences in residual stress). However, the effects of lower conversion can be observed here as well. For the 0% DABo sample, the residual stress has dropped from $> 90\%$ to closer to 80% , with the lower crosslinking density facilitating network mobility. Similarly, the network with 50% DABo relaxes nearly six times as quickly as the mold-cast analog, again due to a decrease in crosslinking density.

This rapidity of stress relaxation opens the door for the possibility of room-temperature self-healing. To investigate the healing ability of these materials, damage was induced in the 50% DABo sample by slicing it in half with a razor blade. These two halves were then placed into close contact in a mold for 24 h, and the result is shown in Figure 7.4. While superficial evidence of the damage remains, the interface of the sample has healed enough to not only support its own weight but also deformation-inducing tensile stress. In contrast, the 0% DABo sample remained in two discrete pieces after undergoing the same process, revealing that the presence of the boronate esters is required for this healing behavior.

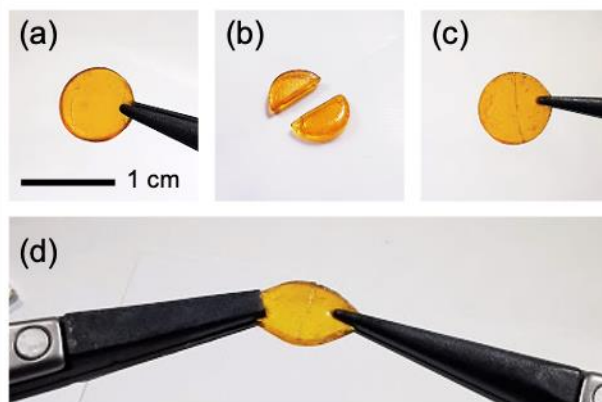


Figure 7.4 Image of 50% DABo sample (a) as printed, (b) cut into half with a razor blade, and (c) after being healed in a mold for 24 h at room temperature. (d) The integrity of the healed sample is demonstrated by applying tensile stress perpendicular to the previously damaged interface.

5.4 Conclusions and Future Directions

With the ever-increasing utilization of 3D printing technology, the need for sustainable alternatives to traditional resins is growing more pressing. Here we present one such strategy, which centers on the inclusion of dynamic boronate ester moieties within a thiol–ene resin. Networks cured from this resin relax stress in the typical manner of vitrimers, with the rate of relaxation partially tunable via the dilution of the boronate with a non-dynamic monomer; however, this versatility is limited at higher boronate incorporations. The resins developed herein were successfully printed using a DLP approach, and the resultant parts not only exhibited stress relaxation but also self-healing characteristics.

While these results are an encouraging demonstration of the potential for 3D-printed boronate vitrimers, there are a few challenges that remain to be addressed. The rapidity with which the printed network relax stress allows for reprocessability at room temperatures, but this low barrier also introduces the risk of creep. In order to extend the lifetime of the parts as printed, a couple of potential avenues are available. The first is to attempt to overcome the low conversion limit currently imposed by the printing parameters. By optimizing the initiator and dye concentrations used, as well as the irradiation time, this conversion could likely be improved, leading to a more tightly crosslinked network and slowing the dynamics considerably. In addition, monomer choice can be utilized to better control the kinetics of stress relaxation. For example, replacing DAP with the reactive diluent 1,3,5-triallyl-1,3,5-triazine-2,4,6(1H,3H,5H) would increase network connectivity and glass transition temperature, both factors that would slow relaxation. Inspiration can also be found in other strategies for curing high- T_g thiol–ene networks, with a number of approaches developed.^{171–173}

Looking beyond the challenges of the current system, there are also several opportunities afforded by the incorporation of boronate moieties into a 3D-printed part. While vitrimer studies often focus on how the dynamic covalent bonds affect the mechanical behavior of a part, dynamic exchange also allows for post-processing; for example, Sumerlin and coworkers demonstrated how the inclusion of β -ketoester moieties into polymethacrylates allowed for various groups to be introduced via exchange with amines.¹⁷⁴ A similar process can be envisioned for the boronate system, in which new functionality is incorporated via exchange with small-molecule boronic acids (readily available due to boron's role in Suzuki coupling).

Furthermore, the ability of boronate esters to undergo not only associative exchange but also to hydrolytically dissociate provides another route for post-printing modification. For printed parts with a majority of the DAP component, hydrolysis would expose hydrophilic diols, dramatically changing the surface energy of the network and enable hydrogel applications. At high enough DABo incorporations, hydrolysis would give full degradation of the part into constituent small molecules and polymers, offering another avenue for transforming the original thermoset into something new.

All these possibilities share one unifying theme: they improve the sustainability of 3D-printed parts. A traditional thermoset is static in character; once it is unable or no longer needed to serve its purpose, its inability to change seals its fate as waste. However, the introduction of self-healing improves the lifetime of the part as originally intended, while the ability to be reprocessed into a new shape, the introduction of new functionality or properties, or the complete dissolution of the part into its molecular building blocks all allow for it to experience new life in a different role. In short, the results discussed here, as well as the potential for future

investigation, serve to present boronate-based vitrimers as a promising platform for sustainable 3D printing.

5.5 Experimental

5.5.1 Materials

1,4-Phenylenediboronic acid (> 97%), 3-allyloxy-1,2-propanediol (> 99%), and phenylphosphonic acid (> 98%) were purchased from TCI America. Pentaerythritol tetrakis(3-mercaptopropionate) (> 95%), diallyl phthalate (97%), phenylbis(2,4,6-trimethylbenzoyl)phosphine oxide (97%), Sudan Orange G (dye content 85%), and 2,6-di-*tert*-butyl-4-methylphenol (> 99%) were obtained from Sigma Aldrich. Anhydrous magnesium sulfate (99%) was purchased from Chem Impex International. All chemicals were used as received. Fluoropolymer films (FEP, 0.001" thick, catalog no. 85905K62) were acquired from McMaster Carr.

5.5.2 Methods

Instrumentation

Nuclear magnetic resonance (NMR) measurements were performed using Varian Unity Inova 500 and 600 MHz instruments. All samples were dissolved in CDCl₃ and chemical shifts (δ) are reported in ppm relative to residual protic chloroform. Infrared (IR) spectra were recorded on a Thermo Nicolet iS10 Fourier-transform infrared (FTIR) spectrometer with a Smart Diamond attenuated total reflectance (ATR) sampling accessory. Differential scanning calorimetry (DSC) was performed on a TA Instruments Q2000 DSC system at a heating rate of 10 °C/min under a nitrogen atmosphere. UV-Vis analysis was performed in quartz cuvettes

on a Shimadzu UV-3600 UV-Vis-NIR spectrophotometer equipped with an integrating sphere. Rheology experiments were performed on a TA Instruments ARES-G2 with an 8 mm parallel plate geometry and a forced convection oven (FCO). All experiments were run at 25 °C in a nitrogen-purged environment. Strain sweeps were used to determine the linear viscoelastic regime (LVE) after which frequency sweeps were run at sufficiently low strains to ensure they were within the regime (with a typical value being 0.1% strain). Stress relaxation experiments were also performed at 0.1% strain.

Sample Preparation

For mold-cast samples, the mold consisted of a 2 mm-thick sheet of stainless steel with an 8-mm diameter disk removed. This sheet was clamped to a piece of flat Teflon, and 100 μ L of resin (containing solely monomers and initiator) was added. After irradiation with 405 nm light for 5 minutes, the Teflon sheet was removed, allowing for the sample to be extricated.

The 3D printer used was modified from a previous set-up,¹⁶⁵ with the addition of a moving build platform to allow for printing in a layer-by-layer approach. The resin chamber is shown in Figure 7.5. The window consists of a fluoropolymer film stretched over a piece of glass and held taut by a 3D-printed base assembly. The walls were machined from Teflon and fastened to the base assembly.

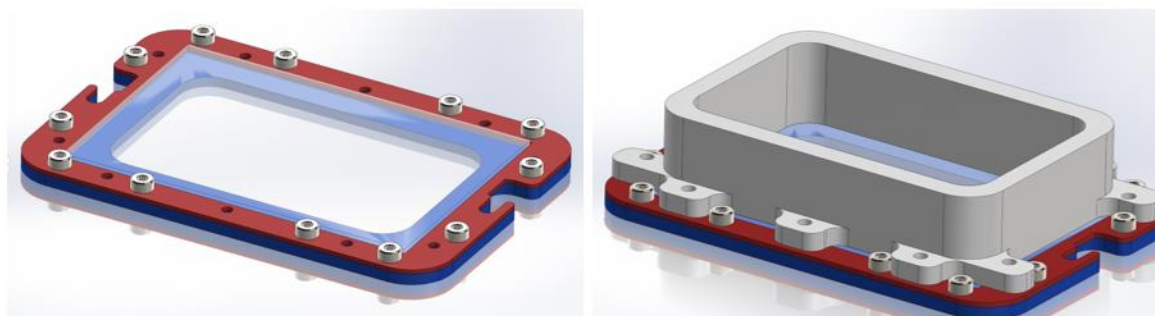


Figure 7.5 Schematics of resin chamber, with base assembly on left and fully assembled chamber on right.

Kinetic studies were performed by exposing the resin in the printing chamber to 3 mm circles of white light for varied durations (0 to 60 s, 5 s intervals). The resultant disks of cured resin were subsequently washed with isopropanol and allowed to cure under bright white light for 24 h before their thickness was measured with electronic calipers. By fitting the data linearly as a function of time (Figure 7.6), the optimal cure times for 100 μm (90 μm layers and 10 μm of over-cure) were found to be 18 s for 0% DABo and 22 s for 50% DABo. The full printing parameters are shown in Table 7.1. After printing, the parts were washed with isopropanol to remove any unreacted resin on the surface and then irradiated with white light for 24 h to increase curing.

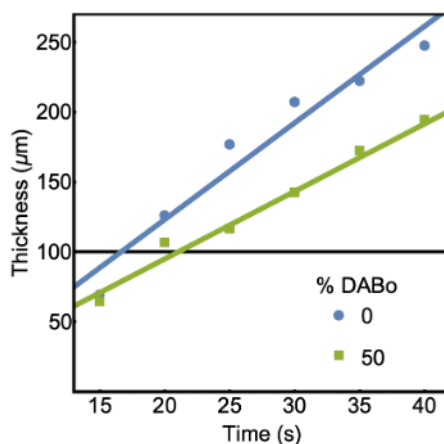


Figure 7.6 Printing kinetics of resins containing 0/100% DABo/DAP and 50/50% DABo/DAP as a function of light exposure duration.

Table 7.1 Printing parameters for 50% DABo resin. For 0% DABo, the exposure time was 18 s.

Parameter	Unit	Value
slice thickness	μm	90
exposure time	s	22
bottom exposure	s	60
no. bottom layers	–	2
z-lift distance	mm	5
z-lift speed	mm/m	25
z-bottom speed	mm/m	50

5.5.3 Synthesis

Synthesis of diallyl boronate (DABo)

To a 100 mL round-bottom flask, was added 1,4-phenyleneboronic acid (4.5 g, 27.1 mmol, 1 equiv.), 3-allyloxy-1,2-diol (6.72 mL, 54.3 mmol, 2 equiv.), and anhydrous THF (45 mL). Magnesium sulfate (9.8 g, 81.4 mmol, 3 equiv.) was added and the mixture stirred at room temperature for 6 h. After filtering off the solid MgSO₄, the solution was concentrated *in vacuo* to give the product as a white solid (8.15 g, 22.8 mmol, 84% yield). ¹H NMR (600 MHz, CDCl₃) δ 7.83 (s, 2H, Ar), 5.89 (ddt, *J* = 17.3, 10.4, 5.7 Hz, 1H, –CH₂–CH=CH₂), 5.28 (dq, *J* = 17.2, 1.6 Hz, 1H, –CH=CH₂), 5.19 (dq, *J* = 10.4, 1.4 Hz, 1H, –CH=CH₂), 4.74 (ddt, *J* = 8.1, 6.6, 5.1 Hz, 1H, –CH₂–C(O–B–)H–CH₂–), 4.43 (dd, *J* = 9.0, 8.1 Hz, 1H, –C(O–)H–CH₂–O–), 4.19 (dd, *J* = 9.0, 6.6 Hz, 1H, –C(O–)H–CH₂–O–), 4.11–4.01 (m, 2H, –O–CH₂–C(O–B–)H–), 3.64 (dd, *J* = 10.3, 5.1 Hz, 1H, –O–CH₂–CH=), 3.57 (dd, *J* = 10.3, 5.1 Hz, 1H, –O–CH₂–CH=). ¹³C NMR (125 MHz, CDCl₃) δ 134.3, 134.1, 117.4, 76.2, 72.5, 71.9, 68.5. FTIR ν_{\max} (cm⁻¹): 3080, 3050, 3029, 2985, 2970, 2940, 2905, 2795, 1520, 1490, 1480, 1465, 1440, 1415, 1405, 1380, 1350, 1345, 1295, 1270, 1255, 1235, 1215, 1160, 1145, 1100, 1090, 1035, 1020, 995,

985, 935, 865, 835, 790, 750, 720, 705, 665, 650, 640, 620. HRMS (EI-TOF) m/z : $[M]^+$ Calcd for $C_{18}H_{24}B_2O_6$ 358.1766; Found, 358.1766.

5.6 Supplemental Results

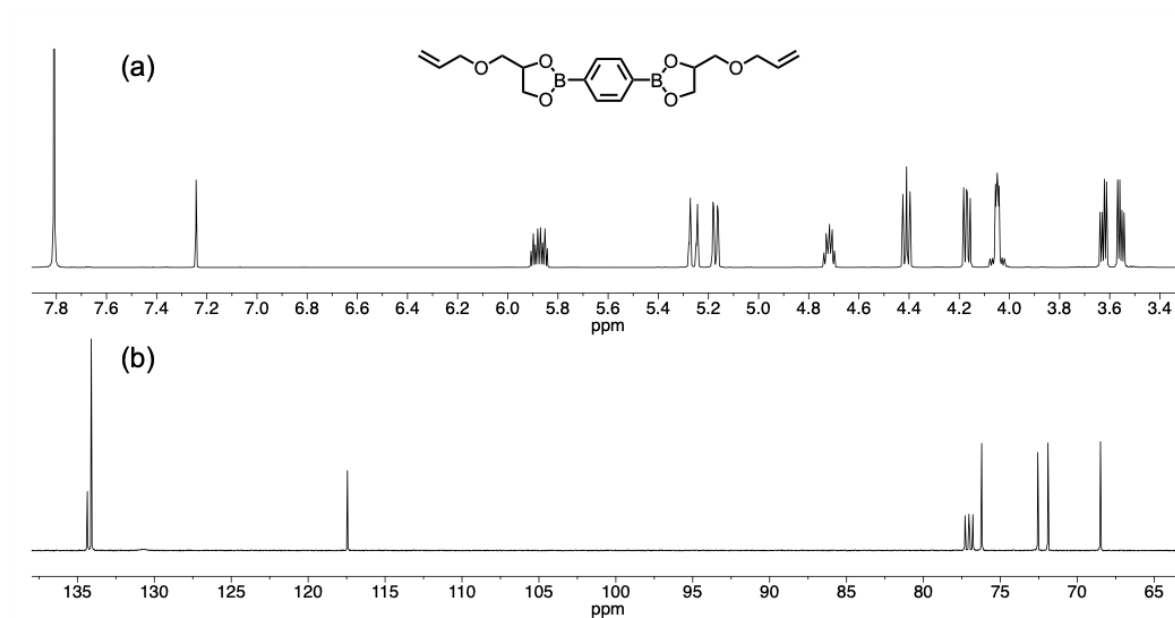


Figure 7.7 (a) 1H NMR and (b) ^{13}C NMR of diallyl boronate (DABo) monomer.

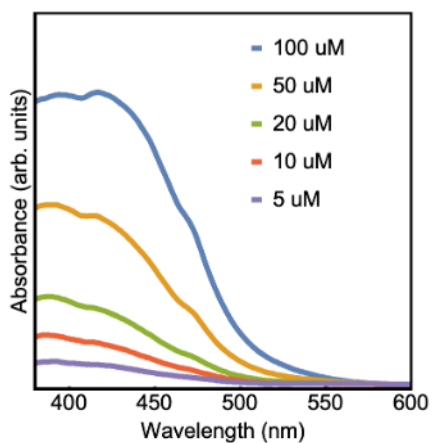


Figure 7.8 UV-vis spectra of solutions of Sudan Orange G with DAP as the solvent at various concentrations.

Table 7.2 Formulation of 50%/50% DABo/DAP resin, with other DABo/DAP ratios calculated such that the total equivalents of allylic monomer always sum to twice that of PETMP. Wt% is measured relative to the total mass of monomer. For mold-cast samples, only the monomers (thiol and ene) and initiator were used.

Reagent	Role	Quantity
PETMP	Thiol	1 equiv.
DABo	Ene	1 equiv
DAP	Ene	1 equiv
BAPO	Initiator	1 wt%
Sudan	Absorber	0.05 wt%
BHT	Inhibitor	0.25 wt%
PPA	Inhibitor	0.1 wt%

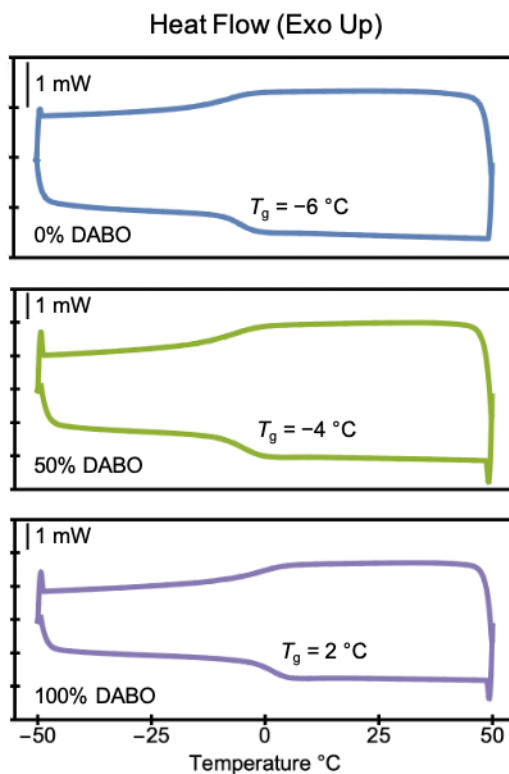


Figure 7.9 DSC traces for 0%, 50%, and 100% DABo cast samples, with glass transition temperatures marked.

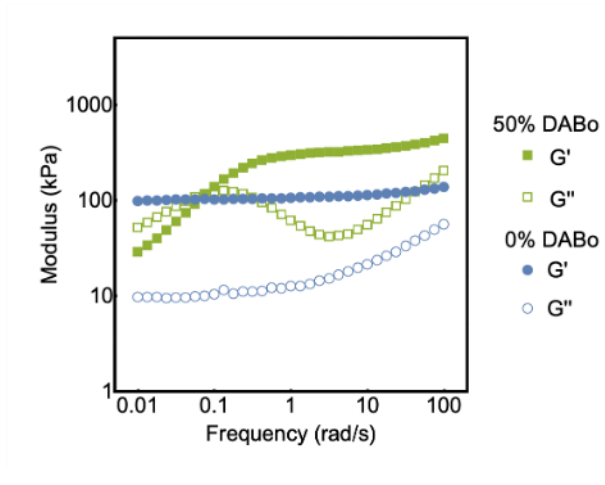


Figure 7.10 Frequency sweeps of printed samples containing (a) 50%/50% DABo/DAP and (b) 0%/100% DABo/DAP.

Chapter 8

References

- (1) Sample, C. S.; Goto, E.; Handa, N. V.; Page, Z. A.; Luo, Y.; Hawker, C. J. Modular Synthesis of Asymmetric Rylene Derivatives. *J. Mater. Chem. C* **2017**, *5*, 1052–1056.
- (2) Sample, C. S.; Lee, S.-H.; Bates, M. W.; Ren, J. M.; Lawrence, J.; Lensch, V.; Gerbec, A.; Bates, C. M.; Li, S.; Hawker, C. J. Metal-Free Synthesis of Poly(Silyl Ether)s under Ambient Conditions. *Macromolecules* **2019**, *52*, 1993–1999.
- (3) Sample, C. S.; Lee, S.-H.; Li, S.; Bates, M. W.; Lensch, V.; Versaw, B. A.; Bates, C. M.; Hawker, C. J. Metal-Free Room-Temperature Vulcanization of Silicones via Borane Hydrosilylation. *Macromolecules* **2019**, *52*, 7244–7250.
- (4) Dimitrakopoulos, C. C.; Mascaro, D. J. Organic Thin-Film Transistors: A Review of Recent Advances. *IBM J. Res. Dev.* **2001**, *45*, 11–27.
- (5) Anthony, J. E.; Facchetti, A.; Heeney, M.; Marder, S. R.; Zhan, X. N-Type Organic Semiconductors in Organic Electronics. *Adv. Mater.* **2010**, *22*, 3876–3892.
- (6) Angadi, M. A.; Gosztola, D.; Wasielewski, M. R. Characterization of Photovoltaic Cells

- Using Poly(Phenylenevinylene) Doped with Perylenediimide Electron Acceptors. *J. Appl. Phys.* **1998**, *83*, 6187–6189.
- (7) Angadi, M. A.; Gosztola, D.; Wasielewski, M. R. Organic Light Emitting Diodes Using Poly(Phenylenevinylene) Doped with Perylenediimide Electron Acceptors. *Mater. Sci. Eng. B Solid-State Mater. Adv. Technol.* **1999**, *63*, 191–194.
- (8) Katz, H. E.; Lovinger, A. J.; Johnson, J.; Kloc, C.; Siegrist, T.; Li, W.; Lin, Y.-Y.; Dodabalapur, A. A Soluble and Air-Stable Organic Semiconductor with High Electron Mobility. *Nature* **2000**, *404*, 478–481.
- (9) Katz, H. E.; Johnson, J.; Lovinger, A. J.; Li, W. Naphthalenetetracarboxylic Diimide-Based n-Channel Transistor Semiconductors: Structural Variation and Thiol-Enhanced Gold Contacts. *J. Am. Chem. Soc.* **2000**, *122*, 7787–7792.
- (10) Chesterfield, R. J.; McKeen, J. C.; Newman, C. R.; Frisbie, C. D.; Ewbank, P. C.; Mann, K. R.; Miller, L. L. Variable Temperature Film and Contact Resistance Measurements on Operating N-Channel Organic Thin Film Transistors. *J. Appl. Phys.* **2004**, *95*, 6396–6405.
- (11) Chen, Z.; Debije, M. G.; Debaerdemaeker, T.; Osswald, P.; Würthner, F. Tetrachloro-Substituted Perylene Bisimide Dyes as Promising n-Type Organic Semiconductors: Studies on Structural, Electrochemical and Charge Transport Properties. *ChemPhysChem* **2004**, *5*, 137–140.
- (12) Liu, C.; Liu, Z.; Lemke, H. T.; Tsao, H. N.; Naber, R. C. G.; Li, Y.; Banger, K.; Müllen, K.; Nielsen, M. M.; Sirringhaus, H. High-Performance Solution-Deposited Ambipolar Organic Transistors Based on Terrylene Diimides. *Chem. Mater.* **2010**, *22*, 2120–2124.
- (13) Zhan, X.; Facchetti, A.; Barlow, S.; Marks, T. J.; Ratner, M. A.; Wasielewski, M. R.;

- Marder, S. R. Rylene and Related Diimides for Organic Electronics. *Adv. Mater.* **2011**, *23*, 268–284.
- (14) Nagao, Y.; Misono, T. Synthesis and Reactions of Perylenecarboxylic Acid Derivatives. VIII. Synthesis of N-Alkyl-3,4,9,10-Perylenetetracarboxylic Monoanhydride Monoimide. *Bull. Chem. Soc. Jpn.* **1981**, *54*, 1191–1194.
- (15) Nagao, Y.; Abe, Y.; Misono, T. Synthesis and Properties of N,N'-Unsymmetrical Dialky-3,4,9,10-Perylenebis(Dicarboximide)S. *Dye. Pigment.* **1985**, *6*, 303–311.
- (16) Korshak, V. V; Vinogradova, S. V. Dependence of Thermal Stability of Polymers on Their Chemical Structure. *Russ. Chem. Rev.* **1968**, *37*, 885–906.
- (17) Mark, J. E. Silicon-Containing Polymers. In *Silicon-Based Polymer Science: A Comprehensive Resource*; Zeigler, J. M., Fearon, F. W. G., Eds.; American Chemical Society: Washington, D.C, 1989; pp 47–68.
- (18) Staple, D.; Hanke, F.; Kreuzer, H. J. Complete Free Energy Landscape and Statistical Thermodynamics of Single Poly(Ethylene Glycol) Molecules. *New J. Phys.* **2007**, *9*, 68–85.
- (19) Mita, I.; Stepto, R. F. T.; Suter, U. W. Basic Classification and Definitions of Polymerization Reactions. *Pure Appl. Chem.* **1994**, *66*, 2483–2486.
- (20) Curry, J. E.; Byrd, J. D. Silane Polymers of Diols. *J. Appl. Polym. Sci.* **1965**, *9*, 295–311.
- (21) Dunnavant, W. R.; Markle, R. A.; Stickney, P. B.; Curry, J. E.; Byrd, J. D. Polyaryloxysilanes by Melt-Polymerizing Dianilino- and Diphenoxysilanes with Aromatic Diols. *J. Polym. Sci. Part A Polym. Chem.* **1967**, *5*, 707–724.
- (22) Dunnavant, W. R.; Markle, R. A.; Sinclair, R. G.; Stickney, P. B.; Curry, J. E.; Byrd, J.

- D. P,P'-Biphenol-Dianilinosilane Condensation Copolymers. *Macromolecules* **1968**, *1*, 249–254.
- (23) Imai, Y. Synthesis of New Functional Silicon-Based Condensation Polymers. *J. Macromol. Sci. Part A - Chem.* **1991**, *28*, 1115–1135.
- (24) Li, Y.; Kawakami, Y. Efficient Synthesis of Poly(Silyl Ether)s by Pd/C and RhCl(PPh₃)₃-Catalyzed Cross-Dehydrocoupling Polymerization of Bis(Hydrosilane)s with Diols. *Macromolecules* **1999**, *32*, 6871–6873.
- (25) Paulasaari, J. K.; Weber, W. P. Ruthenium-Catalyzed Hydrosilation Copolymerization of Aromatic α,ω -Diketones with 1,3-Tetramethyldisiloxane. *Macromolecules* **1998**, *31*, 7105–7107.
- (26) Mabry, J. M.; Paulasaari, J. K.; Weber, W. P. Synthesis of Poly(Silyl Ethers) by Ru-Catalyzed Hydrosilylation. *Polymer* **2000**, *41*, 4423–4428.
- (27) Mabry, J. M.; Runyon, M. K.; Weber, W. P. Poly(Silyl Ether)s by Ruthenium-Catalyzed Hydrosilylation Polymerization of Aliphatic ω -Dimethylsilyloxy Ketones and Copolymerization of Aliphatic α,ω -Diketones with α,ω -Dihydrido-oligodimethylsiloxanes. *Macromolecules* **2002**, *35*, 2207–2211.
- (28) Lázaro, G.; Iglesias, M.; Fernández-Alvarez, F. J.; Sanz Miguel, P. J.; Pérez-Torrente, J. J.; Oro, L. A. Synthesis of Poly(Silyl Ether)s by Rhodium(I)-NHC Catalyzed Hydrosilylation: Homogeneous versus Heterogeneous Catalysis. *ChemCatChem* **2013**, *5*, 1133–1141.
- (29) Lázaro, G.; Fernández-Alvarez, F. J.; Iglesias, M.; Horna, C.; Vispe, E.; Sancho, R.; Lahoz, F. J.; Iglesias, M.; Pérez-Torrente, J. J.; Oro, L. A. Heterogeneous Catalysts Based on Supported Rh-NHC Complexes: Synthesis of High Molecular Weight

- Poly(Silyl Ether)s by Catalytic Hydrosilylation. *Catal. Sci. Technol.* **2014**, *4*, 62–70.
- (30) Li, C.; Hua, X.; Mou, Z.; Liu, X.; Cui, D. Zinc-Catalyzed Hydrosilylation Copolymerization of Aromatic Dialdehydes with Diphenylsilane. *Macromol. Rapid Commun.* **2017**, *38*, 1–5.
- (31) Vijjamarri, S.; Chidara, V. K.; Du, G. Versatile Manganese Catalysis for the Synthesis of Poly(Silylether)s from Diols and Dicarboxyls with Hydrosilanes. *ACS Omega* **2017**, *2*, 582–591.
- (32) Piers, W. E. The Chemistry of Perfluoroaryl Boranes. *Adv. Organomet. Chem.* **2005**, *52*, 1–76.
- (33) Piers, W. E.; Chivers, T. Pentafluorophenylboranes: From Obscurity to Applications. *Chem. Soc. Rev.* **1997**, *26*, 345–354.
- (34) Parks, D. J.; Piers, W. E. Hydrosilylation of Aromatic Aldehydes, Ketones, and Esters. *J. Am. Chem. Soc.* **1996**, *118*, 9440–9441.
- (35) Parks, D. J.; Blackwell, J. M.; Piers, W. E. Studies on the Mechanism of B(C₆F₅)₃-Catalyzed Hydrosilylation of Carbonyl Functions. *J. Org. Chem.* **2000**, *10*, 3090–3098.
- (36) Poelma, J. E.; Fors, B. P.; Meyers, G. F.; Kramer, J. W.; Hawker, C. J. Fabrication of Complex Three-Dimensional Polymer Brush Nanostructures through Light-Mediated Living Radical Polymerization. *Angew. Chemie - Int. Ed.* **2013**, *52*, 6844–6848.
- (37) Fors, B. P.; Poelma, J. E.; Menyo, M. S.; Robb, M. J.; Spokoyny, D. M.; Kramer, J. W.; Waite, J. H.; Hawker, C. J. Fabrication of Unique Chemical Patterns and Concentration Gradients with Visible Light. *J. Am. Chem. Soc.* **2013**, *135*, 14106–14109.
- (38) Discekici, E. H.; Pester, C. W.; Treat, N. J.; Lawrence, J.; Mattson, K. M.; Narupai, B.; Toumayan, E. P.; Luo, Y.; McGrath, A. J.; Clark, P. G.; et al. Simple Benchtop

- Approach to Polymer Brush Nanostructures Using Visible-Light-Mediated Metal-Free Atom Transfer Radical Polymerization. *ACS Macro Lett.* **2016**, *5*, 258–262.
- (39) Pester, C. W.; Narupai, B.; Mattson, K. M.; Bothman, D. P.; Klinger, D.; Lee, K. W.; Discekici, E. H.; Hawker, C. J. Engineering Surfaces through Sequential Stop-Flow Photopatterning. *Adv. Mater.* **2016**, *28*, 9292–9300.
- (40) Page, Z. A.; Narupai, B.; Pester, C. W.; Bou Zerdan, R.; Sokolov, A.; Laitar, D. S.; Mukhopadhyay, S.; Sprague, S.; McGrath, A. J.; Kramer, J. W.; et al. Novel Strategy for Photopatterning Emissive Polymer Brushes for Organic Light Emitting Diode Applications. *ACS Cent. Sci.* **2017**, *3*, 654–661.
- (41) Ligon, S. C.; Liska, R.; Stampfl, J.; Gurr, M.; Mülhaupt, R. Polymers for 3D Printing and Customized Additive Manufacturing. *Chem. Rev.* **2017**, *117*, 10212–10290.
- (42) Layani, M.; Wang, X.; Magdassi, S. Novel Materials for 3D Printing by Photopolymerization. *Adv. Mater.* **2018**, *30*, 1–7.
- (43) Zhu, W.; Ma, X.; Gou, M.; Mei, D.; Zhang, K.; Chen, S. 3D Printing of Functional Biomaterials for Tissue Engineering. *Curr. Opin. Biotechnol.* **2016**, *40*, 103–112.
- (44) Montarnal, D.; Capelot, M.; Tournilhac, F.; Leibler, L. Silica-like Malleable Materials from Permanent Organic Networks. *Science* **2011**, *334*, 965–968.
- (45) Scott, T. F.; Schneider, A. D.; Cook, W. D.; Bowman, C. N. Photoinduced Plasticity in Cross-Linked Polymers. *Science* **2005**, *308*, 1615–1617.
- (46) Lu, Y.-X.; Tournilhac, F.; Leibler, L.; Guan, Z. Making Insoluble Polymer Networks Malleable via Olefin Metathesis. *J. Am. Chem. Soc.* **2012**, *134*, 8424–8427.
- (47) Fortman, D. J.; Brutman, J. P.; Cramer, C. J.; Hillmyer, M. A.; Dichtel, W. R. Mechanically Activated, Catalyst-Free Polyhydroxyurethane Vitrimers. *J. Am. Chem.*

- Soc.* **2015**, *137*, 14019–14022.
- (48) Denissen, W.; Rivero, G.; Nicolaÿ, R.; Leibler, L.; Winne, J. M.; Du Prez, F. E. Vinylogous Urethane Vitrimers. *Adv. Funct. Mater.* **2015**, *25*, 2451–2457.
- (49) Obadia, M. M.; Mudraboyina, B. P.; Serghei, A.; Montarnal, D.; Drockenmuller, E. Reprocessing and Recycling of Highly Cross-Linked Ion-Conducting Networks through Transalkylation Exchanges of C-N Bonds. *J. Am. Chem. Soc.* **2015**, *137* (18), 6078–6083. <https://doi.org/10.1021/jacs.5b02653>.
- (50) Hendriks, B.; Waelkens, J.; Winne, J. M.; Du Prez, F. E. Poly(Thioether) Vitrimers via Transalkylation of Trialkylsulfonium Salts. *ACS Macro Lett.* **2017**, *6*, 930–934.
- (51) Cromwell, O. R.; Chung, J.; Guan, Z. Malleable and Self-Healing Covalent Polymer Networks through Tunable Dynamic Boronic Ester Bonds. *J. Am. Chem. Soc.* **2015**, *137*, 6492–6495.
- (52) Cash, J. J.; Kubo, T.; Bapat, A. P.; Sumerlin, B. S. Room-Temperature Self-Healing Polymers Based on Dynamic-Covalent Boronic Esters. *Macromolecules* **2015**, *48*, 2098–2106.
- (53) Röttger, M.; Domenech, T.; van der Weegen, R.; Breuillac, A.; Nicolaÿ, R.; Leibler, L. High-Performance Vitrimers from Commodity Thermoplastics through Dioxaborolane Metathesis. *Science* **2017**, *356*, 62–65.
- (54) Chen, Y.; Tang, Z.; Liu, Y.; Wu, S.; Guo, B. Mechanically Robust, Self-Healable, and Reprocessable Elastomers Enabled by Dynamic Dual Cross-Links. *Macromolecules* **2019**, *52*, 3805–3812.
- (55) Chen, L.; Li, C.; Müllen, K. Beyond Perylene Diimides: Synthesis, Assembly and Function of Higher Rylene Chromophores. *J. Mater. Chem. C* **2014**, *2*, 1938–1956.

- (56) Herbst, W.; Hunger, K. *Industrial Organic Pigments*, 2nd ed.; Wiley-VCH: Weinheim, 1997.
- (57) Würthner, F. Perylene Bisimide Dyes as Versatile Building Blocks for Functional Supramolecular Architectures. *Chem. Commun.* **2004**, 1564–1579.
- (58) Ford, W. E.; Kamat, P. V. Photochemistry of 3,4,9,10-Perylenetetracarboxylic Dianhydride Dyes. 3. Singlet and Triplet Excited-State Properties of the Bis(2,5-Di-*Tert*-Butylphenyl)Imide Derivate. *J. Phys. Chem.* **1987**, *91*, 6373–6380.
- (59) Seybold, G.; Wagenblast, G. New Perylene and Violanthrone Dyestuffs for Fluorescent Collectors. *Dye. Pigment.* **1989**, *11*, 303–317.
- (60) Sadrai, M.; Bird, G. R. A New Laser Dye with Potential for High Stability and a Broad Band of Lasing Action: Perylene-3,4,9,10-Tetracarboxylic Acid-Bis-N,N'(2',6' Xylidyl)Diimide. *Opt. Commun.* **1984**, *51*, 62–64.
- (61) Reisfeld, R.; Seybold, G. Solid-State Tunable Lasers in the Visible, Based on Luminescent Photoresistant Heterocyclic Colorants. *Chimia (Aarau).* **1990**, *44*, 295–297.
- (62) Gvishi, R.; Reisfeld, R.; Burshtein, Z. Spectroscopy and Laser Action of the “Red Perylimide Dye” in Various Solvents. *Chem. Phys. Lett.* **1993**, *213*, 338–344.
- (63) Law, K. Y. Organic Photoconductive Materials: Recent Trends and Developments. *Chem. Rev.* **1993**, *93*, 449–486.
- (64) Durban, M. M.; Kazarinoff, P. D.; Luscombe, C. K. Synthesis and Characterization of Thiophene-Containing Naphthalene Diimide *n*-Type Copolymers for OFET Applications. *Macromolecules* **2010**, *43*, 6348–6352.
- (65) Yuan, M.; Durban, M. M.; Kazarinoff, P. D.; Zeigler, D. F.; Rice, A. H.; Segawa, Y.;

- Luscombe, C. K. Synthesis and Characterization of Fused-Thiophene Containing Naphthalene Diimide *n*-Type Copolymers for Organic Thin Film Transistor and All-Polymer Solar Cell Applications. *J. Polym. Sci. Part A Polym. Chem.* **2013**, *51*, 4061–4069.
- (66) Jung, B. J.; Tremblay, N. J.; Yeh, M. L.; Katz, H. E. Molecular Design and Synthetic Approaches to Electron-Transporting Organic Transistor Semiconductors. *Chem. Mater.* **2011**, *23*, 568–582.
- (67) Nielsen, C. B.; Holliday, S.; Chen, H. Y.; Cryer, S. J.; McCulloch, I. Non-Fullerene Electron Acceptors for Use in Organic Solar Cells. *Acc. Chem. Res.* **2015**, *48*, 2803–2812.
- (68) O’Neil, M. P.; Niemczak, M. P.; Svec, W. A.; Gosztola, D.; Gaines, G. L.; Wasielewski, M. R. Picosecond Optical Switching Based on Biphotonic Excitation of an Electron Donor-Acceptor-Donor Molecule. *Science* **1992**, *257*, 63–65.
- (69) van der Boom, T.; Hayes, R. T.; Zhao, Y.; Bushard, P. J.; Weiss, E. A.; Wasielewski, M. R. Charge Transport in Photofunctional Nanoparticles Self-Assembled from Zinc 5,10,15,20-Tetrakis(Perylenediimide)Porphyrin Building Blocks. *J. Am. Chem. Soc.* **2002**, *124*, 9582–9590.
- (70) Shinde, S.; Asha, S. K. Temperature Sensitive Emission Color Tuning and White Light Emission in Segmented OPV Polymer: Perylene Bisimide Supramolecular Complex. *Macromolecules* **2016**, *49*, 8134–8145.
- (71) Finlayson, C. E.; Friend, R. H.; Otten, M. B. J.; Schwartz, E.; Cornelissen, J. J. L. M.; Nolte, R. J. M.; Rowan, A. E.; Samorì, P.; Palermo, V.; Liscio, A.; et al. Electronic Transport Properties of Ensembles of Perylene-Substituted Poly-Isocyanopeptide

- Arrays. *Adv. Funct. Mater.* **2008**, *18*, 3947–3955.
- (72) Rajaram, S.; Armstrong, P. B.; Kim, B. J.; Fréchet, J. M. J. Effect of Addition of a Diblock Copolymer on Blend Morphology and Performance of Poly(3-Hexylthiophene):Perylene Diimide Solar Cells. *Chem. Mater.* **2009**, *21*, 1775–1777.
- (73) Tran, H.; Gopinadhan, M.; Majewski, P. W.; Shade, R.; Steffes, V.; Osuji, C. O.; Campos, L. M. Monoliths of Semiconducting Block Copolymers by Magnetic Alignment. *ACS Nano* **2013**, *7*, 5514–5521.
- (74) Langhals, H. Synthese von Hochreinen Perylen-Fluoreszenzfarbstoffen in Großen Mengen – Gezielte Darstellung von Atrop-Isomeren. *Chem. Ber.* **1985**, *118*, 4641–4645.
- (75) Fukuzumi, S.; Ohkubo, K.; Ortiz, J.; Gutiérrez, A. M.; Fernández-Lázaro, F.; Sastre-Santos, A. Formation of a Long-Lived Charge-Separated State of a Zinc Phthalocyanine-Perylenediimide Dyad by Complexation with Magnesium Ion. *Chem. Commun.* **2005**, 3814–3816.
- (76) Nagao, Y. Synthesis and Properties of Perylene Pigments. *Prog. Org. Coatings* **1997**, *31*, 43–49.
- (77) Nagao, Y.; Ishikawa, N.; Tanabe, Y.; Misono, T. Synthesis of Unsymmetrical Perylenebis(Dicarboximide) Derivatives. *Chem. Lett.* **1979**, *8*, 151–154.
- (78) Robb, M. J.; Newton, B.; Fors, B. P.; Hawker, C. J. One-Step Synthesis of Unsymmetrical N-Alkyl-N'-Aryl Perylene Diimides. *J. Org. Chem.* **2014**, *79*, 6360–6365.
- (79) Sakamoto, T.; Pac, C. A “Green” Route to Perylene Dyes: Direct Coupling Reactions of 1,8-Naphthalimide and Related Compounds under Mild Conditions Using a “New” Base Complex Reagent, *t*-BuOK/DBN. *J. Org. Chem.* **2001**, *66*, 94–98.

- (80) Pschirer, N. G.; Kohl, C.; Nolde, F.; Qu, J.; Müllen, K. Pentarylene- and Hexarylenebis(Dicarboximide)s: Near-Infrared-Absorbing Polyaromatic Dyes. *Angew. Chemie - Int. Ed.* **2006**, *45*, 1401–1404.
- (81) Qu, J.; Pschirer, G.; Sens, R. Pentarylene- and Hexarylenetetracarboximides and Preparation Thereof. 8202994 B2, 2012.
- (82) Huang, C.; Barlow, S.; Marder, S. R. Perylene-3,4,9,10-Tetracarboxylic Acid Diimides: Synthesis, Physical Properties, and Use in Organic Electronics. *J. Org. Chem.* **2011**, *76*, 2386–2407.
- (83) Würthner, F.; Stepanenko, V.; Chen, Z.; Saha-Möller, C. R.; Kocher, N.; Stalke, D. Preparation and Characterization of Regioisomerically Pure 1,7-Disubstituted Perylene Bisimide Dyes. *J. Org. Chem.* **2004**, *69*, 7933–7939.
- (84) Kivala, M.; Wu, D.; Feng, X.; Li, C.; Müllen, K. Cyclodehydrogenation in the Synthesis of Graphene-Type Molecules. In *Synthesis of Polymers: New Structures and Methods*; Schlüter, A. D., Hawker, C. J., Sakamoto, J., Eds.; Wiley-VCH: Weinheim, 2012; pp 373–420.
- (85) Vosch, T.; Hofkens, J.; Cotlet, M.; Köhn, F.; Fujiwara, H.; Gronheid, R.; Van Der Biest, K.; Weil, T.; Herrmann, A.; Müllen, K.; et al. Influence of Structural and Rotational Isomerism on the Triplet Blinking of Individual Dendrimer Molecules. *Angew. Chemie - Int. Ed.* **2001**, *40*, 4643–4648.
- (86) Chen, Q.; Gabathuler, R. Synthesis of Camptothecin Melanotransferrin (P97) Conjugate through a Carbamate Bond. *Synth. Commun.* **2004**, *34*, 2415–2424.
- (87) Abd El Samii, Z. K. M.; Al Ashmawy, M. I.; Mellor, J. M. New Routes to Heterocycles via Sulphenylation of Unsaturated Amides. *J. Chem. Soc. Perkin Trans. I* **1988**, 2517–

2522.

- (88) Manning, S. J.; Bogen, W.; Kelly, L. A. Synthesis, Characterization, and Photophysical Study of Fluorescent N-Substituted Benzo[Ghi]Perylene “Swallow Tail” Monoimides. *J. Org. Chem.* **2011**, *76*, 6007–6013.
- (89) Nagasaki, Y.; Matsukura, F.; Kato, M. New Thermosensitive Rubbery Polymers. Synthesis of Poly(Siloxyethylene Glycol) and Its Aqueous Solution Properties. *Macromol. Rapid Commun.* **1996**, *29*, 5859–5863.
- (90) Brook, M. A.; Grande, J. B.; Ganachaud, F. *Silicon Polymers*; Springer: Heidelberg, 2011.
- (91) Parrott, M. C.; Luft, J. C.; Byrne, J. D.; Fain, J. H.; Napier, M. E.; DeSimone, J. M. Tunable Bifunctional Silyl Ether Cross-Linkers for the Design of Acid-Sensitive Biomaterials. *J. Am. Chem. Soc.* **2010**, *132*, 17928–17932.
- (92) Cheng, C.; Watts, A.; Hillmyer, M. A.; Hartwig, J. F. Polysilylether: A Degradable Polymer from Biorenewable Feedstocks. *Angew. Chem. Int. Ed.* **2016**, *55*, 11872–11876.
- (93) Williamson, J. B.; Lewis, S. E.; Johnson, R. R.; Manning, I. M.; Leibfarth, F. C-H Functionalization of Commodity Polymers. *Angew. Chemie* **2018**, *58*, 8654–8668.
- (94) Blackwell, J. M.; Foster, K. L.; Beck, V. H.; Piers, W. E. B(C₆F₅)₃-Catalyzed Silylation of Alcohols: A Mild, General Method for Synthesis of Silyl Ethers. *J. Org. Chem.* **1999**, *64*, 4887–4892.
- (95) Li, Y.; Kawakami, Y. Synthesis and Properties of Polymers Containing Silphenylene Moiety via Catalytic Cross-Dehydrocoupling Polymerization of 1,4-Bis(Dimethylsilyl)Benzene. *Macromolecules* **1999**, *32*, 8768–8773.

- (96) Trost, B. M. Atom Economy—A Challenge for Organic Synthesis: Homogeneous Catalysis Leads the Way. *Angew. Chemie Int. Ed. English* **1995**, *34*, 259–281.
- (97) Nishikubo, T.; Kameyama, A.; Kimura, Y.; Fukuyo, K. Novel Synthesis of Poly(Silyl Ethers) by the Addition Reaction of Bis(Epoxides) with Dichlorosilanes or Bis(Chlorosilanes). *Macromolecules* **1995**, *28*, 4361–4365.
- (98) Nishikubo, T.; Kameyama, A.; Kimura, Y.; Nakamura, T. New Synthesis of Poly(Silyl Ether) and Poly(Germyl Ether) by Addition Reactions of Bisepoxides with Dimethyldiphenoxysilane and Dimethyldiphenoxygermane. *Macromolecules* **1996**, *29*, 5529–5534.
- (99) Minegishi, S.; Ito, M.; Kameyama, A.; Nishikubo, T. Synthesis of Poly(Silyl Ether)s Containing Pendant Chloromethyl Groups by the Polyaddition of Bis(Oxetane)s with Dichlorosilanes. *J. Polym. Sci. Part A Polym. Chem.* **2000**, *38*, 2254–2259.
- (100) Roy, A. K. A Review of Recent Progress in Catalyzed Homogenous Hydrosilation (Hydrosilylation). *Adv. Organomet. Chem.* **2008**, *55*, 1–59.
- (101) Morris, R. H. Asymmetric Hydrosilylation, Transfer Hydrogenation and Hydrogenation of Ketones Catalyzed by Iridium Complexes. *Chem. Soc. Rev.* **2009**, *38*, 2282–2291.
- (102) Troegel, D.; Stohrer, J. Recent Advances and Actual Challenges in Late Transition Metal Catalyzed Hydrosilylation of Olefins from an Industrial Point of View. *Coord. Chem. Rev.* **2011**, *255*, 1440–1459.
- (103) Tondreau, A. M.; Atienza, C. C. H.; Weller, K. J.; Nye, S. A.; Lewis, K. M.; Delis, J. G. P.; Chirik, P. J. Iron Catalysts for Selective Anti-Markovnikov Alkene Hydrosilylation Using Tertiary Silanes. *Science* **2012**, *335*, 567–570.
- (104) Mabry, J. M.; Runyon, M. K.; Weber, W. P. Synthesis of Copoly[Arylene-1,2-

- Dioxy/Oligodimethylsiloxanylene]s by Ruthenium-Catalyzed Dehydrogenative Silylation Copolymerization of o-Quinones with α,ω -Dihydrido oligodimethylsiloxanes. *Macromolecules* **2001**, *34*, 7264–7268.
- (105) Noda, D.; Tahara, A.; Sunada, Y.; Nagashima, H. Non-Precious-Metal Catalytic Systems Involving Iron or Cobalt Carboxylates and Alkyl Isocyanides for Hydrosilylation of Alkenes with Hydrosiloxanes. *J. Am. Chem. Soc.* **2016**, *138*, 2480–2483.
- (106) Discekici, E. H.; Anastasaki, A.; Alaniz, J. R. De; Hawker, C. J. Evolution and Future Directions of Metal-Free Atom Transfer Radical Polymerization. *Macromolecules* **2018**, *51*, 7421–7434.
- (107) Thompson, D. B.; Brook, M. A. Rapid Assembly of Complex 3D Siloxane Architectures. *J. Am. Chem. Soc.* **2008**, *9*, 32–33.
- (108) Kim, D. W.; Joung, S.; Kim, J. G.; Chang, S. Metal-Free Hydrosilylation Polymerization by Borane Catalyst. *Angew. Chem. Int. Ed.* **2015**, *54*, 14805–14809.
- (109) Ma, Y.; Wang, B.; Zhang, L.; Hou, Z. Boron-Catalyzed Aromatic C–H Bond Silylation with Hydrosilanes. *J. Am. Chem. Soc.* **2016**, *138*, 3663–3666.
- (110) Ren, X.; Du, H. Chiral Frustrated Lewis Pairs Catalyzed Highly Enantioselective Hydrosilylations of 1,2-Dicarbonyl Compounds. *J. Am. Chem. Soc.* **2016**, *138*, 810–813.
- (111) Stephan, D. W. The Broadening Reach of Frustrated Lewis Pair Chemistry. *Science* **2016**, *354*, aaf7229.
- (112) Süssle, L.; Hermeke, J.; Oestreich, M. The Asymmetric Piers Hydrosilylation. *J. Am. Chem. Soc.* **2016**, *138*, 6940–6943.

- (113) Addis, D.; Das, S.; Junge, K.; Beller, M. Selective Reduction of Carboxylic Acid Derivatives by Catalytic Hydrosilylation. *Angew. Chem. Int. Ed.* **2011**, *50*, 6004–6011.
- (114) Brook, M. A.; Grande, J. B.; Ganachaud, F. New Synthetic Strategies for Structured Silicones Using B(C₆F₅)₃. *Adv. Polym. Sci.* **2011**, *235*, 161–183.
- (115) Piers, W. E.; Marwitz, A. J. V.; Mercier, L. G. Mechanistic Aspects of Bond Activation with Perfluoroarylboranes. *Inorg. Chem.* **2011**, *50*, 12252–12262.
- (116) Oestreich, M.; Hermeke, J.; Mohr, J. A Unified Survey of Si-H and H-H Bond Activation Catalysed by Electron-Deficient Boranes. *Chem. Soc. Rev.* **2015**, *44*, 2202–2220.
- (117) Chadwick, R. C.; Grande, J. B.; Brook, M. A.; Adronov, A. Functionalization of Single-Walled Carbon Nanotubes via the Piers – Rubinsztajn Reaction. *Macromolecules* **2014**, *47*, 6527–6530.
- (118) Rubinsztajn, S.; Cella, J. A. A New Polycondensation Process for the Preparation of Polysiloxane Copolymers. *Macromolecules* **2005**, *38*, 1061–1063.
- (119) Skjel, M. K.; Houghton, A. Y.; Kirby, A. E.; Harrison, D. J.; Mcdonald, R.; Rosenberg, L. Silane-Controlled Diastereoselectivity in the Tris(Pentafluorophenyl)Borane-Catalyzed Reduction of α -Diketones to Silyl-Protected 1,2-Diols. *Org. Lett.* **2010**, *12*, 376–379.
- (120) Mattson, K. M.; Latimer, A. A.; McGrath, A. J.; Lynd, N. A.; Lundberg, P.; Hudson, Z. M.; Hawker, C. J. A Facile Synthesis of Catechol-Functionalized Poly(Ethylene Oxide) Block and Random Copolymers. *J. Polym. Sci. Part A Polym. Chem.* **2015**, *53*, 2685–2692.
- (121) Nicolson, P. C.; Vogt, J. Soft Contact Lens Polymers: An Evolution. *Biomaterials* **2001**,

- 22, 3273–3283.
- (122) Xia, Y.; Whitesides, G. M. Soft Lithography. *Annu. Rev. Mater. Sci.* **1998**, *28*, 152–184.
- (123) Fudouzi, H.; Xia, Y. Photonic Papers and Inks: Color Writing with Colorless Materials. *Adv. Mater.* **2003**, *15*, 892–896.
- (124) So, J.; Thelen, J.; Qusba, A.; Hayes, G. J.; Lazzi, G.; Dickey, M. D. Reversibly Deformable and Mechanically Tunable Fluidic Antennas. *Adv. Funct. Mater.* **2009**, *19*, 3632–3637.
- (125) Plass, K. E.; Filler, M. A.; Spurgeon, J. M.; Kayes, M.; Maldonado, S.; Brunshwig, B. S.; Atwater, H. A.; Lewis, N. S. Flexible Polymer-Embedded Si Wire Arrays. *Adv. Mater.* **2009**, *21*, 325–328.
- (126) Wang, Y.; Yang, R.; Shi, Z.; Zhang, L.; Shi, D.; Wang, E.; Zhang, G. Super-Elastic Graphene Ripples for Flexible Strain Sensors. *ACS Nano* **2011**, *5*, 3645–3650.
- (127) Görm, P.; Lehnhardt, M.; Kowalsky, W.; Riedl, T.; Wagner, S. Elastically Tunable Self-Organized Organic Lasers. *Adv. Mater.* **2011**, *23*, 869–872.
- (128) Ahmed, S.; Yang, H.; Ozcam, A. E.; Kirill, E.; Weiger, M. C.; Genzer, J.; Haugh, J. M. Poly(Vinylmethylsiloxane) Elastomer Networks as Functional Materials for Cell Adhesion and Migration Studies. *Biomacromolecules* **2011**, *12*, 1265–1271.
- (129) Hénot, M.; Drockenmuller, É.; Léger, L.; Restagno, F. Friction of Polymers: From PDMS Melts to PDMS Elastomers. *ACS Macro Lett.* **2018**, *7*, 112–114.
- (130) Brook, M. A. Silicones. In *Silicon in Organic, Organometallic and Polymer Chemistry*; Wiley: New York, 2000; pp 256–308.
- (131) Treat, N. J.; Sprafke, H.; Kramer, J. W.; Clark, P. G.; Barton, B. E.; Alaniz, J. R. De; Fors, B. P.; Hawker, C. J. Metal-Free Atom Transfer Radical Polymerization. *J. Am.*

Chem. Soc. **2014**, *136*, 16096–16101.

- (132) Wang, J.; Yuan, L.; Wang, Z.; Rahman, A.; Huang, Y.; Zhu, T.; Wang, R.; Cheng, J.; Wang, C.; Chu, F.; et al. Photoinduced Metal-Free Atom Transfer Radical Polymerization of Biomass-Based Monomers. *Macromolecules* **2016**, *49*, 7709–7717.
- (133) Xiao, L.; Chen, Y.; Zhang, K. Efficient Metal-Free “Grafting Onto” Method for Bottlebrush Polymers by Combining RAFT and Triazolinedione–Diene Click Reaction. *Macromolecules* **2016**, *49*, 4452–4461.
- (134) Gonzaga, F.; Yu, G.; Brook, M. A. Polysiloxane Elastomers via Room Temperature, Metal-Free Click Chemistry. *Macromolecules* **2009**, *42*, 9220–9224.
- (135) Rambarran, T.; Gonzaga, F.; Brook, M. A. Generic, Metal-Free Cross-Linking and Modification of Silicone Elastomers Using Click Ligation. *Macromolecules* **2012**, *45*, 2276–2285.
- (136) Feng, L.; Zhou, L.; Feng, S. Preparation and Characterization of Silicone Rubber Cured via Catalyst-Free Aza-Michael Reaction. *RSC Adv.* **2016**, *6*, 111648–111656.
- (137) Zhao, Q.; Liu, Q.; Xu, H.; Bei, Y.; Feng, S. Preparation and Characterization of Room Temperature Vulcanized Silicone Rubber Using α -Amine Ketoximesilanes as Auto-Catalyzed Cross-Linkers. *RSC Adv.* **2016**, *6*, 38447–38453.
- (138) Mincheva, R.; Beigbeder, A.; Pettitt, M. E.; Maureen, E.; Callow, J. A.; Dubois, P. Metal-Free Anti-Biofouling Coatings: The Preparation of Silicone-Based Nanostructured Coatings via Purely Organic Catalysis. *Nanocomposites* **2016**, *2*, 51–57.
- (139) Chadwick, R. C.; Kardelis, V.; Lim, P.; Adronov, A. Metal-Free Reduction of Secondary and Tertiary N-Phenyl Amides by Tris(Pentafluorophenyl)Boron-Catalyzed

- Hydrosilylation. *J. Org. Chem.* **2014**, *79*, 7728–7733.
- (140) Rubin, M.; Schwier, T.; Gevorgyan, V. Highly Efficient B(C₆F₅)₃Catalyzed Hydrosilylation of Olefins. **2002**, No. 6, 1936–1940.
- (141) Keess, S.; Simonneau, A.; Oestreich, M. Direct and Transfer Hydrosilylation Reactions Catalyzed by Fully or Partially Fluorinated Triarylboranes: A Systematic Study. *Organometallics* **2015**, *34*, 790–799.
- (142) Gandhamsetty, N.; Joung, S.; Park, S.-W.; Park, S.; Chang, S. Boron-Catalyzed Silylative Reduction of Quinolines: Selective Sp³ C–Si Bond Formation. *J. Am. Chem. Soc.* **2014**, *136*, 16780–16783.
- (143) Gandhamsetty, N.; Park, J.; Jeong, J.; Park, S.; Park, S.; Chang, S. Chemoselective Silylative Reduction of Conjugated Nitriles under Metal-Free Catalytic Conditions: β-Silyl Amines and Enamines. *Angew. Commun.* **2015**, *54*, 6832–6836.
- (144) Chojnowski, J.; Fortuniak, W.; Kurjata, J.; Rubinsztajn, S.; Cella, J. A. Oligomerization of Hydrosiloxanes in the Presence of Tris(Pentafluorophenyl)Borane. *Macromolecules* **2006**, *39*, 3802–3807.
- (145) Chojnowski, J.; Rubinsztajn, S.; Fortuniak, W.; Kurjata, J. Oligomer and Polymer Formation in Hexamethylcyclotrisiloxane (D₃) – Hydrosilane Systems Under Catalysis by Tris(Pentafluorophenyl)Borane. *J. Inorg. Organomet. Polym. Mater.* **2007**, *17* (1), 173–187.
- (146) Xue, L.; Kawakami, Y. Precise Synthesis of Poly(Silphenylenesiloxane)s with Epoxy Side Functional Groups by Tris(Pentafluorophenyl)Borane as a Catalyst. *Polym. J.* **2007**, *39*, 379–388.
- (147) Zhou, D.; Kawakami, Y. Tris(Pentafluorophenyl)Borane as a Superior Catalyst in the

- Synthesis of Optically Active SiO-Containing Polymers. *Macromolecules* **2005**, *38*, 6902–6908.
- (148) Chojnowski, J.; Rubinsztajn, S.; Fortuniak, W.; Kurjata, J. Synthesis of Highly Branched Alkoxysiloxane - Dimethylsiloxane Copolymers by Nonhydrolytic Dehydrocarbon Polycondensation Catalyzed by Tris (Pentafluorophenyl) Borane. *Macromolecules* **2008**, *41*, 7352–7358.
- (149) Kurjata, J.; Fortuniak, W.; Rubinsztajn, S.; Chojnowski, J. B(C₆F₅)₃ Catalyzed Dehydrocarbon Polycondensation of PhSiH₃ with (MeO)₄Si as Model Polyfunctional Comonomers in New Route to Hydrophobic Silicone TQ Resins. *Eur. Polym. J.* **2009**, *45*, 3372–3379.
- (150) Grande, J. B.; Fawcett, A. S.; Mclaughlin, A. J.; Gonzaga, F.; Bender, T. P.; Brook, M. A. Anhydrous Formation of Foamed Silicone Elastomers Using the Piers–Rubinsztajn Reaction. *Polymer* **2012**, *53*, 3135–3142.
- (151) Fawcett, A. S.; Grande, J. B.; Brook, M. A. Rapid , Metal-Free Room Temperature Vulcanization Produces Silicone Elastomers. *J. Polym. Sci. Part A Polym. Chem.* **2013**, *51*, 644–652. <https://doi.org/10.1002/pola.26414>.
- (152) Zhang, J.; Chen, Y.; Sewell, P.; Brook, M. A. Utilization of Softwood Lignin as Both Crosslinker and Reinforcing Agent in Silicone Elastomers. *Green Chem.* **2015**, *17*, 1811–1819.
- (153) Graiver, D.; Farminer, K. W.; Narayan, R. A Review of the Fate and Effects of Silicones in the Environment. *J. Polym. Environ.* **2003**, *11* (4), 129–136.
- (154) Parks, D. J.; Blackwell, J. M.; Piers, W. E. Studies on the Mechanism of B(C₆F₅)₃-Catalyzed Hydrosilation of Carbonyl Functions. *J. Org. Chem.* **2000**, *65*, 3090–3098.

- (155) Stansbury, J. W.; Idacavage, M. J. 3D Printing with Polymers: Challenges among Expanding Options and Opportunities. *Dent. Mater.* **2016**, *32*, 54–64.
- (156) Zhang, J.; Xiao, P. 3D Printing of Photopolymers. *Polym. Chem.* **2018**, *9*, 1530–1540.
- (157) Bagheri, A.; Jin, J. Photopolymerization in 3D Printing. *ACS Appl. Polym. Mater.* **2019**, *1*, 593–611.
- (158) Ford, S.; Despeisse, M. Additive Manufacturing and Sustainability: An Exploratory Study of the Advantages and Challenges. *J. Clean. Prod.* **2016**, *137*, 1573–1587.
- (159) Wohlers Report 2016: 3D Printing and Additive Manufacturing State of the Industry. Wohlers Associates: Fort Collins, CO 2016.
- (160) Ding, R.; Du, Y.; Goncalves, R. B.; Francis, L. F.; Reineke, T. M. Sustainable near UV-Curable Acrylates Based on Natural Phenolics for Stereolithography 3D Printing. *Polym. Chem.* **2019**, *10*, 1067–1077.
- (161) Voet, V. S. D.; Strating, T.; Schnelting, G. H. M.; Dijkstra, P.; Tietema, M.; Xu, J.; Woortman, A. J. J.; Loos, K.; Jager, J.; Folkersma, R. Biobased Acrylate Photocurable Resin Formulation for Stereolithography 3D Printing. *ACS Omega* **2018**, *3*, 1403–1408.
- (162) Sutton, J. T.; Rajan, K.; Harper, D. P.; Chmely, S. C. Lignin-Containing Photoactive Resins for 3D Printing by Stereolithography. *ACS Appl. Mater. Interfaces* **2018**, *10*, 36456–36463.
- (163) Zhang, B.; Kowsari, K.; Serjouei, A.; Dunn, M. L.; Ge, Q. Reprocessable Thermosets for Sustainable Three-Dimensional Printing. *Nat. Commun.* **2018**, *9*, 1831.
- (164) Hoyle, C. E.; Lee, T. Y.; Roper, T. Thiol–enes: Chemistry of the Past with Promise for the Future. *J. Polym. Sci. Part A Polym. Chem.* **2004**, *42*, 5301–5338.
- (165) Dolinski, N. D.; Page, Z. A.; Callaway, E. B.; Eisenreich, F.; Garcia, R. V.; Chavez, R.;

- Bothman, D. P.; Hecht, S.; Zok, F. W.; Hawker, C. J. Solution Mask Liquid Lithography (SMaLL) for One-Step, Multimaterial 3D Printing. *Adv. Mater.* **2018**, *30*, 1800364.
- (166) Wang, X.; Schmidt, F.; Hanaor, D.; Kamm, P. H.; Li, S.; Gurlo, A. Additive Manufacturing of Ceramics from Pre-ceramic Polymers: A Versatile Stereolithographic Approach Assisted by Thiol-ene Click Chemistry. *Addit. Manuf.* **2019**, *27*, 80–90.
- (167) Esfandiari, P.; Ligon, S. C.; Lagref, J. J.; Frantz, R.; Cherkaoui, Z.; Liska, R. Efficient Stabilization of Thiol-ene Formulations in Radical Photopolymerization. *J. Polym. Sci. Part A Polym. Chem.* **2013**, *51*, 4261–4266.
- (168) Flory, P. J. Molecular Size Distribution in Three Dimensional Polymers. I. Gelation. *J. Am. Chem. Soc.* **1941**, *63*, 3083–3090.
- (169) Stockmayer, W. H. Theory of Molecular Size Distribution and Gel Formation in Branched-Chain Polymers. *J. Chem. Phys.* **1944**, *11*, 45–55.
- (170) Chen, L.; Zhang, L.; Griffin, P. J.; Rowan, S. J. Impact of Dynamic Bond Concentration on the Viscoelastic and Mechanical Properties of Dynamic Poly(Alkylurea-Co-Urethane) Networks. *Macromol. Chem. Phys.* **2020**, *221*, 1–10.
- (171) Li, Q.; Zhou, H.; Wicks, D. A.; Hoyle, C. E. Thiourethane-Based Thiol-ene High T_g Networks: Preparation, Thermal, Mechanical, and Physical Properties. *J. Polym. Sci. Part A Polym. Chem.* **2007**, *45*, 5103–5111.
- (172) Carioscia, J. A.; Schneidewind, L.; O'Brien, C.; Ely, R.; Feeser, C.; Cramer, N.; Bowman, C. N. Thiol-Norbornene Materials: Approaches to Develop High T_g Thiol-ene Polymers. *J. Polym. Sci. Part A Polym. Chem.* **2007**, *45*, 5686–5696.
- (173) Parker, S.; Reit, R.; Abitz, H.; Ellson, G.; Yang, K.; Lund, B.; Voit, W. E. High- T_g Thiol-Click Thermoset Networks via the Thiol-Maleimide Michael Addition.

Macromol. Rapid Commun. **2016**, *37*, 1027–1032.

- (174) Sims, M. B.; Lessard, J. J.; Bai, L.; Sumerlin, B. S. Functional Diversification of Polymethacrylates by Dynamic β -Ketoester Modification. *Macromolecules* **2018**, *51*, 6380–6386.